CHALMERS

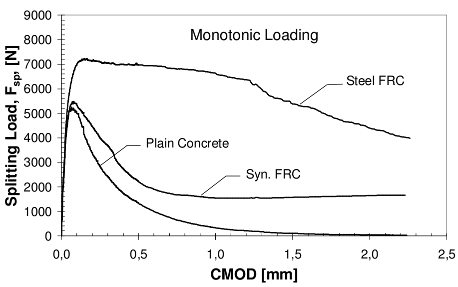

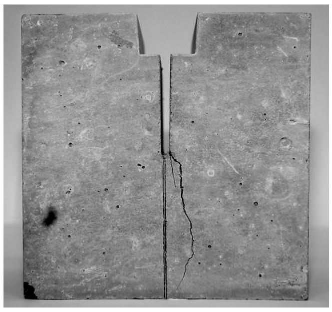

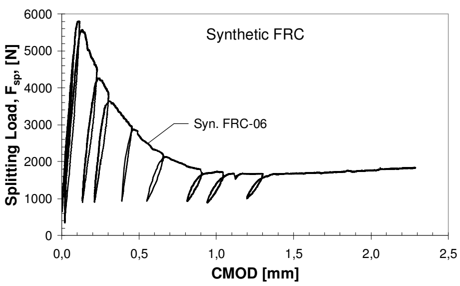

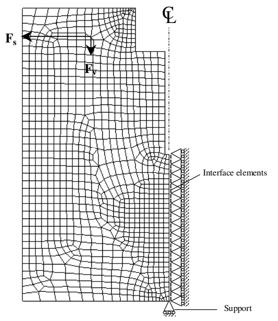

Evaluation of WST Method as a Fatigue Test for Plain and Fiber-reinforced Concrete

- experimental and numerical investigation

Master's Thesis in the International Master's Programme Structural Engineering

KAMYAB ZANDI HANJARI

Department of Civil and Environmental Engineering
Division of Structural Engineering
Concrete Structures
CHALMERS UNIVERSITY OF TECHNOLOGY
Göteborg, Sweden 2006

Master's Thesis 2006:17

MASTER'S THESIS 2006:17

Evaluation of WST Method as a Fatigue Test for Plain and Fiber-reinforced Concrete

- experimental and numerical investigation

KAMYAB ZANDI HANJARI

Department of Civil and Environmental Engineering
Division of Structural Engineering
Concrete Structures
CHALMERS UNIVERSITY OF TECHNOLOGY
Göteborg, Sweden

Evaluation of WST Method as a Fatigue Test for Plain and Fiber-reinforced Concrete
- experimental and numerical investigation

KAMYAB ZANDI HANJARI

Master's Thesis 2006:17

Department of Civil and Environmental Engineering
Division of Structural Engineering
Concrete Structures
Chalmers University of Technology
SE-412 96 Göteborg
Sweden
Telephone: + 46 (0)31-772 1000

Cover:
Top left: experimental result of splitting load, F_{sp}, vs. CMOD for three types of concrete under monotonic loading; see section 6.4, figure 6.3(d)
Top right: photo of the fractured WST specimen under cyclic loading
Bottom left: experimental result of splitting load, F_{sp}, vs. CMOD for synthetic fiber reinforced concrete under cyclic loading; see section 6.5, figure 6.17(c)
Bottom right: the finite element model of half a WST specimen analysed using program package Diana

Chalmers reproservice / Department of Civil and Environmental Engineering

Evaluation of WST Method as a Fatigue Test for Plain and Fiber Reinforced Concrete
Experimental and Numerical investigation

KAMYAB ZANDI HANJARI
Department of Civil and Environmental Engineering
Division of Structural Engineering
Concrete Structures
Chalmers University of Technology

ABSTRACT

In recent years, a profound interest has developed towards the fatigue behaviour of concrete. Firstly because there is always concern about the effect of repeated loads on concrete structures, and secondly, even if repeated loads do not cause a fatigue failure, it may lead to e.g. inclined cracking in a beam at lower than expected loads, or may cause cracking in component materials of a member that alters the static load carrying characteristic. Although there is no standardized method of fatigue testing, fatigue properties of concrete might be estimated by different methods, e.g. Three-point Bending Test (TPBT), Uni-axial Tension Test (UTT), and Wedge Splitting Test (WST). The small dimension of the specimen and stability of the WST method makes it prefect for use as an experimental method in laboratory.

The presented study has been focused on investigating the possibility of using the wedge splitting test method in order to study the fatigue behaviour of concrete. Fatigue behaviour of three types of concrete, i.e. (1) plain concrete, (2) steel fiber reinforced concrete, and (3) synthetic fiber reinforced concrete, were studied experimentally and numerically. In the former part, some experiments were carried out using WST specimens under a monotonic and cyclic loading. In the later part, inverse analyses were conducted using a Matlab® program, developed at DTU by Østergaard (2003), and by conducting FE analyses using the commercial available program package Diana.

Through numerical analysis, bi-linear *σ-w* relationships and the energy dissipation were determined. A systematic approach for material testing based on fracture mechanics presented by Löfgren (2005), which covers material testing, inverse analysis, and adjustment of the *σ-w* relationship for fiber efficiency, were applied. It was found that inclusion of fibers affects the shape of the *σ-w* relationship remarkably, so that for steel and synthetic fiber reinforced concrete, the zero stress is reached at significantly larger crack openings compared to plain concrete.

The stable results of the experiments indicate that the WST method can be applicable for investigating the fatigue behaviour of all three types of tested concrete. The inverse analysis using the Matlab® program for the WST specimen, performed on the plain concrete, suggests that a *σ-w* relationship can be determined for each reloading section on a fatigue test of the WST method. Hence, this study implies applicability of the WST method for exploring the fatigue behaviour of concrete.

Key words: fatigue, concrete, fiber-reinforced, wedge splitting test (WST), inverse analysis, stress-crack opening relationship

Contents

Preface

This thesis is submitted as a partial fulfilment of the requirements for the International Master Degree. The study was carried from September 2005 until February 2006 at Chalmers university of Technology, at the department of Civil and Environmental Engineering, Division of Structural Engineering, Concrete Structures. Parts of experiments have been performed at Thomas Concrete Central Laboratory, Göteborg, Sweden.

At first, I would like to thank my supervisors, Prof. Kent Gylltoft, who was also the examiner, Ingemar Löfgren, PhD, and Rasmus Rempling, current PhD Student for their encouraging support and inspiration, and for giving me the freedom to choose the subjects of my interest. Especially, I am grateful for the many fruitful discussions of the experimental procedures and results and software problems I have had with Ingemar Löfgren and Rasmus Rempling. I would like to give my appreciation to Stefano Battocchi and Andrea Polastri, the opponents, for their comments on the project and all good moments we have had together.

Furthermore, I would like to express my gratitude to all staff at the Division of Structural Engineering. A special thanks to Björn Engström for the concrete knowledge I received during courses, for the well organized master program in structural engineering, and for all his general guidance and kindness during my study at Chalmers.

My warmest thanks to my friends, Farzad for the late night discussions which made me to think deeply, Hosein for his kindness, and all my friends in Iran and Sweden for being nice to me.

Last but not least, I take the opportunity to express my ever lasting love to my father and mother for their never ending supports and my sister for her help during my study at Sweden and my brother for being the best friend to me.

Göteborg, February 2006

Kamyab,

Notations

Roman upper case letters

A	Cross-sectional area
A_f	Fiber cross-sectional area
E	Modulus of elasticity
E_c	Modulus of elasticity of concrete
F_{sp}	Splitting load in a wedge splitting test
F_v	Vertical load in a wedge splitting test
G_F	Specific fracture energy
G_f	Specific energy dissipated during fracture
I	Second moment of inertia
L_e	Embedment length
L_f	Fiber length
M	Bending moment
N	Normal force
N_b	Number of bridging fiber
$N_{f.\exp}$	Number of fibers per unit area in a fracture specimen
V_f	Volume fraction of fibers

Roman lower case letters

a	Crack length
a_1	Initial slope of the bi-linear σ-w relationship
a_2	Second slope of the bi-linear σ-w relationship
b_2	Intersection of the bi-linear σ-w relationship with the y-axis
d_f	Diameter of fiber
f_c	Compressive strength of concrete
f_t	Tensile strength of concrete
l_{ch}	Characteristic length
w	Crack opening
w_c	Critical crack opening for which $\sigma(w) = 0$
w/c	Water cement ratio
w/b	Water binder ratio

Greek letters

α	Wedge angle in the wedge splitting test
δ	Deflection
ε	Strain
ε_c	Concrete strain

ν	Poisson's ratio
μ	Coefficient of friction
η_b	Fiber efficiency factor
λ_f	Aspect ratio of fiber
σ	Stress
$\sigma(w)$	Stress as a function of crack opening
σ_b	Bridging stress
$\sigma(w)$	Stress as a function of crack opening

Abbreviations

ACI	American Concrete Institute
CMOD	Crack Mouth Opening Displacement
CoV	Coefficient of Variance
CTOD	Crack Tip Opening Displacement
C-S-H	Calcium Silicate Hydrate
DTU	Technical University of Denmark
EC2	Eurocode 2
FEA	Finite Element Analysis
FEM	Finite Element method
FRC	Fiber Reinforced Concrete
HSC	High Strength Concrete
NSC	Normal Strength Concrete
PC	Plain Concrete
RILEM	International union of laboratories and experts in construction materials, systems and structures
Steel FRC	Steel Fiber reinforced Concrete
Syn FRC	Synthetic Fiber Reinforced Concrete
UTT	Uni-axial Tension Test
WST	Wedge Splitting Test
TPBT	Three-Point Bending Test
3PBT	Three-Point Bending Test

e.g.	For example
i.e.	That is
vs.	versus
σ-w	stress-crack opening

1 INTRODUCTION

1.1 Background

The use of cementing material is very old. The ancient Egyptians used calcined impure gypsum. The Greeks and the Romans used calcined limestone and later learned to add to lime and water, sand and crushed stone or brick and broken tiles. This might be the first concrete in history. These days, concrete and steel are the two most commonly used structural material. They sometimes complement one another, and sometimes compete with one another so that structures of a similar type and function can be built in either of these materials. And yet, the engineer often knows less about the concrete of which the structure is made than about the steel, especially when it comes to fatigue behaviour of concrete under cyclic loading.

Although the basic knowledge of fracture mechanics theory has been available since the middle of 20th century, design of concrete structures is not yet based on fracture mechanics. This is partly due to the fact that the form of fracture mechanics which was available until recently was applicable only to homogeneous brittle materials such as glass, or to homogeneous brittle-ductile materials such as metals. However, it is also due to the fact that Non-Linear Fracture Mechanics is not easily implemented into design codes. On the other hand, for concrete structures, strain-softening due to distributed cracking, localization of micro cracks into macro cracks prior to failure, and bridging stresses at the fracture front must be taken into account. A form of fracture mechanics that can be applied to such structures and failure processes has been developed only during the last couple of decades.

Fatigue is the process of progressive localized permanent structural change occurring in the material subjected to the conditions that produce fluctuating stresses and strains at some points and that may culminate in cracks or complete fracture after a sufficient number of fluctuations. Fracture mechanics could be a powerful tool in order to interpret the behaviour of concrete elements under cyclic loading provided that a reliable, simple and stable method of material and structural testing under cyclic loading exits. Many different test methods have been applied under monotonic loading which estimate the fracture properties of concrete elements. Among these methods, there are some standardized methods such as Uni-axial Tension Test, Three-point Bending Test, and Wedge Splitting Test methods that characterize fracture properties of concrete while no standardized material and structural test method has been agreed in codes for concrete. Crystal clearly, such a test should be able to characterize fatigue fracture properties of concrete and easy to perform.

The applicability of wedge splitting test for different purposes has been investigated by researcher. The method has proved to be reliable for the determination of fractures properties of ordinary concrete, at early age and later (Østergaard, 2003, Abdalla and Karihaloo, 2003, and Karihaloo *et al.*, 2004), for autoclaved aerated concrete (Trunk *et al.*, 1999), for polymer cement concrete (Harmuth, 1995), for ultra high strength concrete (Xiao *et al.*, 2004), for crushed limestone sand concrete (Kim *et al.*, 1997) for polypropylene fiber reinforced concrete (Elser *et al.*, 1996), and for steel fiber reinforced concrete (e.g. Löfgren, 2005). It has been also used to investigate other properties of concrete rather than fracture properties, e.g. determination of stress-crack opening relationships of interfaces between steel and concrete (Lundgren *et al.*, 2005, and Walter *et al.*, 2005), determination of size effect in the strength of cracked concrete structures (Karihaloo *et al.*, 2005), fracture of rock-concrete (Kishen *et al.*, 2004), numerical evaluation of cohesive fracture parameters (Que *et al.*, 2002), and stability of the crack propagation associated with the fracture energy (Harmuth, 1995). The WST method has been used by a few researchers to investigate the fatigue behavior of concrete, and its applicability for dynamic loading is not approved yet.

1.2 Aim, Scope and Limitations

The main aim of this research is to evaluate the possibility of using wedge splitting test method as a fatigue test to understand the fatigue behaviour of types of concrete, i.e. (1) plain concrete, (2) steel fiber reinforced concrete, and (3) synthetic fiber reinforced concrete.

The worked was limited by following considerations:

- Different types of fatigue load were not studied; a low cycle fatigue load has been applied.
- Size effect of wedge splitting specimens with different dimensions was not considered.
- One mix composition for each concrete type was tested, so the effects of different mix composition and also fiber volume fraction were excluded.

1.3 Scientific Approach

The aim of this project has been studied experimentally and numerically. In the experimental part, some tests were carried out using a WST specimen under a monatomic and cyclic loading. In the numerical part, two inverse analyses were conducted by using a Matlab® program developed at DTU by Østergaard (2003) based on the crack hinged model and FE analysis by commercial available program package Diana under similar loading conditions as the experimental part. Through numerical analysis, bi-linear σ-w relationship and energy dissipation were determined. A systematic approach for material testing based on fracture mechanics presented by Löfgren (2005), which covers material testing, inverse analysis, and adjustment of the σ-w relationship for fiber efficiency were applied.

1.4 Original Features

The study presented in this thesis is an investigation of fatigue behaviour of plain and fiber reinforced concrete using wedge splitting test method. By the result of this study, it has been proved that inclusion of steel and synthetic fibers in concrete affect the shape of the σ-w relationship remarkably and increases the fracture energy. It also has been shown that the wedge splitting method is able to characterize the fatigue behaviour of concrete subjected to low cycle fatigue loading. Right the way through the wok, inverse analysis using Matlab® program developed at DTU by Østergaard (2003) and finite element program package Diana have been apply to experimental data in order to estimate the *σ-w* relationships of tested concretes.

Based on the experimental data, the F_{sp}-*CMOD* curve was divided into different cycles of loading and unloading and inverse analysis using Matlab® program was conducted for loading part of each cycle in order to investigate the applicability of inverse analysis for each loading part of a cyclic test. Moreover, estimation of the *σ-w* relationship for a cyclic test, made it possible to calculate the modulus of elasticity and consequently the stiffness degradation after specific cycles.

1.5 Outline

This report, in 9 chapters, is intended to provide an overview on the fracture mechanics of concrete, fatigue behavior of concrete, fiber reinforced concrete, wedge splitting test method, and present results of experimental and numerical investigations on the fatigue behavior of concrete by the wedge splitting test method.

In *chapter 2*, basic theory and special features of fracture mechanics applicable to concrete structures are presented. After a description of the size effect, a short historical overview of fracture mechanics development e.g. LEFM and NLFM is given, and two crack models, 'Fictitious Crack Model' and 'Crack Band Model', are discussed.

Chapter 3 provides an introduction of the fatigue mechanism, fatigue strength, and parameters which influence the fatigue behaviour of concrete.

Chapter 4 is written so that the reader may gain an overview of the property enhancements of steel fiber reinforced concrete and fracture and fatigue behaviour of fiber reinforced concrete.

In *chapter 5*, a description of the test method and an approach to determine the fracture energy and the *σ-w* relationship is provided. At the end, applications of WST for different purposes are described.

Chapter 6 provides the experimental part of this study including concrete mixture of the tested concrete composites, tests set-up, and experimental results for monotonic loading and cyclic loading, interpreted by inverse analysis. The result of numerical investigations and comparison between numerical and experimental results are not included in this chapter.

In *chapter 7*, the properties and procedures of the FE model are presented and the FEA results are compared with the experimental results based on the F_{sp}-*CMOD*, *σ-w*, and G_{f}-*CMOD* relationships.

Chapter 8 presents the summery and general conclusions together witth suggestions for further research.

2 FRACTURE MECHANICS OF CONCRETE

2.1 Introduction

Failure of concrete structures basically involves stable growth of large cracking zones and the formation of large fracture zones before the maximum load is reached. Although the basic knowledge of fracture mechanics theory has been available since the middle of 20^{th} century, design of concrete structures is not yet based on fracture mechanics. This is partly due to the fact that the form of fracture mechanics which was available until recently was applicable only to homogeneous brittle materials such as glass, or to homogeneous brittle-ductile materials such as metals. However, it is also due to the fact that Non-Linear Fracture Mechanics (NLFM) is not easily implemented into design codes. On the other hand, for concrete structures, strain-softening due to distributed cracking, localization of micro cracks into macro cracks prior to failure, and bridging stresses at the fracture front must be taken into account. A form of fracture mechanics that can be applied to such structures and failure processes has been developed only during the last couple of decades.

Fracture mechanics, in a broad sense, is a failure theory which (1) uses energy criteria, possibly in conjunction with strength criteria, and (2) takes into account crack propagation through the structure. There are some compelling reasons for applying fracture mechanics for the design of concrete structures, such as: need for an energy criteria; the lack of a yield plateau; consideration of energy absorption; but the most important reason is the size effect observed for concrete structures. Application of fracture mechanics is highly linked to the size of the concrete structures and the fracture model used for analysis. According to Brühwiler (1989), the applicability of Linear Elastic Fracture Mechanics (LEFM) is limited to analyse the bottom part of large gravity dams. Whereas, Non-Linear Fracture Mechanics (NLFM) should be applied for fracture mechanics analysis of arch/buttress dams and the top part of gravity dams. Consequently, all concrete structures, which dimensions are smaller than dams, are expected to fall into the range of NLFM.

Concrete is a composite material, consisting of hardened cement paste, aggregate, water, and pores, but the observed behaviour of concrete cannot be linked directly with the structure of hardened cement paste. In order to apply existing knowledge of fracture mechanics to concrete, Wittmann (1980) proposed three different levels of concrete modelling so-called the 3L-approach as follows:

1. MicroLevel: on this level, concrete consist of silicate calcium hydrate (C-S-H) layers with primary and secondary bonds. The water absorbed by these layers plays an important role also. This level is not suited for fracture mechanics applications.

2. Meso-Level: this level considers the composite nature of concrete and distinguishes between hardened cement paste, aggregate, and a bond layer between these two constituents. If the properties of the three components are known then LEFM can be applied by numerical approaches, however this is not the level of practical application.

3. Macro-Level: homogeneous isotropic material properties are assumed for concrete at this level, and it suits purpose of applying LEFM best.

Surveys of concrete fracture mechanics have been prepared by various committees (see e.g. Wittmann, 1983, Elfgren, 1989, ACI 446.1R, 1991, Karihaloo, 1995), but to be able to interpret and explain the result of this project, basic theory and special features of fracture mechanics applicable to concrete structures are presented in this chapter. After a description of the size effect in the following section a short historical overview of fracture mechanics' development e.g. LEFM and NLFM will be given, and two crack models, 'Fictitious Crack Model' and 'Crack Band Model', will be discussed.

2.2 Size Effect

The most significant implication of the quasi-brittle behaviour of concrete structures is the observed structural size effect, which implies that most results of concrete fracture experiments cannot be uniquely described by the common used strength of material approach. On the other hand, LEFM considers the size effect but overestimates the load bearing capacity of usual dimensions. Moreover, adjacent to the fracture surface, a relative large microcracking zone exist, called the fracture process zone, in which the material behaves nonlinearly; while LEFM requires this zone to be small. Therefore, there exists a gradual transition from the strength of material criterion to LEFM that can be modelled by NLFM approach. In this transition range, the size of the fracture process zone or the discontinuous microcracking ahead of a stress-free crack in the concrete specimen is large compared to the structural size; see Shah (1991).

The size effect is defined through a comparison of geometrically similar structures of different sizes, and is conveniently characterized in terms of the nominal stress, σ_N, at the maximum (ultimate) load, P_u. When the σ_N–values for geometrically similar structures of different sizes are the same, it indicates that there is no size effect. A dependence of σ_N on the structures size (dimension) is called the size effect.

The nominal stress dose not need to represent any actual stress in the structure but may be defined simply as:

$$\sigma_N = P_u / bd \qquad \text{When the similarity is two-dimensional} \qquad (2.1)$$

$$\sigma_N = P_u / d^2 \qquad \text{When the similarity is three-dimensional} \qquad (2.2)$$

Where, b is thickness of the two-dimensional structure,

d is the characteristic dimension of the structure, which may be chosen as any dimension, e.g., the depth of the beam, or its span, since only the relative values of σ_N matter.

Based on the classical theories, such as elastic analysis with allowable stress, plastic limit analysis, as well as any other theories which use some types of strength limit or failure criterion in terms of stresses (e.g. viscoelasticity, viscoplasticity), σ_N is constant, that is, independent of the structure size. This may be illustrated, for instance, by considering the elastic and plastic relations for the strength of beams in bending, shear, and torsion[1]. It is seen that these relations are of the same form except for a factor. Thus, if log σ_N is plotted versus log d, the failure states according to a strength or yield criterion are always given by a horizontal line (dashed line in Figure 2.1). Therefore failures according to strength or yield criteria exhibit no size effect.

By contrast, failures governed by linear elastic fracture mechanics exhibit a rather strong size effect, which in Figure 2.1 is described by the inclined dashed line of slope $-1/2$. The reality for concrete structures is a transitional behaviour illustrated by the solid curve in Figure 2.1. The curve approaches the horizontal line for the strength criterion if the structure is very small. This size effect, which is generally ignored by current codes (with a few exceptions), should obviously be important for design.

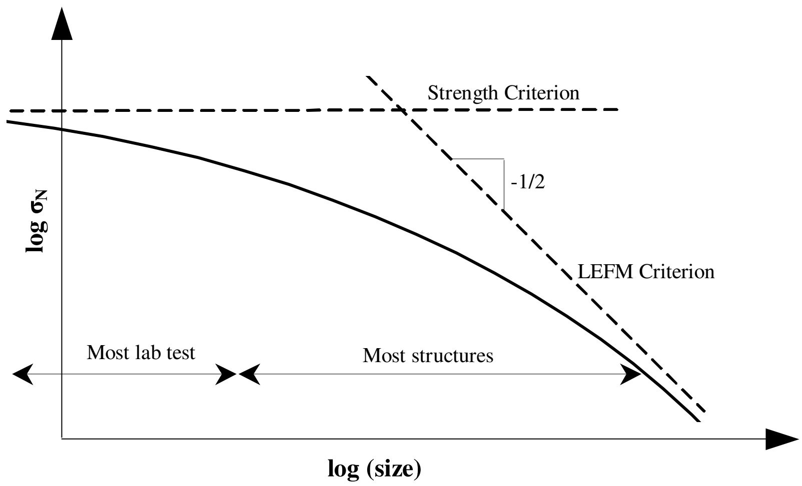

Figure 2.1 Fracture mechanics size effect for geometrically similar structures of different sizes based on LEFM and Strength of material criterion.

Another size effect which calls for the use of fracture mechanics is the effect of size on ductility. The ductility of a structure may be characterized by the deformation at which the structure fails under a given type of loading. For loading in which the load is controlled, structures fail (become unstable) at their maximum load, while structural elements that are loaded under displacement control (i.e. imposed displacement) fail in their post-peak, strain-softening range. In a plot of σ_N versus deflection, the failure

---

[1] Regarding to the definition $\sigma_N = P_u / bd$ for torsion; note that one may set $P_u = T_u / r$ where,
T_u is the ultimate torque, and
P_u is the force acting on an arm, r, such that r / H or r / a is constant for similar structures of different sizes; H is the cross section depth, a is the crack length).

point is characterized by a tangent (dashed line in Figure 2.2) of a certain constant slope, $-C_s$, where C_s is the stiffness of the device (see e.g. Baiant and Cedolin, 1990, Sec. 13.2). Geometrically equivalent structures of different sizes typically have yield curves of the type shown in Figure 2.2. As illustrated, as the size increases failure occurs closer to the peak. This effect is again generally predicted by fracture mechanics, due to the fact that in a larger structure more strain energy is available to drive the propagation of the failure zone. A decrease of ductility of a structure represents an increase in its brittleness.

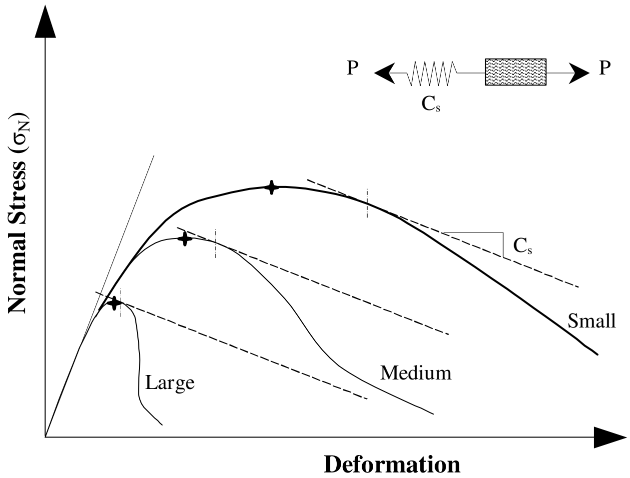

Figure 2.2 Load-deflection diagrams of geometrically similar structures of different sizes

2.3 Linear Elastic Fracture Mechanics

In linear elastic fracture mechanics (LEFM) it is assumed that all of the fracture processes occurs at the crack tip and the entire volume of the body remains elastic. With reference to this assumption, the crack propagation and structural failure are solved by methods of linear elasticity.

It is convenient to consider three elementary fracture modes, Modes I, II, and III[1]. These modes are used to define tensile and shear loading but not for compressive loading, since compression does not cause a stress intensity in a homogenous crack-free material such as concrete. The definition of different fracture modes is shown in Figure 2.3.

[1] For the definition of Mode 1, 2, and 3 see APPENDIX A: Standard Terminology Relating to Fatigue and Fracture Testing

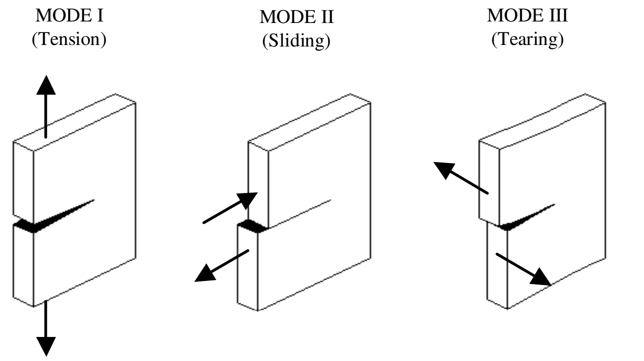

Figure 2.3 Definition of different fracture modes (Mode I: tension; Mode II: Sliding; Mode III: Tearing).

If a crack, in a homogenous isotropic material, is loaded by normal forces it will open in Mode I (so-called Opening mode). However, what usually happens is that mode I, and II occur simultaneously in a mixed mode which can be calculated for linear elastic materials. As far as concrete is concerned, there is very little information available about fracture mode III. Modes I and II are planar symmetric and anti-symmetric, while Mode III is three-dimensional. General fracture is a linear combination of these three modes.

Stress Singularity

The introduction of a crack into a linear elastic body produces stress concentrations near the crack tip. This may be illustrated by the perturbation of the trajectories of the maximum principal stress shown in Figure 2.4-(a). The stress field is singular at the crack tip, with all the nonzero stress components approaching infinity as the radial distance, r, from the crack tip tends to zero, see Figure 2.4-(b). In a sufficiently close neighbourhood of the sharp crack tip, the stress components σ_{ij} are the same regardless of the shape of the body and the manner of loading, and may be expressed as:

$$\sigma_{ij}^{I} = \frac{K_I}{\sqrt{2\pi r}} f_{ij}^{I}(\theta) \tag{2.3}$$

$$\sigma_{ij}^{II} = \frac{K_{II}}{\sqrt{2\pi r}} f_{ij}^{II}(\theta) \tag{2.4}$$

$$\sigma_{ij}^{III} = \frac{K_{III}}{\sqrt{2\pi r}} f_{ij}^{III}(\theta) \tag{2.5}$$

Where the subscripts I, II, and III refer to the elementary modes, θ is the polar angle, K_I, K_{II}, and K_{III} are parameters called the stress intensity factors, and functions f_{ij} are the same regardless of the body geometry and the manner of loading, for example;

$$f_{11}^{I}(\theta) = \cos\alpha(1-\sin\alpha\sin 3\alpha) \tag{2.6}$$

$$f_{22}^{I}(\theta) = \cos\alpha(1+\sin\alpha\sin 3\alpha) \tag{2.7}$$

$$f_{12}^{I}(\theta) = \cos a \sin 2\alpha \cos 3\alpha \tag{2.8}$$

Where $\alpha = \theta / 2$; see e.g. Knott (1973), Broek (1974), Owen and Fawkes (1983), Hellan (1984), and Kanninen and Popelar (1985).

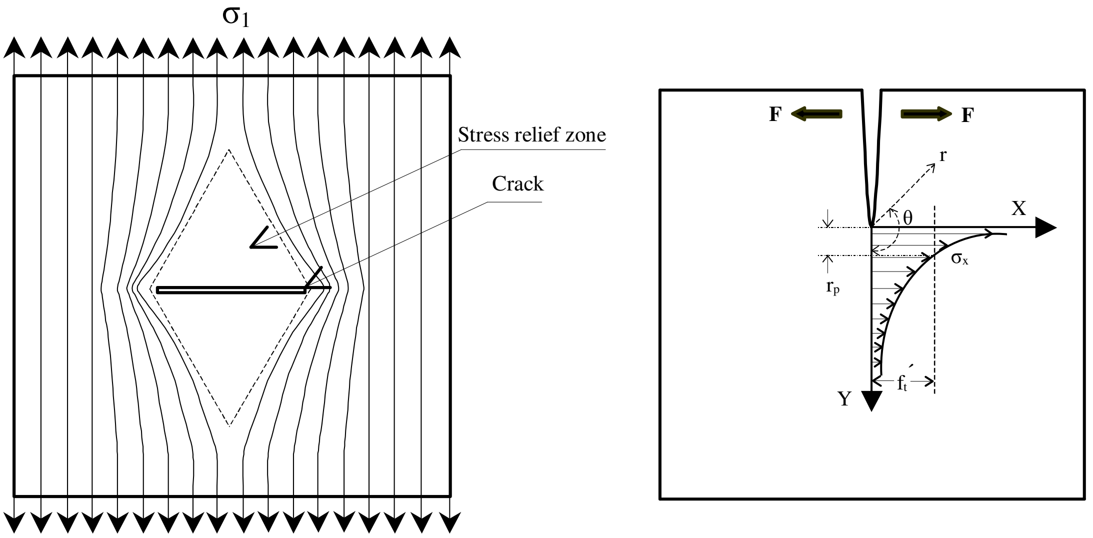

Figure 2.4 (a) Principal stress trajectories in a cracked specimen, (b) Stress distribution near crack tip

Energy criterion

According to the theory of elasticity, the stress near the crack tip approaches infinity independent of the load magnitude; investigated by Griffith (1921, 1924). He concluded that if linear elasticity is used then the failure condition cannot be stated by strength criteria but must be instead introduced by energy criteria. As the crack propagates, energy flows into the crack tip where it is dissipated by the fracture process. The energy flow is characterized by the energy release rate, which is expressed as:

$$Gb = -\frac{\partial \Pi(a)}{\partial a} \approx -\frac{1}{\Delta a}\left[\Pi(a+\frac{\Delta a}{2}) - \Pi(a-\frac{\Delta a}{2})\right] \tag{2.9}$$

Where $\Pi = U - W =$ Potential energy of the structure,

$U =$ Strain energy of the structure as a function of the crack length a,

$W =$ Work of loads,

a = Crack length

Equation (2.9) also gives a finite difference approximation which may be used to calculate G by the finite element method. Thus, the crack can be modelled as a line gap between adjacent elements, and the strain energy stored in the mesh can be calculated for the crack tip displaced by either $\frac{\Delta a}{2}$ or $-\frac{\Delta a}{2}$. Rather than using a line gap of crack, one may, for the sake of convenience, model the crack by assuming a band of elements to have zero stiffness.

According to Griffith, the condition of crack propagation is:

$G = G_F$; $\frac{\partial G}{\partial a} > 0 \Rightarrow$ The crack is unstable under load control (i.e., the structure fails);

$G = G_F$; $\frac{\partial G}{\partial a} < 0 \Rightarrow$ The crack can grow under load control on a stable manner;

$G < G_F$ $\Rightarrow$ The crack cannot propagate;

$G > G_F$ $\Rightarrow$ Equilibrium is impossible

Where; G is the fracture energy; from the physical viewpoint, it is recognized that while crack initiation depends on stress, the actual formation of cracks requires a certain energy, named the fracture energy, which represents the surface energy of a solid. Fracture energy has the dimension of j/m^2 (Nm/m^2) and introduces a basic material property.

The energy release rate for modes I, II, and III may be expressed on the basis of the stress intensity factors as follows:

$$G_I = K_I^2 / E', \qquad G_{II} = K_{II}^2 / E', \qquad G_{III} = K_{III}^2 / \mu \tag{2.10}$$

Where, μ Elastic shear modulus;

$E' = E$ Young's elastic modulus, for the case of plane stress;

$E' = E/(1-\nu^2)$ Young's elastic modulus, for the case of plane strain;

ν Poisson's ratio

For general loading, the total energy release rate is:

$$G = G_I + G_{II} + G_{III} \tag{2.11}$$

The stress intensity factors are proportional to the applied load, and may generally be expressed in the form:

$$K_I = \frac{P}{bd}\sqrt{\pi a} f(\alpha) = \frac{P}{bd}\sqrt{d}\varphi(\alpha), \qquad \alpha = a/d \tag{2.12}$$

Where, f is a certain non-dimensional function of the relative crack length α

d is characteristic structure dimension;

$\varphi(\alpha) = f(\alpha)\sqrt{\pi a}$ is another non-dimensional function.

For various simple geometries of notched fracture specimens, accurate expression for the function f is available in textbooks and handbooks (see e.g. Tada et al., 1985, and Murakami, 1987). For other geometries, the function f can always be calculated by linear elastic analysis; e.g., through a finite element program. For the special case of a single line crack of length a in an infinite solid subjected at infinity to nominal stress σ_N in the direction normal to the crack plane, one has $f(\alpha) = 1$. Equation (2.12) shows that, for geometrically similar structures of different sizes, the stress intensity factor is proportional to the square root of the size, and the energy release rate is proportional to the size of the structure.

Instead of the condition of crack propagation stated by Griffith, the condition of Mode I crack propagation (critical state) can be expressed in terms of the stress intensity factor as:

$$K_I = K_{Ic} \tag{2.13}$$

Where, $K_{Ic} = G_F E'$ is the critical value of K_I which is also called fracture toughness and represents a material property.

If Equation (2.13) is substituted into Equation (2.12), the nominal stress at failure (critical state) is obtained as:

$$\sigma_N = \frac{K_{IC}}{\sqrt{\pi a} f(\alpha)} = \frac{K_{IC}}{\sqrt{d}\varphi(\alpha)} \tag{2.14}$$

It may be noted that, according to Equation (2.14),

$$\log \sigma_N = -\frac{1}{2}\log d + const. \tag{2.15}$$

This relation illustrates that the size effect plot according to LEFM is an inclined straight line of slope $-\frac{1}{2}$; see Figure 2.1.

Limits of Applicability

In reality, the fracture process cannot take place at a point. The fracture process zone must have some finite size. According to Irwin (1958) a crude estimate of the length r_f of the fracture process zone may be obtained by setting the transverse normal stress in equations (2.3), (2.4), and (2.5) to be equal to the tensile strength f_t' ; this yields:

$$r_f = \frac{1}{2\pi}\frac{K_{IC}^2}{f_t'^2} = \frac{l_0}{2\pi}, \qquad l_p = \frac{K_{IC}^2}{f_t'^2} = \frac{E'G_F}{f_t'^2} \tag{2.16}$$

Note that this length is expressed only in terms of material properties, and may therefore be considered as a material property too. An alternative estimate of the size of the fracture process zone of concrete can be based on the maximum aggregate size d_a. Bažant and Oh (1983) concluded that the length and effective width of the fracture process zone of concrete in three-point bend specimens are roughly $12d_a$ and $3d_a$, respectively. Values of l_p for typical cementitious materials are compared in Table 2.1 with those of glass.

Table 2.1 Typical length of fracture process zone; reported by Karihaloo (1995)

Material	l_p**, mm**	**Reference**
Glass	10-6	Bache (1986)
Cement paste densified by silica fume	1	Bache (1986)
Hardened cement past	5 – 15	Hillerborg (1983)
Mortar	100 – 200	Hillerborg (1983)
High strength concrete (50 – 100 MPa)	150 – 300	Hilsdorf & Brameshuber (1991)
Normal concrete	200 – 500	Hillerborg (1983)
Dam concrete ($d_a = 38mm$)	700	Brühwiler et al. (1991)

Linear elastic fracture mechanics is applicable when r_f is much smaller than the cross section dimension of the structure. This condition is not satisfied for most concrete structures, with the possible exception for some very large structures such as concrete dams. However, a more precise criterion for the applicability of linear elastic fracture mechanics, which also takes into account the structure shape and the manner of loading, can be given in terms of the so-called brittleness number, β, but discussion about that is not in the scope of present report; for more explanation see ACI 446.1R

2.4 Non-linear Fracture Mechanics

The main reason for applying Non-Linear Fracture Mechanics (NLFM) to concrete structures is the development of a relatively large fracture process zone which undergoes progressive softening damage due to microcracking. This microcracking reduces the flux of energy that can be released into the crack tip; and on the other hand it increases the combined surface area of cracking, and thus enhances the energy absorption capability of the fracture zone; see 446.1R-91 (2003)

The fracture process zone is defined as the total region, in front of or in the wake of a traction-free macrocrack, in which the material undergoes strain softening; i.e., the stress normal to the crack plane decreases with increasing strain. It may even be surrounded by a zone where the material response is nonlinear because of microcracking but it is not yet softening. Due to the microcracking effect, the material in the fracture process zone progressively softens. This has been illustrated in Figure 2.5-(a) for the case of a notched specimen subjected to a tensile load. The pre-peak and post-peak nonlinearity (AB and BC) in Figure 2.5-(a) correspond to microcracking and crack coalescence in the fracture process zone and the load keeps decreasing with increasing strain in the strain softening diagram (CD). The post-peak behaviour is a result of aggregate bridging[1] caused by aggregate interlock and other frictional effects. In fact, the pre-peak nonlinearity does not have any significant influence on passing from LEFM to NLFM for concrete as a quasi-brittle material; see 446.1R-91 (2003). In fact it is the strain-softening response, the post-peak nonlinearity, which causes reduction of energy flux released into the crack tip and increases the fracture surface and thereby the energy dissipation.

[1] The bridging stress, referred to as crack bridging, is mainly composed of aggregate bridging in plain concrete and both of aggregate bridging and fiber bridging in fiber reinforced concrete (FRC). The crack bridging in these materials is achieved by the bond defined as the shearing stress along the interfaces between fibers or aggregate and surrounding matrix. The structural performance of concrete and FRC is strongly influenced by the crack bridging which, in turn, depends on the bond behaviour of fiber-matrix and aggregate-matrix interfaces.

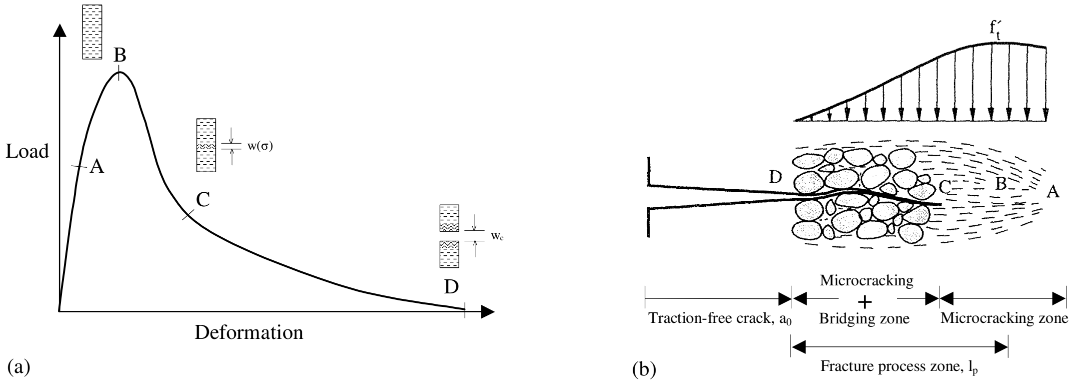

Figure 2.5 Typical tensile load-deformation response of a pre-cracked concrete specimen (a), and the fracture process zone ahead of the real traction-free crack (b)[1] *(from Karihaloo, 1995).*

From a purely micro-mechanical point of view, the introduction of a macrocrack into a concrete specimen initiates microcracks at nearby pre-existent flaws and second phase particles (i.e. sand and gravel); see Figure 2.6-(a). The microcracks, next to the aggregate-cement matrix, cause the second phase particles to debond from the surrounding cement paste; see Figure 2.6-(b). The flaws, such as microcracks and pores, are present in abundance in normal concrete even prior to the introduction of a macrocrack or the application of a load. Under external loading microcracks can coalesce with one another or with debond cracks to form cracks of larger size which may even join up with the macrocrack, if there are no obstacles such as other particles and/or pores to prevent this from happening; see Figure 2.6-(c). The second phase particles in the cement matrix arrest the progress of a growing crack which therefore requires additional external work for sustained growth. The crack may choose the path which requires least energy and thus may be forced to grow around a particle[2] leaving the latter to bridge its faces. Bridged crack faces may give rise to numerous crack branches; see Figure 2.6-(d). The crack bridging is the primary reason for extended tail region of the strain-softening diagram (part CD in Figure 2.6); see Karihaloo (1995).

---

[1] Note that fracture process zone extends only over the strain-softening region (BCD) and it may be surrounded by a nonlinear (but not a softening) region, e.g. the region AB.

[2] This behaviour is true in the case of non-impact loading when the crack has the chance to find the path with least energy

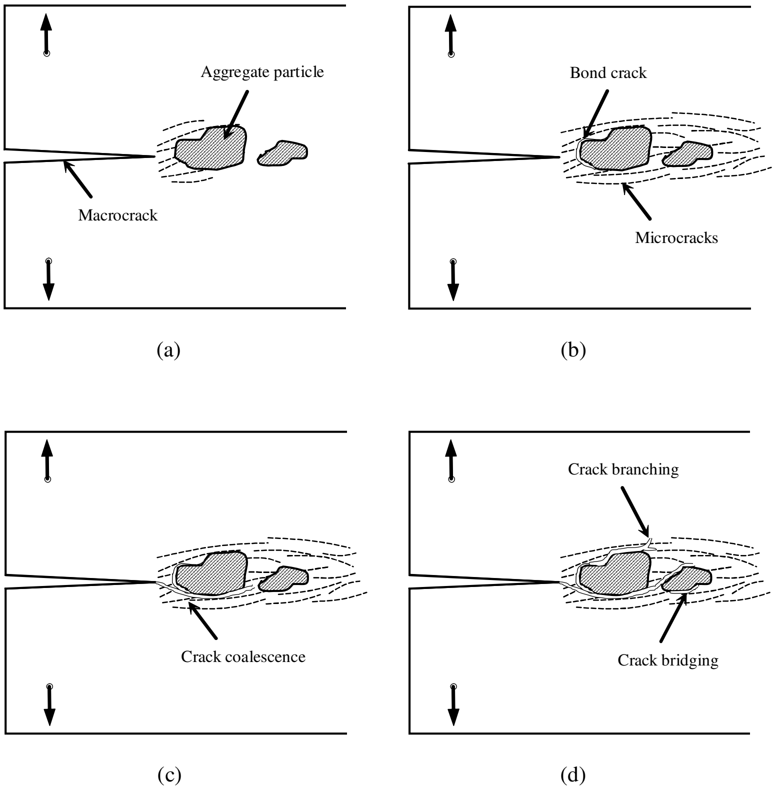

Figure 2.6 Schematic representation of the development of fracture zone (a) microcracking at aggregate due to the presence of macrocrack, (b) debonding and microcracking, (c) coalescence of debond crack with macrocrack, and microcracking, (d) crack bridging, debonding, crack branching and microcracking, from Karihaloo (1995).

2.5 Material Model Classification

Various models have been developed to describe the fracture process zone, and examples of such are the Fictitious Crack model and the Crack Band theory, proposed by Hillerborg et al. (1976) and Bažant et al. (1983), respectively. Both models are based on the tensile strength, f_t', the specific fracture energy, G_F, and the strain-softening diagram of the material. However, before presenting these models, it is wise to realize the conceptual framework of concrete models based on fracture mechanics. In this section, a classification proposed by Elices and Planas (1989), based on essential features that any fracture model for concrete should take into account, is described. It is hoped that this classification will provide a deeper understanding of the models that will be introduced, later on, in this chapter.

As stated before, based on Wittmann's classification, three different levels are defined for concrete. At the microlevel, the structure of hardened cement paste is treated. At the meso-level, the main characteristics are big pores, pre-existing cracks and inclusions. At macro-level, concrete is treated as a continuum and homogeneous medium. This section deals only with models at the macro-level and is restricted to physical models. Models at micro and meso-level would make this introduction lengthy and are not considered at this stage.

The propagation of a single crack, modelled as a single surface discontinuity, is the main concern of fracture mechanics. This case was basically investigated by means of a fracture criterion added to the classical field equations of continuum mechanics. Actually this is the sharp conceptual and computational distinction between fracture methods, when the dominant collapse mode is crack propagation, and methods derived from limit analysis, which apply when collapse is dominated by yielding. As concrete is concerned, this classification is not helpful any longer since for most practical situation the actual structural behaviour is not dominated by these extreme modes, therefore new fracture models were developed to gain a better description of the actual behaviour. Such models, called progressive fracture models, permit a description of a smooth transition from a continuous medium to the discontinuous (fully fracture) one and they rely on two basic concepts: *Strain Softening* and *Strain localization*.

According to Bažant, Lin, and Pijaudier (1987) the term 'localization limiter' is interpreted as a mathematical restriction forcing the strain-softening region to have a certain minimum finite size, while one may extend this concept to conditions where mathematical restrictions force the dissipation energy within strain softening region to attain a non-vanishing value. This interpretation enables different models such as Bažant's Crack Band Model and Hillerborg's Fictitious Crack Model, based on different mathematical treatment for hardening and softening regimes. For instance, in the Crack Band Model stress-strain variables are used on both hardening and softening parts, while in the Fictitious Crack Model stress-strain variables on hardening and stress-displacement variables on softening must be used.

The fundamental idea of material model classification is that softening of the material occurs inside a fracture process zone, whose shape and size is specified by a localization criterion, while the material outside the fracture process zone, the bulk material, unloads. Thus a complete fracture model must be able to specify: material behaviour outside (bulk material) and inside of the fracture process zone as well as the localization criterion which define the shape and size of fracture process zone. A classification, according to Elices and Planas (1989), may then be set up by specifying a three-alphabet code, (ABC) where:

A is a single code for bulk material behaviour,

B is a single code for material behaviour inside the fracture process zone, and

C is a single code for the localization criterion.

For each code, three different alternatives are taken into account. This classification, sketched in Figure 2.7, and explained as follows.

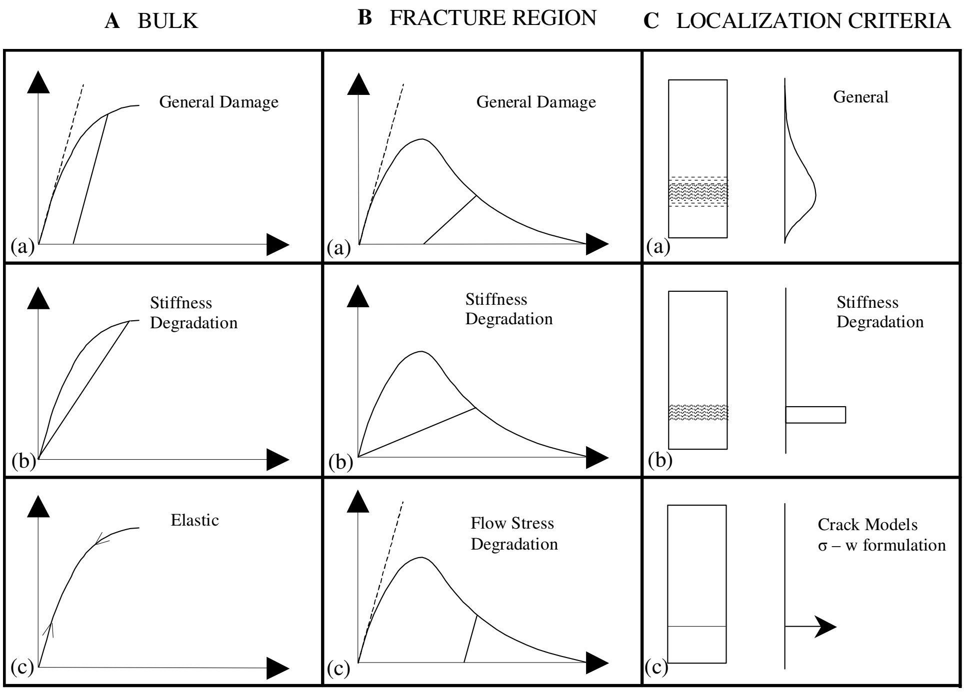

Figure 2.7 Material model classification, proposed by Elices and Planas (1989)

Bulk material behaviour (as presented in Figure 2.7A-a): in General Damage, both energy dissipation and strain irreversibility, including plastic softening (flow-stress degradation without stiffness loss), are considered. In some softening models, it unloads back to the origin. Such a process leads to a sort of stiffness loss so-called stiffness degradation; see Figure 2.7A-b. A set of particular but widely used models assumes no energy dissipation for bulk material named Elastic behaviour; see Figure 2.7A-c. Since after strain localization in the fracture process zone, unloading occurs in the bulk material and a statement of unloading behaviour of the bulk material is always needed.

Material behaviour inside the fracture process zone: three different behaviours are distinguished for material behaviour inside the fracture process zone such as: General Damage considering plastic-softening and stiffness loss, Stiffness degradation allowing for secant unloading, and Flow Stress Degradation taking into account the elastic unloading; see Figure 2.7B-a, b, and c.

Localization criterion: In general, strains are localized in a gradual way; see Figure 2.7C-a, however difficulties in implementing this general hypothesis lead to more simple criteria such as localization within a band or along a line crack called the Band Model and the Crack Model, respectively; see Figure 2.7C-b and c.

For instance, the Crack Band Model developed by Bažant (1976) may be falls into (c,x[1],b) category, while his Microplane Model should be classified as (a,a,b); the Fictitious Crack Model proposed by Hillerborg (1983) is usually considered as a (c,x,c) model.

---

[1] x indicates unspecified behaviour.

2.6 Fictitious Crack Model

The first nonlinear theory of fracture mechanics for concrete - called the Fictitious Crack Model – was proposed by Hillerborg et al. (1976); the model used a similar approach previously formulated for metals. Dugdale (1960) and Barenblatt (1959, 1962) proposed that a plastic (yielding cohesive) zone of a certain finite length must exist at the front of a crack; see Figure 2.8-(a). The length of this zone must be such that the stresses from the fracture process zone cancel the stress singularity caused at the top of the equivalent elastic crack by the applied load (i.e., $K_I = 0$). The crack opening at the beginning of the plastic zone, where the stress suddenly drops to zero, may be regarded as a material property which controls propagation; see Figure 2.8-(b).

For concrete, this type of model was proposed by Hillerborg, Modeer and Petersson (1976) under the name of the Fictitious Crack Model. The term "fictitious" refers to the fact that the portion of a crack which transmits tensile stress cannot be a continuous crack with full separation of the surfaces; the real crack ends at the point where the stress is reduced to zero; see Figure 2.9. Like the Dugdale and Barenblatt models, the Fictitious Crack Model assumes that the fracture process zone is of negligible thickness and the crack tip faces close smoothly. This smooth closure condition requires that K_I vanish at the top and thus determines the size of the process zone. This model however differs from both Dugdale and Barenblatt models based on its closing stress distribution and the size of fracture process zone (cohesive zone in Barenblatt models). The closing stress in the Fictitious Crack Model is not constant, i.e. it increases from a zero value at the tip of the pre-existing traction-free macrocrack to the full uniaxial tensile strength value of the material, f_t', at the tip of the fictitious crack and its distribution over the fracture process zone depends on the opening of the fictitious crack faces, w. On the other hand the size of fracture process zone is not small in comparison with the length of the pre-existing macrocrack.

In the Fictitious Crack Model, which has been widely applied in finite element analysis of concrete fracture, the material fracture properties are defined by the softening stress- displacement relation, $\sigma(w)$ [1]. The area under the curve represents the fracture energy of the material, i.e.:

$$G_F = \int_0^{w_c} \sigma(w)dw = \int_{f_t'}^{0} w(\sigma)d\sigma \qquad (2.17)$$

Where, f_t' is the uniaxial tensile strength limit of material; and

w_c is the critical crack opening displacement at which the stress is zero.

[1] $\sigma(w)$ is the stress in the direction normal to the crack.

According to the strain softening diagram it is concluded that the fracture of concrete cannot be described by a single material parameter, such as f_t', w_c, K_{Ic}, G_F, l_{ch} [1]. For this description it is now necessary to have at least two material parameters, while any combination of two independent parameters as (G_F , f_t'), (G_F , w_c), and etc. can be taken.

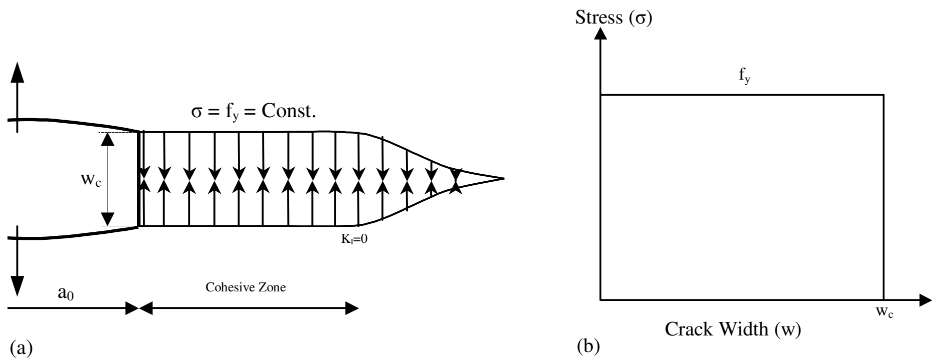

Dugdale and Barenblatt model, (1960)

Figure 2.8 Stress distributions in and near the fracture process zone in Dugdale and Barenblatt model, (a) Stresses are constant over the fracture process zone, (b) the material behaviour is presented by stress-strain diagram.

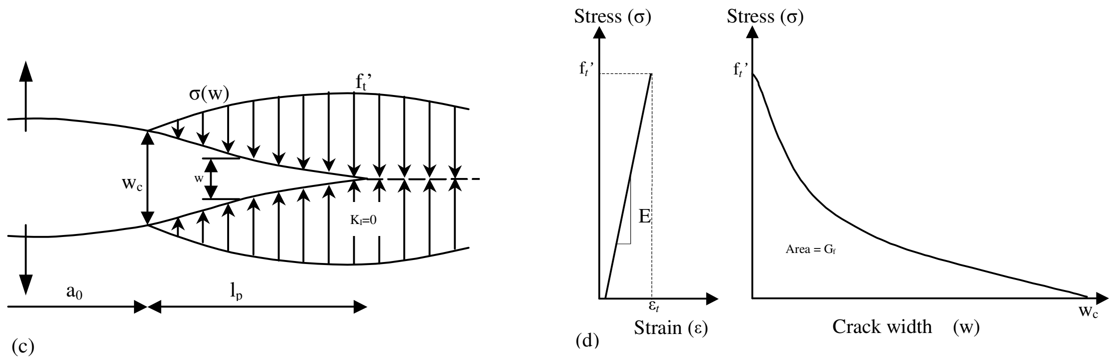

Fictitious Crack Model, Hillerborg (1976)

Figure 2.9 Stress distributions in and near the fracture process zone in the Fictitious Crack Model, (a) The stress distribution over the fracture process zone depends on the opening of the fictitious crack faces, w, (b) The hardening behaviour is presented by stress-strain diagram while the softening behaviour is presented by stress-displacement diagram.

---

[1] Called the characteristic length of the material and defined as $l_{ch} = E'G_F / f_t'^2$, the derived material parameter l_{ch} is nothing but the length of the fracture process zone l_0 introduced at Equation (2.16).

The Fictitious Crack Model has been applied successfully to describe fatigue fracture of plain and fiber reinforced concrete by different researchers, for example the ‘’prediction of crack width in steel FRC structures’’ by Stang et al. (1995). It will be discussed more in detail in chapters 3 and 4.

2.7 Crack-Band Model

Since cracks in concrete are not straight, and the microcracking zone in front of the continuous fracture is not likely to develop along a straight line, the behavior of the fracture process zone can equally be described by stress-strain relations with strain-softening, i.e. declining stress at increasing strain. However, this strain is related to the inelastic deformation, w, and fracture energy G_F, consequently the ultimate strain at complete rupture, ε_c, is related to w_c. This approach is quite convenient for computer programming since no separation of the nodes of two adjacent elements needs to be introduced and fracture is handled by adjustments of the incremental stiffness of finite elements, basically in the same way as any inelastic behavior. The basic idea of the Crack Band Model, proposed by Bažant (1976), is:

(1) to characterize the material behavior in the fracture process zone in a smeared manner through a strain-softening constitutive relation, and

(2) to impose a fixed width, h, of the front of the strain-softening zone (crack band), representing a material property.

The imposition of constant h is required in order to avoid spurious mesh sensitivity and achieve objectivity, assuring that the energy dissipation due to fracture per unit length (and unit width) is a constant, equal to the fracture energy of the material, G_F. The stress softening curve has been approximated by many simple functions such as linear or exponential. The fracture energy G_F is now:

$$G_F = h\int_0^{\varepsilon_c} \sigma_{yy}(\varepsilon)d\varepsilon \qquad (2.18)$$

Where; $\varepsilon_c = w_c / h$ corresponds to the critical crack opening displacement, w_c of the Fictitious Crack Model.

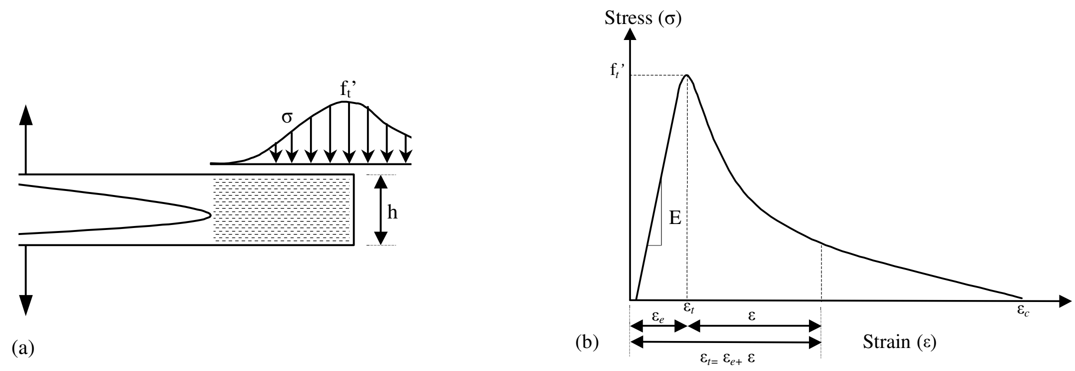

Crack Band Model, Bažant (1976)

Figure 2.10 *Stress distributions in and near the fracture process zone in the Crack Band Model, (a) The stress distribution over the fracture process; microcracking smeared over a band of width h, (b) the inelastic deformation in the fracture process zone is represented by an equivalent inelastic strain ε which is related to w and G_f of the Fictitious Crack Model.*

In the discussion above, no distinction was made between fracture energy, G_F, used in the Fictitious Crack Model and the Crack Band Model. It means that whenever $h \to 0$, two models will merge and the fully cracked state is obtained for $h \to 1$. However the fracture energy, G_F, used in the Crack Band Model is not determined experimentally in the same manner, as the G_F used in the Fictitious Crack Model.

3 FATIGUE BEHAVIOUR OF CONCRETE

3.1 Introduction

These days, concrete and steel are the two most commonly used structural materials. They sometimes complement one another, and sometimes compete with one another so that structures of a similar type and function can be built in either of these materials. And yet, the engineer often knows less about the concrete of which the structure is made than about the steel, especially when it comes to fatigue behaviour of concrete under cyclic loading.

The outstanding pioneering character in the experimental study of the strength of materials under repeated stress was born June 22. Wöhler's famous tests were made between the years 1852 and 1862 on ductile material such as metal. His machine is still preserved, and it is very similar to the machine used today for repeated stress testing - the rotating beam machine. In fact, the names ''Wöhler machine'' and ''Wöhler test'' are frequently used in connection with rotating-beam fatigue test. Wöhler passed away March 21, 1914, in the city of Hanover, a few months before his ninety-fifth birthday.

Some years later, Moore (1927) gathered and published the result of several research projects, related to fatigue behaviour of cement and concrete, and dedicated one chapter of his book, entitled '' The Fatigue of Metal'', to estimate the fatigue strength of concrete. These estimations were mostly based on extrapolation of the available test data, such as beam tests by Berry and compression test by Williams, assuming a general similarity of behaviour under test between concrete and metals.

In recent years, the interest to investigate fatigue strength of concrete has increased. First, because there is always a concern about the effect of repeated loads on concrete structures such as bridge slabs and crane beams. Second, since the introduction of prestressed concrete railroad ties and continuously reinforced concrete pavement, a demand for high performance concrete with assured fatigue strength was raised. Third, even if repeated loading dose not cause a fatigue failure, it may lead to inclined cracking in prestressed beam at lower than expected loads, or may cause cracking in component materials of a member that alters the static load carrying characteristic.

It is of importance to clearly distinguish between static, dynamic, fatigue, and impact loading. Actual static loading remains constant with time; however, a load which increases slowly is often called static loading. The maximum load capacity, under such conditions, is referred to as static strength. Dynamic loading varies with time in any arbitrary manner while fatigue and impact loadings are special cases of dynamic loading. A fatigue loading consists of a sequence of load repetitious that may cause a fatigue failure in several cycles.

The fatigue behaviour of concrete, reinforcing bars, and prestressing tendons has been described in some references, e.g. Holmen (1979), ACI 215R-74 (2003), and etc; however in this chapter just an introduction of the fatigue mechanism, fatigue strength, and parameters which influence the fatigue behaviour of concrete are reviewed. As already mentioned, concrete behaviour, in different aspects, are more complicated than steel; moreover, when it comes to fatigue behaviour, further complexity appears and, to some extent, disagreements can be found in scientific publications. On the other hand, due to the lack of a unified language of fatigue mechanisms in different literature, this complication has intensified. In order to avoid confusion in this report, ‘‘Standard Terminology Relating to Fatigue and Fracture Testing’’, ASTM (2001), has been utilized throughout to explain the fatigue behaviour of concrete and is provided in Appendix A[1].

3.2 Fatigue Mechanisms of Plain Concrete

Fatigue is the process of progressive localized permanent structural change occurring in a material subjected to conditions that produce fluctuating stresses and strains at some points and that may culminate in cracks or complete fracture after a sufficient number of fluctuations. These fluctuations may occur both in load and with time (frequency) as in the case of ‘’random vibration’’, see ASTM (2001). However, there are different hypotheses concerning the crack initiation and propagation, for instance Murdock and Kesler formulated the following hypothesis:

> The initiation of fatigue failure may reasonably be attributed to the progressive deterioration of the bond between the coarse aggregate and the binding matrix, together with an accompanying reduction of section of the specimen. The final failure of the specimen occurs by fracture of the matrix. The development of the cracks may be intensified if the modulus of elasticity of the coarse aggregate exceeds that of the binding matrix; see Murdock (1960).

Antrim developed the following hypothesis:

> Fatigue failure in plain concrete occurs because small cracks form and propagate in the cement paste and the resulting crack pattern weakens the section to the point where it cannot maintain the applied load. The development of this damaging cracks pattern depends primarily, if not entirely, on the water-cement ratio of the cement paste and the presence of shrinkage stresses in the cement paste; see Antrim (1976).

Test results, from different investigators, such as Holmen (1979), have proved both theories; thus, it may be concluded that fatigue behaviour of concrete is caused by the development of internal micro cracks, both at cement matrix-aggregate interface and in the cement matrix itself, see Holmen (1979).

As general, the initiation and propagation of fatigue failure is related to the bonding between aggregate and cement matrix. It has been shown that very fine bond cracks exist at the interface between aggregates, coarse or fine, and hydrated cement paste even prior to application of load. Such weak regions appear as a result of a difference in volume changes between the cement paste and the aggregate, i.e. due to the difference in stress-strain behaviour, in shrinkage performance, and in thermal and moisture movements. These bond cracks remain stable and do not grow under stress

[1] This terminology was issued under the jurisdiction of ASTM Committee E-8 on Fatigue and Fracture and contains definitions of terms specific to certain standards, Symbols, and abbreviations.

up to about 30 percent of the ultimate strength of the concrete; see Neville (2003). With increased load, these microcracks will grow and coalesce steady, as long as the aggregate bridging action is sufficient, and finally the formation of microcracks starts to localize in a narrow zone. Under fatigue loading, these microcracks undergo several cycles of crack opening and closing. These cycles will cause a progressive deterioration of the bond between aggregate and cement matrix. Therefore, the microcracks will grow and connect to each other and finally a dominant macrocrack is created. Consequently, due to the degradation of aggregate-cement matrix interface, the dominant fatigue crack propagates gradually until fatigue failure; see Zhang (1998).

Based on the description above, the propagation of fatigue damage of plain concrete might be summarized into the following stages; see M.K. Lee (2004):

I. Flaw initiation: formation of weak regions within concrete due to difference in volume changes between the aggregates and cement paste.

II. Microcracking: slow and progressive growth of the inherent flaws to a critical size.

III. Fatigue failure: when a sufficient number of unstable cracks has formed, a continuous or macrocrack will develop and eventually it leads to failure.

Overall, the fatigue life of concrete structures is the sum of the cycles needed for these three stages until reaching fatigue failure. The part of the fatigue life that are related to microcracking, is highly influenced by the microstructure of concrete matrix such as water/cement ratio, aggregates properties, and air content. The second part of the fatigue life, related to macrocracking, depends strongly on the bridging behaviour within the fracture zone, which is controlled by the bond degradation laws of aggregates and cement matrix interfaces during cyclic loading. Therefore, if these cyclic constitutive laws are known, it is possible to predict the fatigue crack propagation for a given structure and further estimate the fatigue life.

According to Hideyuki Horii (1992), three stages of fatigue crack growth has been observed experimentally, involving a decelerated stage, a steady state stage, and an accelerated stage towards the final fatigue failure. The development of these three stages of fatigue damage is schematically depicted in Figure 3.1. This curve is obtained by plotting the deformation, recorded during a fatigue test, versus the number of cycles undergone. The second stage makes up to 80% of the total curve, while the first and last stages make up to 10% of the total curve, respectively. The slope of the steady state stage is highly correlated with the fatigue life of the concrete.

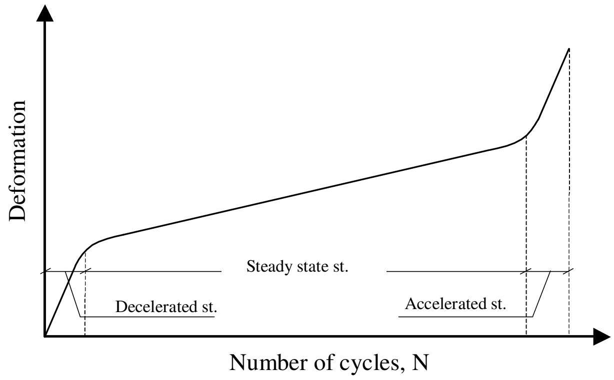

Figure 3.1 Schematic curve of the fatigue crack growth during a fatigue test, from M.K. Lee (2004)

According to Holmen (1979), Fatigue of concrete structures can be divided into six main categories: fatigue in compression, fatigue in flexure, fatigue in tension, fatigue in bond, fatigue in reinforced concrete, and fatigue in prestressed concrete. As in the case of static tests, different loading arrangements have been used in fatigue testing, including compression, tension and bending tests. The most common method of fatigue testing, by far, is via flexural tests. To a lesser extent, compressive fatigue tests have also been investigated. In recent years, there has been more interest in the fatigue characteristics of concrete in uni-axial tension, especially since the advent of nonlinear fracture mechanics in the analysis of concrete structures.

3.3 Fatigue Strength of Concrete

Fatigue strength is a value of stress that results in failure at *N* cycles as determined from a *S-N* curve. The *S-N* curve, referred to as the Wöhler curve or stress-fatigue life curve is a plot of stress against the number of cycles to failure. The stress can be the maximum stress ratio, S_{max}/S_{static}, minimum stress ratio, S_{min}/S_{static}, stress range, $\Delta S= S_{max}- S_{min}$, or stress level, $R=S_{min}/S_{max}$. The curve indicates the *S-N* relationship for a specified probability of survival. For *N*, a logarithmic scale is commonly used, while for *S*, either a logarithmic or a linear scale is used, see Holmen (1979) and ASTM (2001). An example of a *S-N* curve is presented in Figure 3.2.

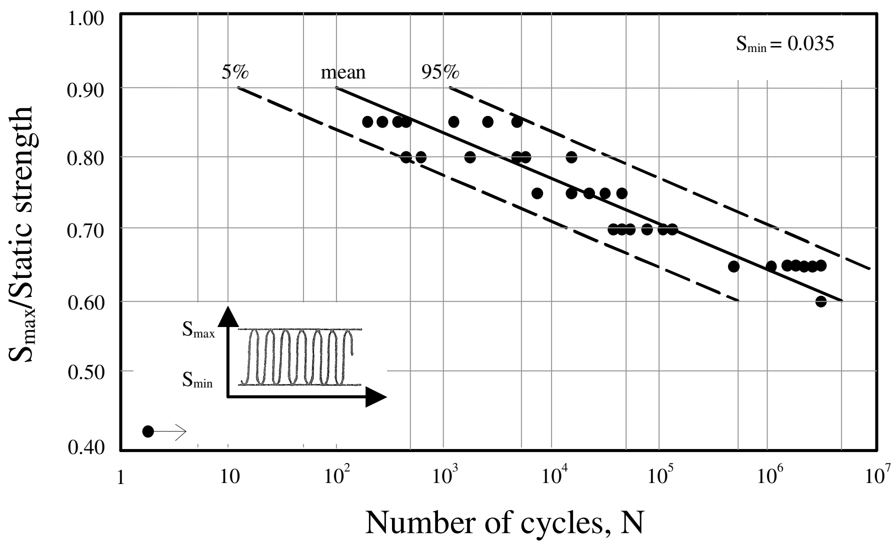

Figure 3.2 Typical S-N relationship for concrete in compression, from Holmen (1979)

The *S-N* curves are usually plotted for a given constant minimum stress level ($S_{min}=constant$) or for a constant stress level ($S_{min}/S_{max}=constant$). Fatigue tests usually exhibit a large scatter and it is necessary to test a number of specimens at several stress levels in order to establish the *S-N* curve of a particular concrete. By applying probabilistic procedures, a relationship between probability of failure and number of cycles until failure can be obtain as indicated in Figure 3.2. For instance, fatigue strength of concrete for a life of ten million cycles (for compression, tension, or flexure) is roughly about *60* percent of the static strength.

Fatigue strength depends on the maximum as well as on the minimum stress level of a specific cycle. This effect is represented by a Goodman-diagram and a Smith-diagram based on a constant minimum stress level, and constant mean stress level, $S_m=(S_{min}+S_{max})/2$, respectively, see Figure 3.3. From the Goodman-diagram, it appears that an increase of the minimum stress level results in increased fatigue strength for a given number of cycles, see Holmen (1979).

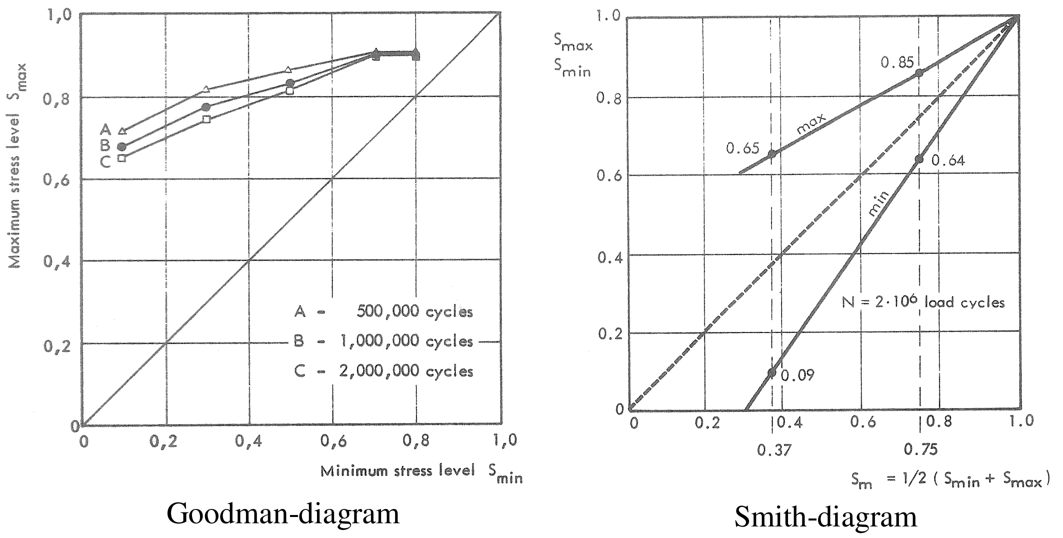

Figure 3.3 Goodman-Diagram, Based on constant minimum stress level; Smith-diagram, based on Constant mean stress level, from Holmen (1979)

In contrast to fatigue of steel, no fatigue limit of plain concrete has been reported. This means that no stress level is known below which the fatigue life would be infinite, see Holmen (1979). This has been also verified for concrete with normal strength, see Svensk-Byggtjänst (2000).

In general, parameters such as mixture, moisture content, and temperature of concrete as well as stress level, loading configurations and boundary conditions will influence the fatigue performance of the concrete specimen. However, the quantitative and qualitative nature of these parameters on the fatigue performance of concrete is not yet agreed upon in the literature.

3.4 Material-dependent Effects on Fatigue Behaviour of Concrete

Variables such as water-cement ratio, cement content, air content, curing condition, and age at loading does not seem to influence the fatigue strength when the fatigue strength is expressed in terms of static strength. These experienced is based on normal concrete strength, i.e. static strength up to 60 MPa, see Holmen (1979).

High strength, lightweight-aggregate concrete has been investigated and appears to have higher fatigue strength than one produced with normal aggregates under the same maximum load amplitude. This behaviour is interpreted by the fact that cement paste and lightweight aggregate have almost the same stiffness and the stresses are thus distributed more uniformly and local stress peaks are prevented. Adding fly ash as a pozzolane may lead to reduced fatigue strength, while silica powder has the opposite effect; see Taylor and Tait (1999). Obviously, the fatigue strength decreases with increasing air content because it decreases the static strength of concrete. High strength concrete specimens stored and tested in air have shown longer working life than corresponding specimens stored in water; see Svensk Byggtjänst (2000).

It is of interest to investigate the fatigue behaviour of high strength concrete subjected to fatigue loading because of its increased use in structures such as long-span bridges, offshore structures, and reinforced concrete pavements. The total strain at failure has been found to be approximately the same for fatigue loading as for monotonic loading. It is reasonable too say that the fatigue strain at failure decreases with increased concrete strength. The rate of strain increment, in contrast to the fatigue strain, increases with the strength of concrete. Therefore, the fatigue life should decrease with increased concrete strength. As a result, it can be concluded that high strength concrete is more brittle than low strength concrete under fatigue loading, see Holmen (1979).

Test results indicate that different moisture conditions affect the fatigue strength in the same proportion as the static strength. This can also be concluded from flexural tests of plain concrete beams tested under four different conditions: saturated, oven-dried then soaked in water, surface-dry and oven dried. With the fatigue strength expressed in terms of static strength, no significant effect of moisture conditions seems to be present, see Holmen (1979). According to Svensk Byggtjänst (2000), both static and fatigue strength of concrete decrease with increased moisture content. Decreasing temperatures improve the static and fatigue strength at least at a very low temperature.

3.5 Loading-dependent Effects on Fatigue Behaviour of Concrete

Fatigue loading usually falls into two categories, i.e. low-cycle and high-cycle loading. Low-cycle loading involves the application of a few load cycles at high stress levels. On the other hand, high-cycle loading is characterized by a large number of cycles at lower stress levels. M.K. Lee (2004) presented a wider range of fatigue load spectrum with the inclusion of super-high cycle loading. Table 3.1 summarizes the different classes of fatigue loading.

Table 3.1 Class of fatigue load; from M.K. Lee (2004)

Low-cycle fatigue			High-cycle fatigue				Super-high-cycle fatigue		
1	10^1	10^2	10^3	10^4	10^5	10^6	10^7	10^8	10^9
Structures subjected to earthquake			Airport pavements and bridges		Highway and railway bridges, highway pavements		Mass rapid transit structures		Sea structures

The fatigue strength of concrete, defined as a fraction of the static strength that it can support repeatedly for a given number of cycles, is influenced by the range of loading, the rate of loading, load history, eccentricity of loading, and lateral loading. These effects are described briefly as follows.

Range of Loading

The effect of range of loading may be illustrated by *S-N* curves shown in Figure 3.4. These curves are the result of tests (see ACI 215R-74 (2003)) on 6×6 in. (152×152 mm) plain concrete beams loaded at the three-point-bending test of a 60 in. (1.52 m) span. In the figure, the ratio of the maximum flexural tensile stress, $S_{\max}$, and the static strength, f_r, versus the number of cycles to failure, N, is shown. Curve *a* and *c* were obtained from tests with two stress levels, equal to 75 and 15 percent, respectively. It indicates that a decrease of the stress level results in increased fatigue strength for a given number of cycles. When the minimum and maximum loads are equal, the strength of the specimen corresponds to the static strength of concrete, determined under otherwise similar conditions; see ACI 215R-74 (2003).

As already stated, the results of fatigue tests usually exhibit considerably larger scatter than static tests. This inherent statistical nature of fatigue test results can best be accounted for by applying probabilistic procedures, i.e. for a given maximum load, minimum load, and number of cycles, the probability of failure can be estimated from the test results. By repeating this for several numbers of cycles, a relationship between probability of failure and number of cycles until failure at a given level of maximum load can be obtained. From such relationships, *S-N* curves for various probabilities of failure, so called *S-N* curve for *p %* survival[1], can be plotted. Curves *a* and *c* in Figure 3.4 are averages, representing *50* percent probability of failure. Curve *d* represents *5* percent probability of failure, while Curve *b* corresponds to an *80* percent chance of failure. The usual fatigue curve is that shown for a probability of failure of *50* percent[2]. However, design may be based on a lower probability of failure.

---

[1] See Appendix A, definition of the term: *S-N* curve for *p %* survival.

[2] See Appendix A, discussion-2 made in the definition of the term: *S-N* curve for *50 %* survival.

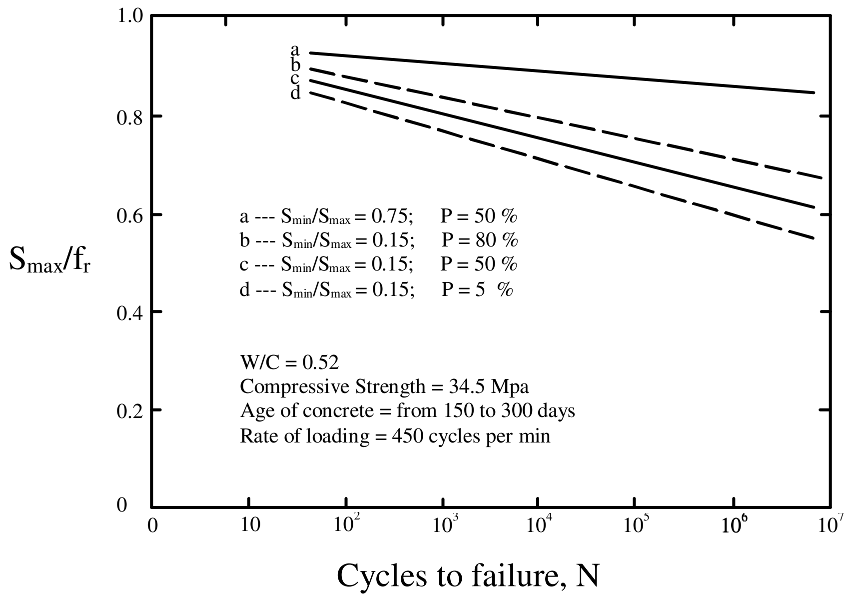

Figure 3.4 Fatigue strength of plain concrete beam (P is Probability of failure so-called survival); from ACI 215R-74 (2003)

Modified Goodman-diagrams, Figure 3.5, may be applied to make a simple design for fatigue. This diagram is based on the observation that the fatigue strength of plain concrete is essentially the same, independent of loading modes, i.e. tension, compression, or flexure. The diagram also incorporates the influence of range of loading. For a zero minimum stress level, the maximum stress level that concrete can support for one million cycles without failure is taken conservatively as *50* percent of the static strength. As the minimum stress level is increased, the stress range that the concrete can support decreases. The approximately linear decrease of stress range with increasing minimum stress has been observed by many investigators. Hence, the maximum stress that concrete can withstand for one million repetitions and for a given minimum stress can be determined; for example, consider a structural element to be designed for one million repetitions. If the minimum stress is *15* percent of the static ultimate strength, then the maximum load that will cause fatigue failure is about *57* percent of static ultimate load.

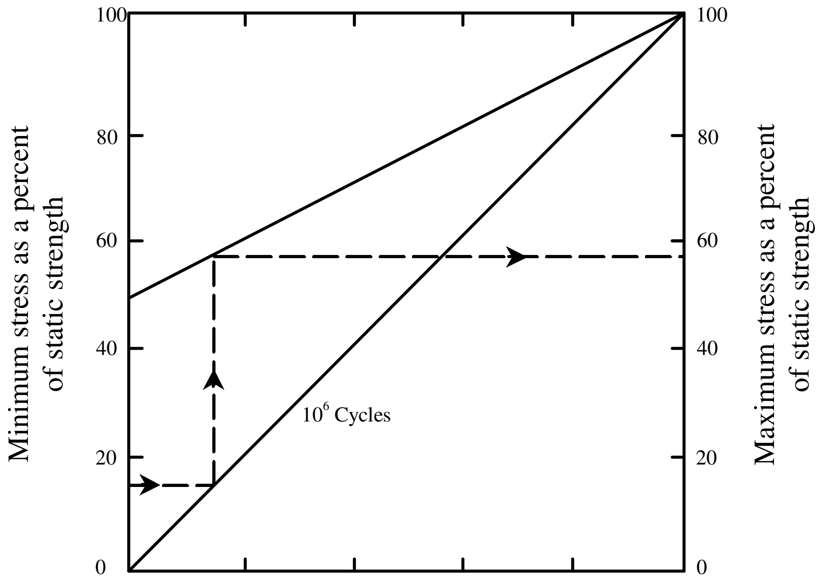

Figure 3.5 Modified Goodman-Diagram for failure after one million cycles in tension, compression, or flexure; from ACI 215R-74 (2003)

The number of cycles to failure increases with decreasing maximum stress. Large stress range and high frequency loading entail more fatigue like condition, i.e. the number of cycles determines the degree of degradation. On the other hand, a small stress range and low frequency loading imply sustained loading condition, i.e. the degree of degradation depends on how long the load has been applied. As in static loading, high stress rate results in high static strength; increased loading rate may lead to higher fatigue strength; see Svensk Byggtjänst (2000).

The sinusoidal function is the most commonly used, since wind and wave load may be assumed to have this shape; however special structure, such as machine foundation, may be exposed to other loading pattern. The rectangular load shape yields less cycle to failure than the sinusoidal, while the triangular load shape entails longer fatigue life, see Holmen (1979) and Svensk Byggtjänst (2000).

Rate of loading

The loading frequency effects have been investigated by many researchers. A common conclusion is that a frequency of loading between 50 and 900 cycles per minutes (c.p.m.) has little effect on fatigue strength, provided that the maximum stress level is less than about 75 percent of the static strength. For higher stress levels, a significant influence of the rate of loading has been observed. Under such condition, creep effects become more important, leading to a reduction in fatigue strength with decreasing rate of loading; see Holmen (1979).

Load History

Most of the topics discussed, so far, are gained from fatigue tests with constant amplitude loading. However, concrete in structural members may be subjected to randomly varying loads. The first investigation, where the effect of variable stress level on the fatigue behaviour of plain concrete was studied, was done by Hilsdorf and Kesler (1960). This research was conducted in order to study the validity of the

Palmgren-Miner (PM) hypothesis in flexural tests of plain concrete beam. The PM hypothesis is very simple, since it is assumed that damage accumulates linearly with the number of cycles, applied at a particular load level. The failure criterion of PM hypothesis is written as:

$$\sum_{i=1}^{K}\left(\frac{N_i}{N_{Fi}}\right)=1.0 \qquad (3.1)$$

Where, $N_i =$ number of cycles applied at stress level i.

$N_{Fi} =$ number of cycles to failure at stress level i.

The hypothesis was first proposed by Palmgren in 1924 for ball-bearings and was used by Miner, in 1945, in tests with notched aluminium specimen. In the tests, conducted by Hilsdorf and Kessler (1960) and Miner (1945), the loading histories consisted of blocks with two different stress levels as shown in Figure 3.6. The results indicated that the hypothesis may lead to conservative or unsafe predictions of the fatigue strength depending on the load history; see Figure 3.6.

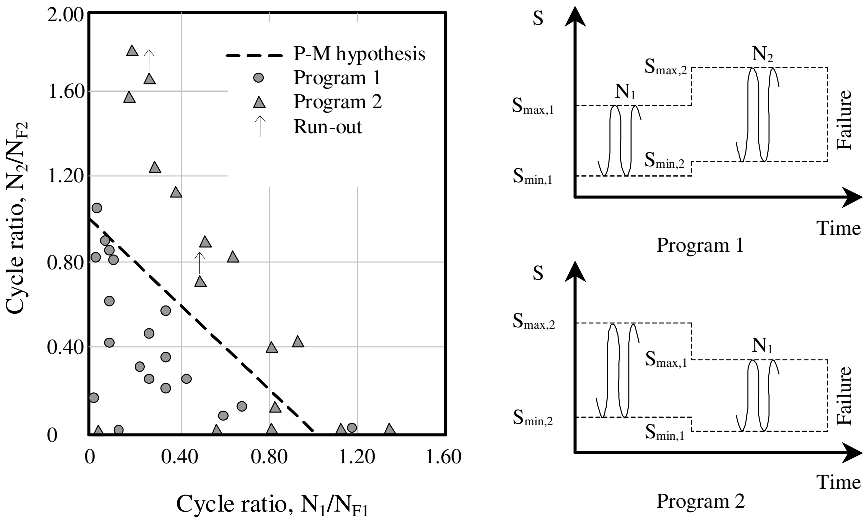

Figure 3.6 Behaviour of specimens subjected to two-stage loading; from Holmen (1979)

In two-stage tests, the PM hypothesis overestimated the strength where the lower stress level was applied first, and the strength was underestimated where the higher stress level was applied first, as:

$$\frac{N_1}{N_{F1}}+\frac{N_2}{N_{F2}}<1$$ Where the lower stress level was applied first

$$\frac{N_1}{N_{F1}}+\frac{N_2}{N_{F2}}>1$$ Where the higher stress level was applied first

After 1960, a number of corresponding tests have been done in compression and these showed that the PM hypothesis could not predict the cumulative fatigue behaviour of concrete satisfactorily. In multi-stage tests, i.e. tests with three or more stages of different stress levels, both unsafe and conservative predictions of the PM hypothesis have been found; see Holmen (1979).

The effect of rest periods and sustained loading on fatigue behaviour of concrete has been investigated by some researcher, but it is still not sufficiently explored. Laboratory tests have shown that if a sustained load is imposed with a stress level that is higher than *75* percent of static strength may be detrimental, while if the sustained load remains lower than *75* percent it would increase the fatigue strength of concrete. Rest periods between repeated load cycles tend to increase the fatigue strength of concrete; see Hilsdorf (1966). According to Svensk Byggtjänst (2000), the recovering period may be justifies since the traffic and wind load is of this character. The benefit of the recovering period has its maximum after about *5* minutes, if a stop is made every *4-500* cycle.

Eccentricity of loading

The fatigue strength is increased for eccentric loading, but if the stress level of the fatigue load is expressed in terms of static stress by corresponding eccentricity, then both static and fatigue loading are affected in the same proportion; see Holmen (1979).

Figure 3.7 presents results from tests on $100 \times 150 \times 300$ mm prisms under repeated compressive stress and three different eccentricities; see Holmen (1979). The diagram shows the ratio of the maximum stress, defined as the extreme fiber stress, over the static compressive strength, f_c', versus the number of cycles to failure, plotted on a logarithmic scale.

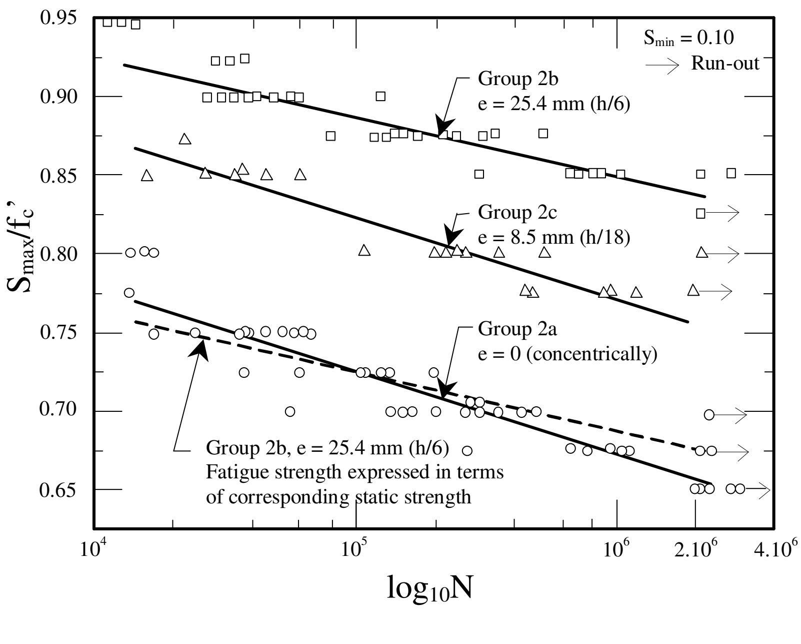

Figure 3.7 Iinfluence of eccentric loading on fatigue strength, from Holmen (1979)

It can be seen that the fatigue strength is increased with eccentricity. The three *S-N* curves, in Figure 3.7, will practically coincide, as shown by the stippled curve in the same figure for $e = 25.4$ mm, if the fatigue strength is expressed in terms of corresponding static strength.

Lateral Loading

The fatigue behaviour is affected by lateral confining load. Some results, from fatigue tests of cylindrical specimens with and without lateral confining load, applied to the circumference of the specimen, are shown in Figure 3.8. It can be concluded that the lateral confining load prolongs the fatigue life of concrete considerably. This effect seems to be dependent on the maximum stress level of the fatigue load; see Holmen (1979).

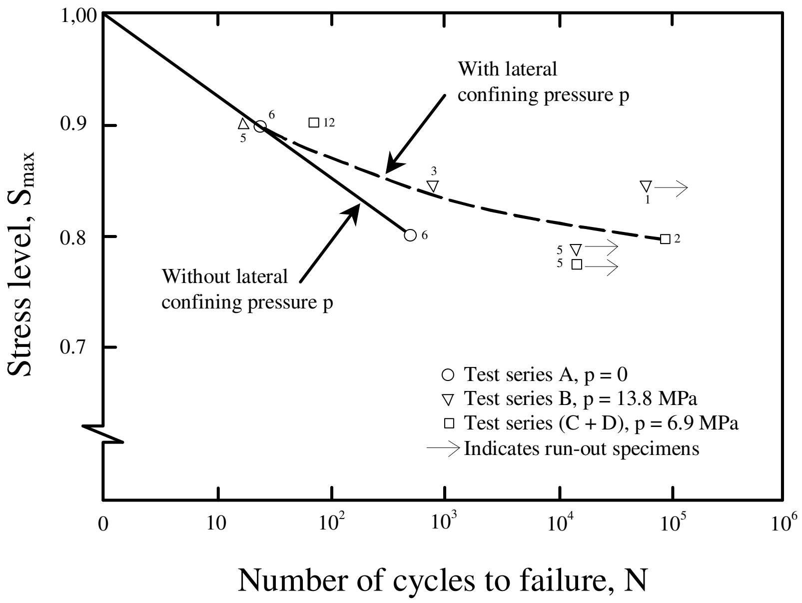

Figure 3.8 S-N relationship for specimens with and without lateral confining load, from Holmen (1979)

3.6 Fatigue Design in SLS and ULS

Concrete structures, such as bridges, pavements, offshore structures, and railroad ties, exposed to frequently varying stresses, should be design against fatigue damage. Design of concrete structures regarding to fatigue loading is a huge subject and there is no complete agreement between different building codes yet. Similar to other kind of loadings, structural elements should provide resistance against induced stresses in both Service Limit State (SLS) and Ultimate Limit State (ULS). Discussion about fatigue design methods and approaches in different buildings regulations is beyond the scope of this study; but the present section is devoted to this subject in order to make a general perspective of how fatigue loadings are considered in design of a structural element. Since all building codes do not include fatigue loading in design procedure, fatigue design in SLS, presented in this section, is in accordance with ACI 215R-74, and fatigue design in ULS is in accordance with CEB-FIP Model Code 1990. As this text is an introduction to fatigue design, readers who may wish to use the design procedure and equations are recommended to follow the original source.

Fatigue Design[1] in SLS

In order to ensure adequate performance at service load levels, beams subjected to repeated loads should be checked for the possibility of fatigue distress[2]. In order to check a design for safety in fatigue, subsequent three steps should be followed:

1. Projection of a load histogram for structural members: requires a study of many factors related to the nature of the repetitive loading, which is beyond the scope of this report.

2. Identification of location where fatigue stresses may be critical: any location where high stress ranges occur may be critical for fatigue. Locations of stress concentrations in steel reinforcement such as at tendon anchorage are especially critical.

3. Determination of critical fatigue stresses and comparison of these stresses with permissible values: requires calculation of a minimum and maximum stress for specified loadings. Typically, the minimum stress is due to dead load, and the maximum stress is due to dead plus live load. To determine whether these stresses may possibly produce fatigue distress, ACI Committee 215 recommends the following criteria:

   - The stress range in concrete shall not exceed 40 percent of its compressive strength when the minimum stress is zero, or a linearly reduced stress range as the minimum stress is increased so that the permitted stress range is zero when the minimum stress is $0.75 f_c'$.

   - The stress range in straight deformed reinforcement shall not exceed the value computed from the following expression:

     $$S_r = 161 - 0.33 S_{\min}$$

     Where S_r = Stress range, in MPa; and

     $S_{\min}$ = Algebraic minimum stress, for tension (+) and compression (-), in MPa

---

[1] A beam element is discussed in this section.

[2] According to ''Cement and Concrete Terminology'', reported by ACI Committee 116; **distress** is a physical manifestation of cracking and distortion in a concrete structure as the result of stress, chemical action, or both.

But S_r does not need to be taken less than 138 MPa. For bent bars or bars to which auxiliary reinforcement has been tack welded, the stress range computed from the above equation should be reduced by 50 percent.

Fatigue Design in ULS

Ultimate Limit States of fatigue may be associated with the failure of reinforcing steel, prestressing steel, or concrete. Fatigue design shall ensure that in any fatigue endangered cross-section the expected damage *D* will not exceed a limiting damage D_{lim}. The verifications of this requirement can be performed according to the following four methods with increasing refinement.

(a) First Method

This is a qualitative verification that no variable action is able to produce fatigue. If the conclusion of this verification is not positive, a verification according to one of the following methods shall be made.

(b) Second Method

Following conditions should be verified:

- For steel

$$\gamma_{sd} \max \Delta\sigma_{Ss} \le \Delta\sigma_{Rsk} / \gamma_{s,fat} \tag{3.2}$$

- For concrete in compression

$$\gamma_{sd}\sigma_{c,\max}\eta_c \le 0.45 f_{cd,fat} \tag{3.3}$$

- For plain concrete in tension

$$\gamma_{sd}\sigma_{ct,\max} \le 0.33 f_{ctd,fat} \tag{3.4}$$

Where; γ_{sd}, $\gamma_{s,fat}$ Partial safety factors depending on material;
$max\Delta\sigma_{Ss}$ Maximum acting stress range;
$\Delta\sigma_{RSk}$ Characteristic fatigue strength at 10^8 cycles;
$f_{cd,fat}$ ($f_{ctd,fat}$) Fatigue reference compressive (tensile) strength;
$\sigma_{c,max}$ ($\sigma_{ct,max}$) Maximum compressive (tensile) strength; and
η_n Averaging factor considering the stress gradient.

(c) Third Method

This verification refers to a representation of the variable load dominant for fatigue by a single magnitude, *Q*, associated with a number of repetitions, *n*, during the required lifetime.

The stresses (or stress range) due to the application of Q (possibly due to applications in two senses or due to successive load arrangements) are multiplied by a factor γ_{sd}[1]. These design values shall be smaller than the resistance to fatigue[2] for n cycles divided by a specific γ_M-factor ($\gamma_{s,fat}$ or $\gamma_{c,fat}$[3] depending on the material).

(d) Fourth Method

This is a verification based on an assessment of the fatigue damage resulting from various magnitudes of loads. The load history during the required life should usually be represented by a spectrum in a discretized form. The accumulation of fatigue damage is calculated on the basis of the Palmgren-Miner summation.

According to Svensk Byggtjänst (2000), since the probability of failure in the case of small oscillating load, in comparison with total load, is low then an accurate fatigue calculation may be unnecessarily time consuming. A simplified method may then be used and if the calculations show that fatigue is not decisive, further detailed fatigue analysis is not required. In the simplified method, the structure is considered as being subjected to a non-fatigue load, where the amplitude of the fatigue load is multiplied by a factor μ depending on the number of cycles according to Table 3.2. The resulting load may then be treated as a non-fatigue load and multiplied by appropriate partial coefficients (considering the load combination factor as $\psi = 1$).

Table 3.2 the factor by which the design fatigue load is decreased when the calculations are performed according to the simplified method; from Svensk Byggtjänst (2000)

Stress oscillation between compression and tension	Number of Cycles, N					
	$\leq 5.10^5$	10^3	10^4	10^5	6.10^5	$\geq 10^6$
	μ					
Dose occur	1.0	1.3	2.2	3.2	4.2	4.6
Dose not occur	1.0	1.0	1.1	1.6	2.1	2.3

1 Given in CEB-FIP Model Code 1990 – subsection 1.6.4.4

2 Given in CEB-FIP Model Code 1990 – subsection 6.7.4

3 Given in CEB-FIP Model Code 1990 – subsection 1.6.4.4.

3.7 Methods Used to Determine Fatigue Behaviour of Concrete

Various approaches have been used for fatigue life assessment of structural elements. A widely accepted approach for engineering practice is based on empirically derived *S-N* diagrams. In addition, the effects of minimum stress in the loading cycle may be represented in so-called Goodman diagrams; see Figure 3.3. These empirical curves give a graphical representation of the fatigue performance for certain loading parameters. Another method is based on fracture mechanics concepts and has been incorporated in the finite element approach. This method is more demanding but provides an insight into the underlying physical behaviour.

Unlike experimental test methods to determine fracture properties of concrete, there are no standard test methods to investigate fatigue behaviour of concrete. A variety of tests with different geometry, boundary conditions, and loading arrangement have been applied to concrete in order to investigate the fatigue behaviour under cyclic loading. As in the case of static test, different loading conditions have been used in fatigue testing, including compression, tension, and bending tests however the most common method of fatigue testing, so far, is via flexural tests. Some of the experimental methods have been summarized in Appendix B.

4 FIBER REINFORCED CONCRETE (FRC)

4.1 Introduction

Fiber reinforced concrete (FRC) is made primarily of hydraulic cement, aggregates, and discrete reinforcing fibers. Different kind of fibers, mostly from steel, glass, and organic polymers (synthetic fibers), have been used for reinforcing concrete. The concrete matrices may be mortar, normally proportioned mixes, or mixes specifically formulated for a particular application. Generally, the length and diameter of the fibers used for FRC do not exceed 80 mm and 1 mm, respectively; see ACI (2003).

Since brittle materials are considered to have no significant post-cracking ductility, fibrous composites have been developed to provide brittle materials with ductile mechanical properties. These unreinforced brittle matrices initially deform elastically under tension loading, which is followed by micro-cracking, localized macrocracking, and finally fracture. Introduction of fibers into the concrete results in a change of the post-elastic property that range from subtle to substantial, depending upon several factors including matrix strength, fiber type, fiber modulus, fiber aspect ratio, fiber strength, fiber surface bonding characteristics, fiber content, fiber orientation, and aggregate size effects. For many practical applications, the matrix first-crack strength is not increased. In these cases, the most significant enhancement from the fibers is the post-cracking composite response. This is most commonly evaluated and controlled through toughness testing, such as measurement of the area under the load-deformation curve.

If properly designed, one of the greatest benefits with FRC is improved long-term serviceability of the structure or product. Serviceability is the ability of the specific structure or part to maintain its strength and integrity and to provide its designed function over its intended service life. One aspect of serviceability that can be enhanced by the use of fibers is control of cracking. Fibers can prevent the occurrence of large crack widths that are either unsightly or permit water and contaminants to enter, causing corrosion of reinforcing steel or potential deterioration of concrete. In addition to crack control and serviceability benefits, use of fibers at high volume percentages (5 to 10 percent or higher with special production techniques) can substantially increase the composite tensile strength; see ACI (2003).

The main characteristics of fibers which determine their efficiency as reinforcement of brittle matrices are:

- Aspect ratio, which means length to diameter ratio, l/d
- Surface properties and additional anchorage at the ends (e.g. hooked ends)
- Mechanical properties of the material, which means tensile strength and ductility

The total amount of fibers in a composite material is defined as a volume fraction of the total volume rather than mass. Generally the applied volumes vary between 0.25 and 2.0% and the upper limit is based on the following arguments:

- The workability of fresh mix decreases rapidly when a large volume of fibers is added and the porosity, due to entrapped air voids, is increased. Even with intensive vibration it is difficult to place and to compact correctly the fresh mix into forms when too many fibers are added.

- The fibers have a tendency to form balls and with a higher fraction it is very difficult to distribute them properly.

- The total price of composite increases considerably with high fiber fraction.

- The optimal efficiency of fibers – i.e. that the post-cracking tensile strength is equal to or larger than the matrix cracking strength – depends on several factors, but in most cases it corresponds to a volume between 1 and 2%.

Special technologies have been developed in order to introduce significantly larger volume fractions of fibers, even up to 20% by volume. One such technology is called SIFCON (slurry Infiltrated Concrete) and has been applied in the repair works of concrete structures.

However, there are different types of fibers (steel, glass, synthetic, and natural fibers) used to produce fiber reinforced concrete, the report is written so that the reader may gain an overview of the property enhancements of steel fiber reinforced concrete.

4.2 Steel Fibers

The use of fibres in concrete is not a novel concept; early patents on fibre-reinforced concrete date back to 1874 (A. Berard, USA) and fibres with shapes similar to those currently used were patented already in 1927 (G. Martin, USA), 1939 (Zitkevic, Britain) and 1943 (G. Constantinesco, England) – for a more comprehensive historical review see e.g. Naaman (1985) and Beddar (2004).

at the present time, there are different kinds of steel fibers used as reinforcement for concrete; some examples are shown in Figure 4.1.

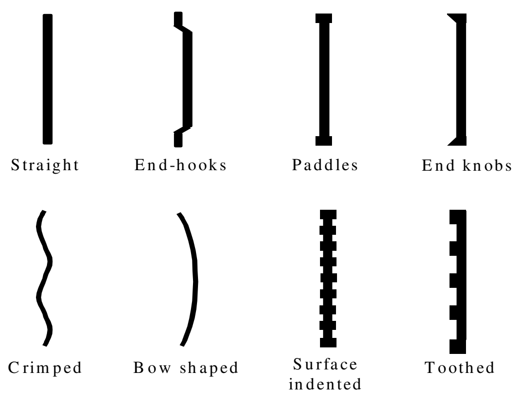

Figure 4.1 Examples of some kinds of short steel fiber; from Brandt (1995)

According to Brandt (1995), fibers are produced by various methods, e.g.:

1. Chopped from cold drawn wire of circular cross–section, mostly indented, waved with hooks, or enlargement at the end.

2. Cut out from strips of thin plates, of square or rectangular cross-section; often twist along their longitudinal axes during cutting, some kinds also with enlargements at the ends.

3. Machined, of rough surface and varied cross-section related to the technology of machining.

4. Obtained from molten metal, with a rough surface (Johnson and Nephew).

Fibers of type 1 were produced years ago and their unit cost is relatively high due to the complicated technology of cold drawing and cutting. Moreover, additional operations are required to increase their binding by surface indentation or waving. Plain, straight fibers are rarely used because of their low efficiency due to poor bonding. Fibers of type 2 are less expensive and have better bond strength without special operations. Fibers of type 3 were applied later and their application is quickly developing. They are less expensive than fibers chopped from wires and their uniform distribution in the fresh matrix is easier. Shape of this kind of fibers ensures better adherence to the matrix. Fibers of type 4 are also inexpensive and have increased bond strength. There are, however, few results available from test or practical applications of these fibers.

4.3 Fiber-cement Paste Interface

The fiber-cement paste interface has been investigated by many researchers for different kinds of fibers such as steel, polypropylene, glass and carbon fibers. Initially, attempts were made to use numerous results obtained for steel bars and cement mortar in reinforced concrete elements. It appears that because of the different scale and role of steel bars and thin fibers with respect to other components of material structure, like aggregate and pores, only few similarities exist.

There is no significant chemical reaction between cement paste and steel fibers. Following parameters mostly influences the interfacial layer:

- The natural roughness of the fiber surfaces

- The shape of the fibers and special indentations and deformation

- Modification of cement paste in the vicinity of the finer surface e.g. increased water-cement ratio and higher porosity due to restraints in vibration.

The transition zone at a steel fiber is, as for aggregate-cement paste interface, composed of different layers: duplex, CH layer, porous layer of CSH and ettringite[1]; see Bentur A. (1985) for more information, this is shown schematically in Figure 4.2. The Porous Layer is characterized by lower strength and is the weakest zone in which cracks between fiber and matrix are observed; see Figure 4.3.

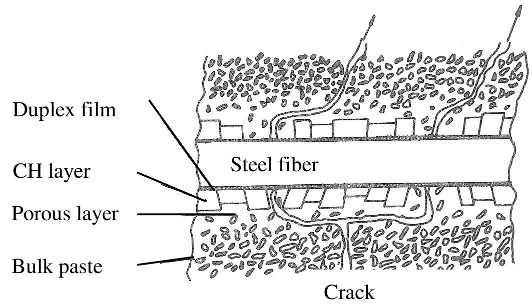

Figure 4.2 Scheme of steel fiber-cement paste interface with a crack propagating in transversal direction; see Bentur A. (1985).

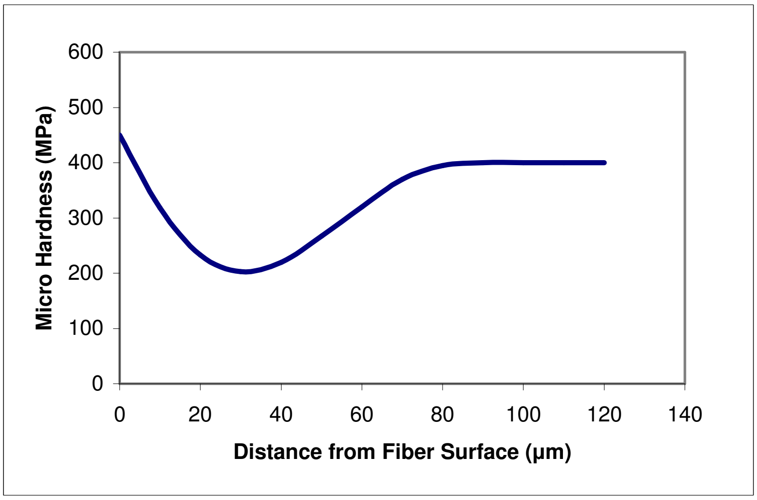

Figure 4.3 Microhardness of the cement paste measured from the steel fiber surface; see Brandt (1995).

One of the effects of a weak zone around fibers are the mechanism of crack arrest observed in many test and described by Brandt (1995). In this mechanism the interface fails ahead of the crack tip due to tensile stress concentrations, which is shown schematically in Figure 4.1 – this is also referred to as the Cook-Gordon effect;

[1]Ettringite ($3CaO.Al_2O_3.3CaSO_4.32H_2O$) forms as a natural part in the cement hydration reaction. Moreover In sulfate attack on concrete, ettringite is also produced; see Neville (2003).

See Cook, J. & Gordon, J. E. (1964) . The following sequence of events is then supposed as shown in the figure.

- Crack approaches a weak interface
- Interface fails ahead of the main crack
- Crack stops in a T-shape or may be diverted.

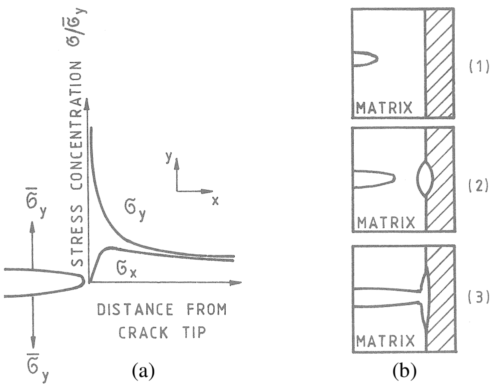

Table 4.1 The Cook-Gordon arrest mechanism of a crack; from Brandt (1995)

4.4 Fracture Properties of Fiber Reinforced Concrete

Potentially useful improvements in the mechanical behavior of concrete matrices can be obtained by the inclusion of fibers; see Figure 4.4. Similar to the behavior of plain concrete, composite failure under most types of loading is initiated by the tensile cracking of the matrix along planes where the normal tensile strains exceed the corresponding permissible values. This may be followed by multiple cracking of the matrix prior to composite fracture if the volume fraction of fibers are sufficiently high (or if the fibers are continuous), see Aveston et al. (1971). However, when short fibers are used, once the matrix has cracked, one of the following types of failure will occur; see Figure 4.4:

a) The composite fractures immediately after matrix cracking. This results from inadequate fiber content at the critical section or insufficient fiber lengths to transfer stresses across the matrix crack.

b) Although the maximum load on the composite is not significantly different from that of the matrix alone, the composite continues to carry decreasing loads after the peak. The post-cracking resistance is primarily attributed to gradual (rather than sudden) fiber pull-out associated with crack bridging. While no significant increase in composite strength is observed, the composite fracture energy and toughness are considerably enhanced.

c) Even after matrix cracking, the composite continues to carry increasing loads. The peak load-carrying capacity of the composite and the corresponding deformation are significantly greater than that of the plain matrix. During the pre-peak inelastic regime of the composite response, progressive debonding of the interface and distributed microcracks in the matrix may be responsible for the energy dissipation process. It is clear that this mode of composite failure results in the efficient use of both the constituents; see Mobasher and Shah (1989), Stang, Mobasher and Shah (1989), Mobasher, Stang and Shah (1989).

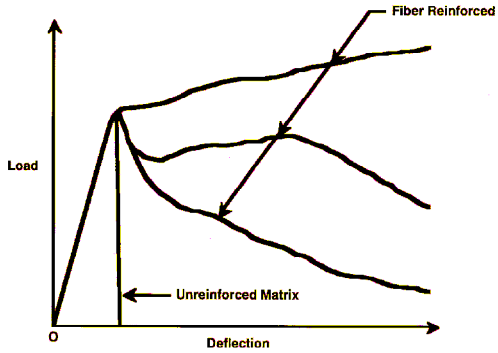

Figure 4.4 *Range of load versus deflection curves for unreinforced and reinforced matrix; from ACI 544.1R-96 (2003)*

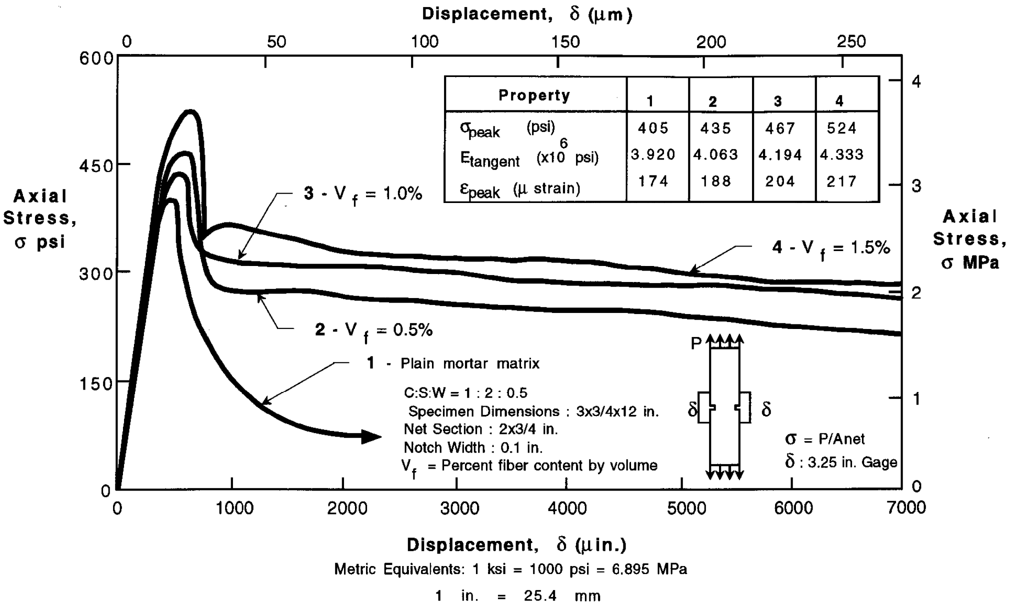

Figure 4.5 *Typical results of stress-displacement curves obtained from direct tension tests on plain mortar matrix and SFRC; from ACI 446.1R (2003)*

One or more of the above types of failure mechanisms may be modeled by analytical approaches in order to predict the mechanical behavior of fibrous composites. The analytical models can be categorized as: models based on the theory of multiple fracture, composite models, strain-relief models, fracture mechanics models, interface mechanics models, and micro-mechanics models. Fairly exhaustive reviews of these models are available in the scientific literature, e.g. Gopalaratnam and Shah (1987), and Mindess (1983).

4.5 Toughness

Toughness is a measure of the energy absorption capacity of a material and is used to characterize the material's ability to resist against fracture when subjected to static strains or to dynamic or impact loads. The difficulties of conducting direct tension tests on FRC prevent their use in evaluating toughness. Hence, the simpler flexural test is recommended for determining the toughness of FRC. In addition to being simpler, the flexural test simulates the loading conditions for many practical applications of FRC. The flexural toughness and first-crack strength can be evaluated under third-point loading. The flexural strength may also be determined from the maximum load reached in this test. Energy absorbed by the specimen is represented by the area under the complete load-deflection *(P-Δ)* curve. The P-Δ curve has been observed to depend on:

a. The specimen size (depth, span, and width).

b. The loading configuration (midpoint versus third-point loading).

c. Type of control (load, load-point deflection, cross-head displacement, and etc.).

d. The loading rate.

To minimize at least some of these effects, normalization of the energy absorption capacity is necessary. This can be accomplished by dividing the energy absorbed from the FRC beam by that absorbed from an unreinforced beam of identical size and matrix composition, tested under similar conditions. The resultant non-dimensional index I_t represents the relative improvement in the energy absorption capacity due to the inclusion of the fibers. It is an index for comparing the relative energy absorption of different fiber mixes as well; see ACI 544.2R-89 (2003).

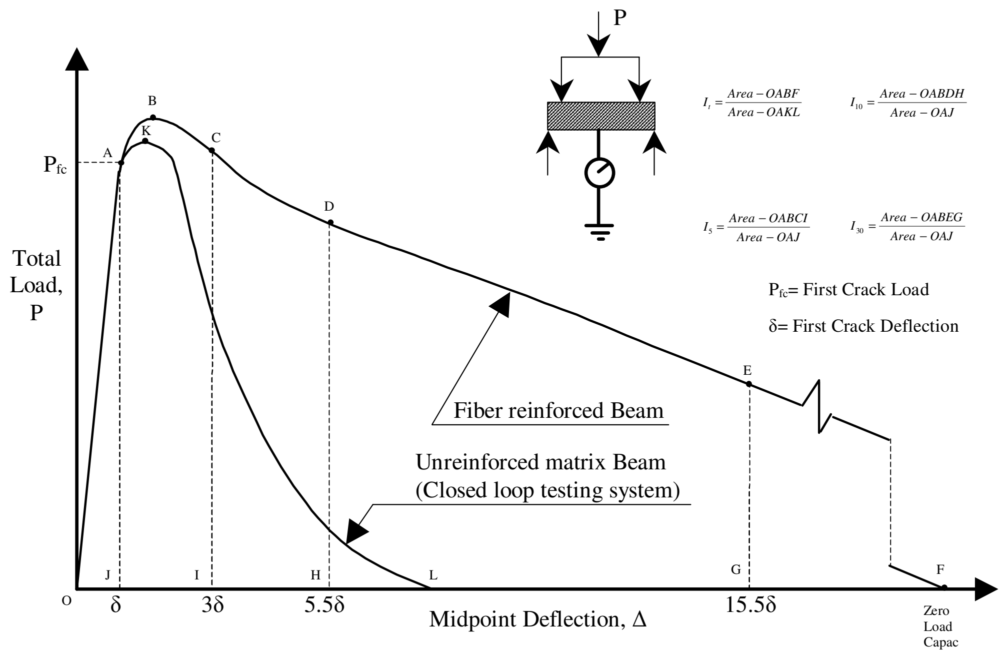

Figure 4.6 Toughness index from flexural load-deflection diagram, from ACI 544.2R-89 (2003)

Several useful methods for evaluating toughness that do not require determining I_t, have been adopted, see ACI (2003). These methods are based on the facts that:

a. It may not always be practical to obtain the complete *P- Δ* characteristics of FRC (time constraints in slow tests or rate-dependent behaviour in rapid tests).

b. A stable fracture test of the unreinforced beam requires a stiff testing machine, or closed-loop testing.

c. Each toughness test using the I_t measure would require both FRC and unreinforced beams of identical matrix to be cast, cured, and tested.

d. I_t does not reflect the relative toughness estimates at specified levels of serviceability appropriate to specific applications.

ASTM C 1018 provides a mean for evaluating serviceability-based toughness indexes and the first-crack strength of fiber reinforced concretes. The procedure involves determining the amount of energy required to deflect the FRC beam a selected multiple of the first-crack deflection based on serviceability considerations. This amount of energy is represented by the area under the load-deflection curve up to the specified multiple of the first-crack deflection. The toughness index is calculated as the area under the *P- Δ* diagram up to the prescribed deflection, divided by the area under the *P- Δ* diagram up to the first-crack deflection (first-crack toughness).

Indexes I_5, I_{10}, and I_{30} at deflections of 3, 5.5, and 15.5 times the first-crack deflection, respectively, are illustrated in Figure 4.6. These indexes provide an indication of

a. The relative toughness at these deflections, and

b. The approximate shape of the post-cracking *P- Δ* response.

The indexes I_5, I_{10}, and I_{30} have a minimum value of 1 (elastic-brittle material behaviour) and values of 5, 10, and 30, respectively, for perfectly elastic-plastic behaviour (elastic up to first crack, perfectly plastic thereafter). The unreinforced matrix is assumed to be elastic-brittle. It is possible for the defined indexes to have values larger than their respective elastic-plastic values, depending on fiber type, volume fraction, and aspect ratio.

4.6 Fatigue Behaviour of Fiber Reinforced Concrete

As previously stated, the action of fiber bridging and fiber pullout in FRC dissipates energy in the wake of crack tip. Consequently, it is feasible to retard and inhibit the growth of the flaws in the second stage of fatigue failure development by introducing dispersed fibers as reinforcements. This mechanism plays a significant role in decreasing the crack growth and increasing the load carrying capacity of FRC.

The addition of fibers has been found to have a dual effect on the cyclic behaviour of concrete. Fibers are able to bridge microcracks and retard the crack growth by enhancing the composite performance under cyclic loading. On the other hand, the presence of fibers increases the pore and initial microcracks density, resulting in decreased strength. The overall outcome of these two competing effects depends significantly on the fiber volume; see M. Grzybowski (1993).

The main benefit of the addition of fibers in the concrete matrix is the increased ability to absorb energy. Increasing the fiber content and aspect ratio increases the amount of energy spent in crack growth of SFRC under fatigue loading. Based on research conducted by M. Grzybowski (1993), there seems to be a reduction in the fatigue life of FRC compared to plain concrete for volume percentage above 0.25%: On the other hand, T. Paskova (1994) reported that fibers substantially improve fatigue life of concrete for all volume percentage of fibers. From the conflicting evidence available, M.K. Lee (2004) concluded that there could be an optimum fiber content, above which the effectiveness of the inclusion of fibers towards enhancing the fatigue performance increases. For example, Zhang (1998) reported an optimum fiber volume concentration of 1% by volume.

Fiber type also affects the fatigue performance of FRC. Steel fibers seem to be more effective compared to polypropylene fibers. For volumes up to 1%, steel fibers are up to two times as effective as polypropylene fibers; see Zhang (1998). The effectiveness of fiber on fatigue strength is increased if they are hooked rather than straight; see M.K. Lee (2004).

Based on an overview of the fatigue behaviour of plain and fiber reinforced concrete, done by M.K. Lee (2004), there is no agreement whether *S-N* curves may be used for all types of specimens, load configuration, testing condition and etc. However, some of these comparisons are presented here to see whether the fatigue data could show any qualitative benefits of fiber additions.

Figure 4.7(a) shows *S-N* curve for plain concrete in compression and Figure 4.7(b) and (c) present the *S-N* curve for SFRC containing 0.5% and 1.0% of fiber under compression fatigue loading respectively. Furthermore, in Figure 4.8 results for flexural fatigue loading are presented. It can be concluded that the lack of a well-established test procedure for executing and evaluating fatigue tests makes it difficult to correlate or extend published test results. The presence of fibers does not seem to enhance the fatigue life of concrete under compressive fatigue loading. On the other hand, fiber addition benefits the fatigue performance under tensile and flexural fatigue loading. A possible explanation is that under tensile forces, the fibers are able to bridge cracks and prolong fatigue life. On the contrary, the presence of fibers cannot display their true effectiveness under compressive loading, as the mode of failure is different; see M.K. Lee (2004).

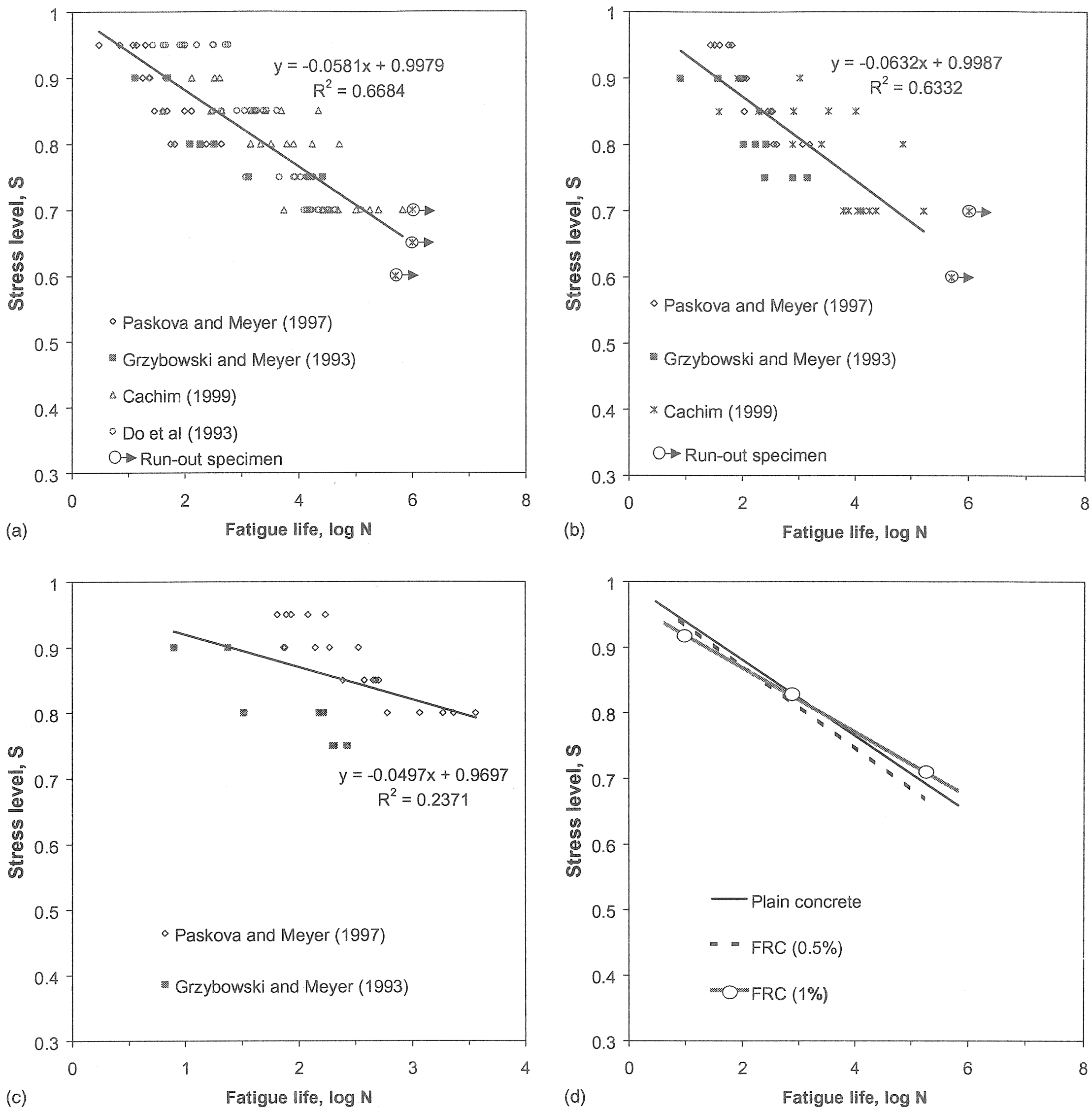

Figure 4.7 S-N curve under compressive loading for (a) plain concrete; (b) SFRC (0.5% fiber content); (c) SFRC (1.0% fiber content); (d) comparison between plain concrete and SFRC (0.5 & 1.0% fiber content); from M.K. Lee (2004)

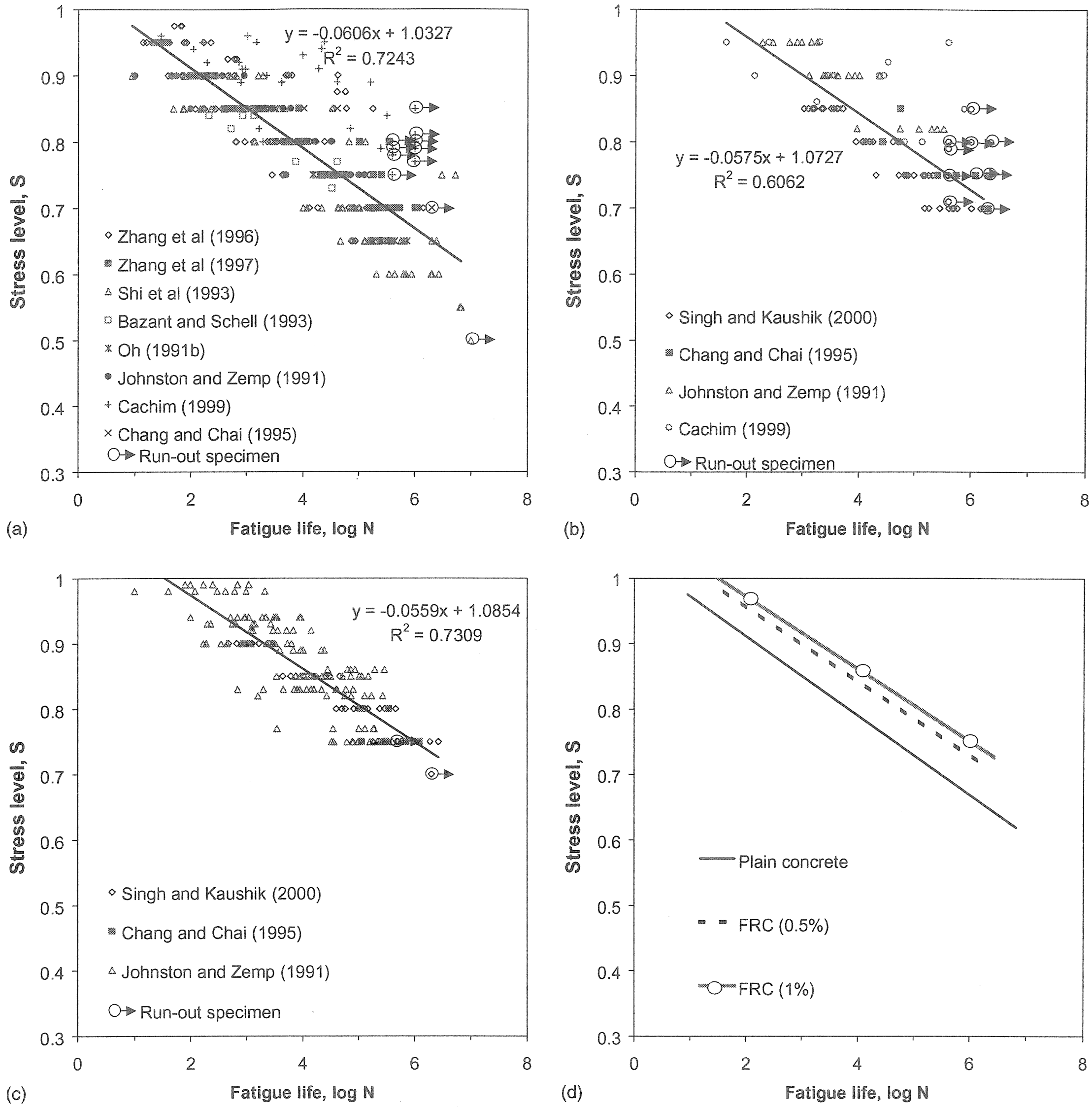

Figure 4.8 S-N curve under flexural loading for (a) plain concrete; (b) SFRC (0.5% fiber content); (c) SFRC (1.0% fiber content); (d) comparison between plain concrete and SFRC (0.5 & 1.0% fiber content); from M.K. Lee (2004)

4.7 Fatigue Mechanism of Fiber Reinforced Concrete

According to Murdock (1960) and Antrim (1976) and the three main stages of fatigue failure stated in section 3.2, the initiation of fatigue failure is attributed to the progressive deterioration of the bond between the coarse aggregates and the binding matrix. This theory can also be applied to fiber reinforced concrete, i.e. in FRC the initiation and propagation of fatigue failure is related to the bonding between both aggregate-matrix and fiber-matrix.

Therefore, the fatigue life of FRC depends on both aggregate-matrix and fiber-matrix interfaces. Under fatigue loading microcracks, initiated due to different volume changes of different components of concrete, undergo a cycle of crack opening and closing. During the following deterioration of the bond between aggregate-matrix and fiber-matrix, the microcracks will grow and coalesce together, and ultimately a dominant macrocrack is created and fatigue failure takes place. Over all, in order to explain the fatigue behaviour of FRC, three stages of fatigue damage similar to those stated for plain concrete, i.e. flaw initiation, microcracking, and fatigue failure, can be described by considering the bond bridging on fiber-matrix interface.

Most likely, the growth of microcracks in the second stage is delayed and inhibited by introducing closely spaced and randomly dispersed fibers as reinforcement. Steel fibers dissipate energy in the crack tip by the action of fiber bridging and fiber pullout. These phenomena play a dominant role in inhibiting crack growth and therefore increase the load carrying capacity of FRC both under static and cyclic loading.

4.8 Flexural Fatigue of Fiber Reinforced Concrete

The endurance in dynamic cyclic flexural loading is an important property of FRC, particularly in applications involving repeated loadings, such as airport, highway, railway and bridge's pavements and industrial floor slabs. Although there is no current standard for flexural fatigue performance, tests similar to that employed for conventional concrete has been conducted using reversing and non-reversing loading, with applied loads normally corresponding to 10 to 90 percent of the static flexural strength. Short beam specimens with small deflection movements have been successfully tested at 20 cycles per second (cps) when hydraulic testing machines with adequate pump capacity were available. However, verification that the full load and specimen response has been achieved at these high frequencies is desirable. Specimens with large deflections may need to be tested at reduced rates of 1 to 3 cps, to minimize inertia effects. Strain rates of 6000 to 10,000 $\mu\varepsilon$/s (microstrain per second) may result from testing at 20 cps versus a strain rate of 600 to 1000 $\mu\varepsilon$/s at 2 cps; see 544.2R-89 (2003).

Loadings are selected so that testing can continue to at least, two million cycles, and applications to 10 million cycles are not uncommon. The user should be aware that 10 million cycles at 2 cps will require over 57 days of continuous testing, and the influence of strength gain with time may have to be considered in addition to the influence of strain rates. Specimen testing at later ages may reduce the influence of aging when testing at the lower strain rates. Test results in the range of 60 to 90 percent of the static flexural strength for up to 10 million cycles have been reported for non-reversed loading to steel fiber reinforced concrete with 0.5 to 1.0 volume percent fiber content. Data on reversed loading cyclic testing and the influence of strain rate and load versus time parameters are not available; see 544.2R-89 (2003).

In general, it has been concluded in related literature, such as 544.2R-89 (2003), that the addition of steel fibers to concrete mixture can significantly improve the flexural fatigue performance of concrete elements. The extent of improvement on the fatigue properties of FRC is expected to be dependent upon the fiber volume content, fiber type and geometry. Actually, the addition of fibers has added a further difficulty to the study of fatigue behaviour of concrete and has increased the complexity of analysis.

It was hoped that fibers in concrete would endow the FRC with a fatigue limit, thus making it more attractive material by comparison with plain concrete, which appears to have no fatigue limit.

5 Overview on Wedge Splitting Test (WST)

5.1 Introduction

The Wedge Splitting Test (WST) is a test method to determine the fracture properties of concrete. The test is similar to the compact tension test, used for metals, and was studied for concrete by Hillemier and Hilsdorf (1977). The present shape of the WS specimen, characterized by a starter notch and a guiding groove which can be either molded or sawn, was proposed by Linsbauer and Tschegg (1986). The test was subsequently refined by Brühwiler (1988) and Brühwiler & Wittmann (1989) who conducted (at the Swiss Federal Institute of Technology) wedge splitting tests on normal concrete, dam concrete, and other cementitious materials. Very large wedge splitting specimens, of sizes up to 1.5 m, have been tested by Saouma, Broz, Brühwiler and Boggs (1989) at the University of Colorado, to study the size effect in dam concrete, reported by ACI 446.1R-91 (2003).

Usually three types of concrete test methods are recommended to measure the fracture parameters for Mode I. These are the method of ''Three-point Bending Test (3PBT) on a notched beam[1]'', ''Uni-axial Tension Test (UTT)[2]'', and ''wedge splitting test (WST)''; See Figure 5.1 for schematic view of the tests set-up. A possible problem associated with the use of the 3PBT is that when the size of the beam tested is relatively large, the effect of self-weight of the beam should be carefully considered in the evaluation of fracture properties. Moreover, although the three-point bending beam can be handled in the laboratory, it is not possible to fabricate on the building site or to use material drilled from existing structures. While, direct uniaxial tensile test, both single and double notched, is not easy to carry out. Hence, the 'compact' 3PBT, which actually is a wedge splitting test, was recommended by Subcommittee B within RILEM TC 89-FMT to be used for investigating the fracture behaviour of concrete.

In this chapter a description of the test method and an approach to determine the fracture energy and the σ-w relationship is provided. At the end, applications of WST for different purposes are described.

---

[1] Proposed by RILEM TC 162-TDF (2002): Test and Design Methods for Steel Fiber Reinforced Concrete, Bending Test, Final Recommendation

[2] Proposed by RILEM TC 162-TDF (2001): Test and Design Methods for Steel Fiber Reinforced Concrete, Recommendations for uni-axial tension test

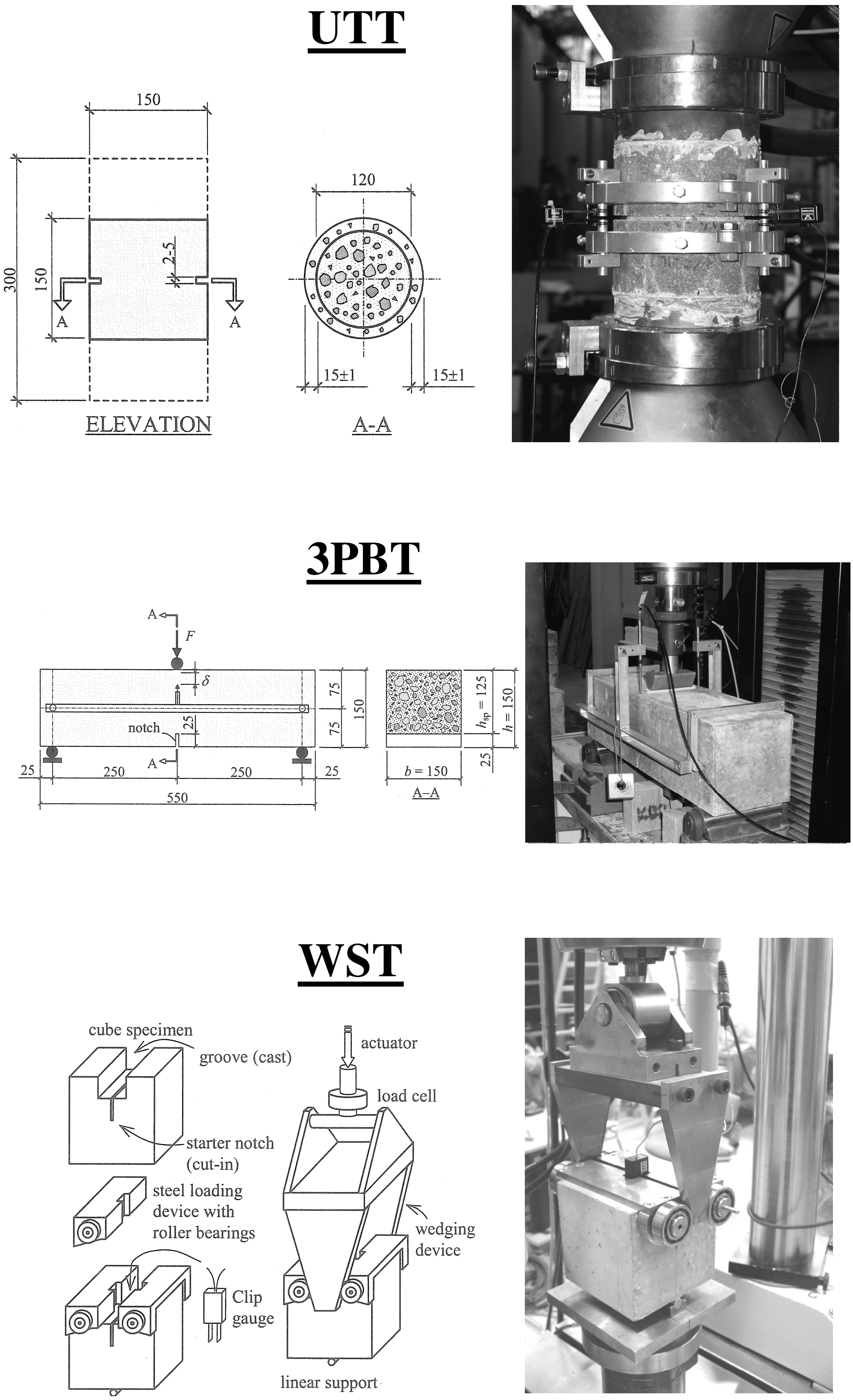

Figure 5.1 Schematic view and photo of the equipments and test set-up of the UTT, 3PBT, and WST

5.2 Description of the Wedge Splitting Test

Various possible wedge splitting specimen shapes are shown in Figure 5.2. Although both cubical and cylindrical specimens are applicable for the WST method, but the cubical specimen were used more by investigators. The specimens, shown in the Figure 5.2(c), requires either a deep notch or a longitudinal groove on both sides, in order to prevent shear failure of one of the cantilevers, see Shah and Carpinteri (1991).

Figure 5.3 illustrates the method of testing. At first, the wedge splitting specimen is placed on a linear support, which has been fixed to the lower plate of the testing machine; see Figure 5.3(a). Two steel loading devices, equipped with roller or needle bearings on each side, are placed on the top of the specimen; see Figure 5.3(b). A steel profile with two wedges is fixed at the upper plate of the testing machine. The actuator[1] of the testing machine is moved so that the wedges enter between the bearings, resulting in a horizontal splitting force component; see Figure 5.3(c). The fracture section of the specimen is essentially subjected to a bending moment. The wedge assembly is loaded in a statically determinate manner so that each wedge receives the same load. The dimensions of the notch and the groove must be chosen so that the crack propagates symmetrically.

During the test, the vertical force, F_v, must be measured with sufficient accuracy, Figure 5.3(d). The crack mouth opening displacement, CMOD, is measured by a clip gage, which should be attached at the level of the splitting forces. In this case CMOD represents the load-point displacement, associated with the horizontal component of the splitting force, F_{sp}. The test is controlled by CMOD in a closed-loop servo-hydraulic testing machine. However, a stable test can also be performed under actuator stroke control or under crosshead displacement control, using conventional testing machines. In that case, the appropriate notch length, which is necessary to ensure stability, must be identified by considering the interaction between testing machine stiffness, specimen stiffness and material properties (Brühwiler, 1988; Brühwiler and Wittmann, 1989).

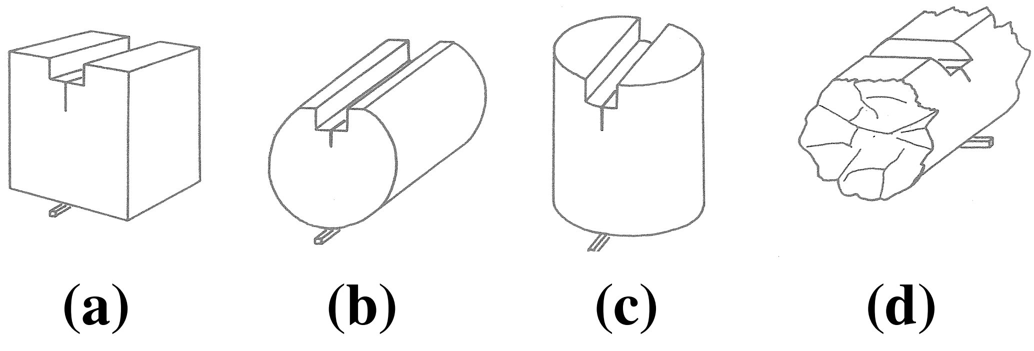

(a) (b) (c) (d)

Figure 5.2 Wedge splitting specimen shapes; from Brühwiler (1990).

[1] a mechanical device for moving or controlling the cross-head of the testing machine

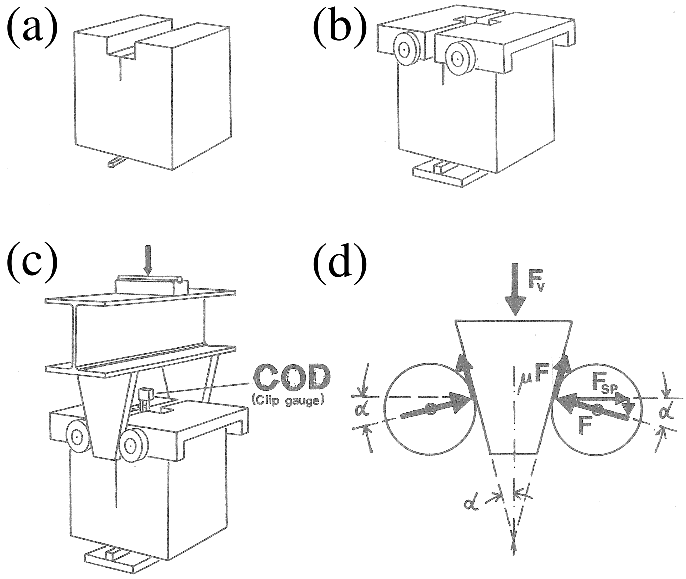

Figure 5.3 *Principle of wedge splitting test: (a) test specimen on a linear support, (b) placing of two loading devices with roller bearings, (c) the wedge are pressed between the bearings in order to split the specimens into two halves, and (d) forces acting on the wedge; from Brühwiler (1990) and Shah and Carpinteri (1991).*

To achieve a stable fracture test on a concrete specimen is particularly difficult due to the high specimen stiffness compared to the testing machine stiffness and the small rupture deformation of concrete. According to Shah and Carpinteri (1991), the WST overcomes these difficulties by the use of wedges:

- The frame of the testing machine is deformed only by the vertical load component in the wedge splitting test. By using a small wedge angle, the vertical force is reduced relative to the splitting force for a given specimen. Consequently a very stiff testing machine is not needed for the wedge splitting test.

- The actuator displacement which is perpendicular to the specimen deformation is increased with respect to the CMOD, if a small wedge angle is chosen. Hence, a small wedge angle should be used to increase the stiffness of the specimen; however it increases the friction effect.

The advantages of the wedge splitting test are as follows:

1. The specimens are compact and light, since the ratio of fracture area to the specimen volume is larger than other test methods (e.g., 5.2-times larger than that for the three-point bending test according to RILEM, 1985). This is especially useful for the study of size effect, since larger fracture areas can be obtained with smaller specimen weight. Due to lesser weight large specimens are easier to handle and there is a lower risk of breaking them during handling.

2. The cubical or cylindrical specimens, as shown in Figure 5.2, can be easily cast at the construction site using the same molds as for strength tests; the cylindrical shapes can also be obtained from drilled cores of existing structures.

3. The use of wedges, for inducing the load, increases the stiffness of the test set-up and thus enhances stability of the test and makes it possible to conduct the test even in a machine that is not very stiff.

4. The effect of self-weight is negligible in contrast to notched beam tests where the bending moment due to own weight can be over *50%* of the total bending moment.

On the other hand, it must be noted that the wedge-loading device has also a disadvantage when it comes to frictional effects. During the test, the load in the vertical direction, F_v, and the CMOD are monitored. The splitting force, F_{sp}, is the horizontal component of the vertical force and can be calculated by taking the wedge angle, α, and frictional forces, μF, into account; see Figure 5.3(d).

The splitting force can be calculated by force equilibrium as follow; see Shah and Carpinteri (1991):

$$F_{sp} = \frac{F_v}{2.\tan\alpha}.\frac{(1-\mu.\tan\alpha)}{(1+\mu.\cot\alpha)} \approx \frac{F_v}{2.\tan\alpha}.\frac{1}{(1+\mu.\cot\alpha)} \tag{5.1}$$

Where α is the wedge angle according to Figure 5.3(d), and

μ is the coefficient of friction.

The manufacturers of roller bearings give k-values ranging from *0.1%* to *0.5%*. For the typical wedge angle $\alpha = 15°$, the effect of frictional forces on F_{sp} is about *0.4%* for μ*=0.1%* and *1.9%* for μ*=0.5%*. This frictional effect is significant and is about 6-times larger than for the short notched beams of Bazant and Pfeiffer (1987), and about 20-times larger than for the longer notched beams recommended by RILEM, for the same value of μ; see Shah and Carpinteri (1991) and 446.1R-91 (2003). This disadvantage of the wedge splitting test is surmountable, and frictional effects can be reduced by (1) attaching hardened steel inserts along the inclined wedge surface, (2) using needle bearings, and (3) carefully polishing the wedge surface as shown by Hillemeier and Hilsdorf (1977) who experimentally determined a μ -value of *0.031%* for their wedge loading set-up with needle bearings.

As Shah and Carpinteri (1991) stated, for the μ*>0.5%,* the frictional effects should be taken into consideration in the evaluation of the test data. However, if the frictional effects can be kept lower that *2%*, it can be neglected and the splitting force is calculated from the measured vertical force as:

$$F_{sp} = \frac{F_v}{2.\tan\alpha} \tag{5.2}$$

However, since the value of the friction coefficient is often quite uncertain, it is better to measure the splitting force, F_{sp}, directly by instrumenting the wedges and the shafts that carry the bearings with strain gages. The foregoing analysis shows that a very small wedge angle, α, is unfavorable from the viewpoint of friction. The angle $\alpha=15^{\circ}$ is a reasonable compromise. Also, a large wedge angle, $\alpha>30^{\circ}$, is undesirable because it leads to a significant normal stress parallel to the crack plane in the fracture process zone. The presence of such stresses may affect the softening curve for the fracture process zone, and the area under the softening curve is then no longer equal to the fracture energy, G_f, nor to the area under the load-displacement curve; see ACI 446.1R-91 (2003).

5.3 Determination of the Fracture Energy and the *σ-w* Relationship

Basically, the fracture energy, G_F, is calculated from the area under the splitting force versus CMOD curve divided by the fracture surface. The fracture surface in the WST specimen is obtained by l_{ligament} times *Width* of the specimen; see Figure 5.4(a). The input energy could be obtained from the area under the vertical force versus actuator displacement, *u*-curve. From theoretical point of view, the input energy and the fracture energy should be the same, but larger energy is determined from the vertical load vs. vertical displacement curve. Because the vertical displacement includes not only the specimen displacement but also testing machine displacement, thus the energy calculated based on the total vertical displacement is larger than the fracture energy. It should be noted that, in the WST, the effect of self-weight is negligible even for large specimens; this is an important advantage compared to the Three-point Bending Test (3PBT), where the fracture energy due to the self-weight of the beam reaches up to *40 – 60 %* of the total fracture energy; see Shah and Carpinteri (1991).

The contribution of the vertical force, F_v, in the fracture energy should also be taken into consideration. During the loading, when the specimen opens, the place of resultant undergoes some displacement in the vertical direction as well; see Figure 5.4(b). The energy, dissipated in the vertical direction, can be estimated from the area under the F_v versus vertical displacement curve, which is obtained by comparing the geometrical situation of the untracked (zero crack opening displacement) with the cracked (crack opening displacement of some finite value) specimen. A portion of *5%* to *9%* of the fracture energy, obtained under the F_s – CMOD curve, was estimated for the cubical and cylindrical specimen by Shah and Carpinteri (1991). Based on the analysis, done in the current project, this value was approximated about *7.5%* for cubic specimen of $150x150x150\ mm^3$; for the detail calculation see Chapter 6. The more the load point is away from the axis of symmetry, the more important is this contribution (cylindrical specimen), and a very long WST specimen would correspond to the 3PBT beam; see Figure 5.4(c).

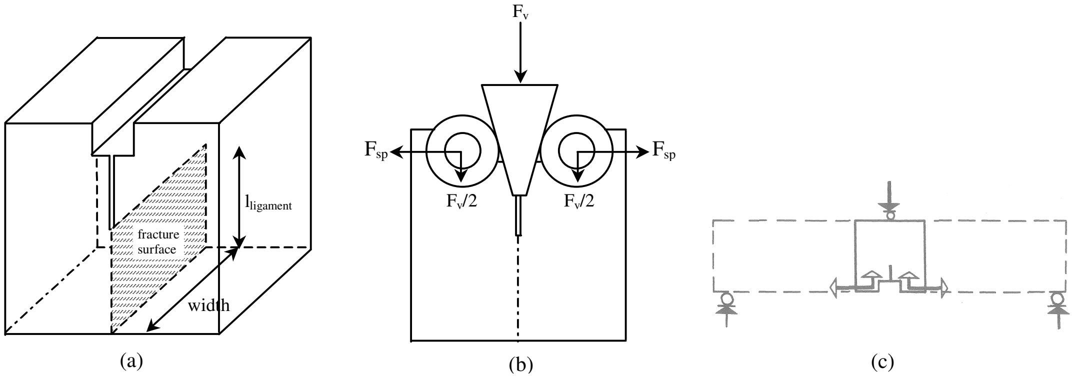

Figure 5.4 WST specimen, (a) Fracture surface, (b) Vertical and horizontal component of force, (c) Wedge splitting specimen as a ''compact'' three-point-bending test; from Shah and Carpinteri (1991)

In order to determine *σ-w* relationship, the approach which has been developed by Löfgren (2005) can be used. The approach has been developed for FRC and includes three steps: (1) the material testing, e.g. the WST or the 3PBT; (2) inverse analysis (using non-linear fracture mechanics) where the *σ-w* relationship is determined; and (3) adjustment of the *σ-w* relationship for any differences in fiber efficiency (the number of fiber) between the experiment and random 3-D orientation or the member where the material is to be used. The same approach, but without the inverse analysis step, may be used for the uni-axial tension test.

Material Testing

The general requirements that has been stated by Löfgren (2005) for the first step, i.e. material testing, are as follows:

- The material testing must provide results which readily can be interpreted as constitutive material parameters (the *σ-w* relationship).
- It should, preferably, provide a relationship between load and crack opening (or CMOD) which can be used for inverse analysis.
- The specimen should be designed such that a single, well-defined crack is formed, which generally means that the specimen has to be equipped with a notch of sufficient dimension.
- It should give representative values;
- It should, if possible, not require an advanced testing equipment or demand a high machine stiffness.
- It should be easy to handle and execute.
- The specimen size should be as small as possible but still be representative.

Inverse Analysis

The σ-w relationship can be determined by bi-linear, exponential or poly-linear (multi-linear) approximation; see Figure 5.5. Inverse analysis is achieved by minimising the difference between calculated displacement and target displacement, e.g. CMOD, obtained from test results; see Figure 5.6. The results taken from the 3PBT and the WST, can be analysed by inverse analysis in order to determine the σ-w; for more comprehensive review of inverse analysis the reference is made to Löfgren (2005).

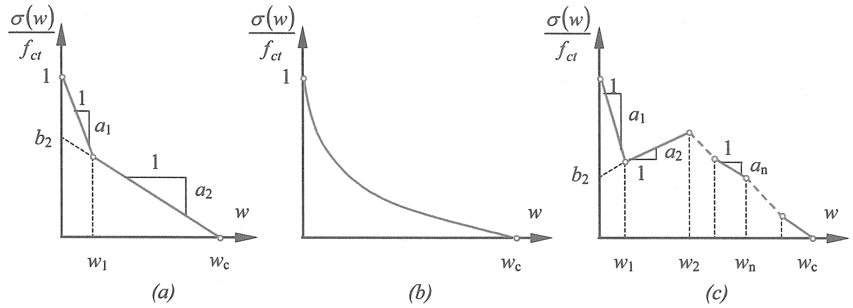

Figure 5.5 Different σ-w relationship: (a) bi-linear; (b) exponential; and (c) poly-linear (or multi-linear); from Löfgren (2005).

In the present project, the bi-linear approximation of the σ-w relationship is investigated by inverse analysis for both plain and fiber reinforce concrete. The recommendations, proposed by Löfgren (2005), has been taken into consideration when the inverse analysis was performed on FRC; see Chapter 6.

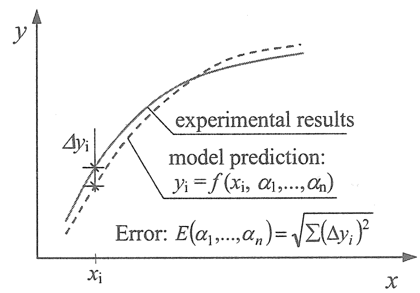

Figure 5.6 Principle of inverse analysis; from Löfgren (2005)

Adjustment of the *σ-w* relationship for fiber efficiency

The last step is to adjust the σ-w relationship for specific fiber efficiency by considering the actual number of fibers crossing the fracture surface. Löfgren (2005) has shown that the specimen size, in relation to the fiber length, has a considerable impact on the fiber efficiency factor. He has also shown that if the material test specimen, used for material characterisation, has a more or less random 3-D fiber orientation but with a different fiber efficiency factor compared to random 3-D; an experimentally determined fiber efficiency factor, $\eta_{b.exp}$, can be used to modify the stress-crack opening relationship so that it more closely corresponds to that of a completely random 3-D orientation. A linear relationship between the number of fibers and the fiber bridging stress exists and it is possible to adjust the σ-w relationship obtained from inverse analysis, $\sigma_{b.exp}(w)$, considering the difference in fiber efficiency factor between material test specimen and the theoretical value for random 3-D orientation, $\eta_{b.3\text{-}D}$, according to:

$$\sigma_{b.3-D}(w) = \sigma_{b.\exp}(w).\frac{\eta_{b.3-D}}{\eta_{b.\exp}} \tag{5.3}$$

Where $\sigma_{b.3\text{-}D}(w)$ is the σ-w relationship for random 3-D orientation,

$\sigma_{b.exp}(w)$ is the σ-w relationship obtained from inverse analysis (experimental data),

$\eta_{b.exp}$ is the experimentally determined fiber efficiency factor, and

$\eta_{b.3\text{-}D}$ is the theoretical fiber efficiency factor for the 3-D case, which is equal to 0.5; see Löfgren (2004).

The Equation (5.3) provides the σ-w relationship for random 3-D orientation, $\sigma_{b.3\text{-}D}(w)$. The experimental fiber efficiency factor, $\eta_{b.exp}$, for the material test specimen can be determined by counting the number of fibers crossing the fracture plane and calculating with the following experiences:

$$\eta_{b.\exp} = \frac{N_{f.\exp}}{V_f / A_f} \tag{5.4}$$

Were $N_{f.exp}$ is the number of fibers per unit area,

V_f is the fiber volume fraction, and

A_f is the cross-sectional area of a fiber.

Since the number of fibers crossing a crack has a significant influence on the toughness and the σ-w relationship the approach explained above is used in this project; see Chapter 6.

5.4 Applications of the WST (Overview on Experimental Results)

Researches have used the WST method to investigate the fracture properties of different types of concrete and recently there has been an increasing interest in this method. The method has proved to be applicable for the determination of fracture properties of ordinary concrete, at early age and later (Østergaard, 2003, Abdalla and Karihaloo, 2003, and Karihaloo *et al.*, 2004), for autoclaved aerated concrete (Trunk *et al.*, 1999), and for polymer cement concrete (Harmuth, 1995). It also has been applied for ultra high strength concrete (Xiao *et al.*, 2004), crushed limestone sand concrete (Kim *et al.*, 1997), polypropylene fiber reinforced concrete (Elser *et al.*, 1996), and steel fiber reinforced concrete (e.g. Löfgren, 2005). This method has been used to investigate other properties of concrete rather than fracture properties, e.g. determination of stress-crack opening relationships of interfaces between steel and concrete (Lundgren *et al.*, 2005, and Walter *et al.*, 2005), determination of size effect in the strength of cracked concrete structures (Karihaloo *et al.*, 2005), fracture of rock-concrete (Kishen *et al.*, 2004), numerical evaluation of cohesive fracture parameters (Que *et al.*, 2002), and stability of the crack propagation associated with the fracture energy (Harmuth, 1995).

The WST method has also been used by a few researchers to investigate the fatigue behavior of concrete, and its applicability for dynamic loading is not approved yet. The results of two researches, done by the wedge splitting test on the fatigue behavior of concrete, are described in this section.

Wedge splitting tests were carried out for the investigation of low cycle fatigue crack growth behaviour of high strength concrete by Jin-Keun Kim (1999). On the basis of the comparison between the test data and the predicted curve of fatigue crack growth, it was found that the empirical-model predictions and the test data were in good agreement. However, the differences, between the test data and the predicted numerical values, are because of the inherent feature of fatigue failure (i.e., wide scatter of fatigue life data).

Another wedge splitting test was performed to study the fracture behavior of concrete under cyclic loading by Rossi (1986). Geometrically similar specimens with different sizes were adopted. In the experiments, the specimens were pre-cracked and a fracture process zone was present. Specimens of both normal and high strength concrete with sinusoidal steel fibers were investigated. Results show a strong influence of the fracture process zone on damage accumulation, improve performance of high strength concrete, and the size effect on fracture behavior of concrete under cyclic loading.

6 EXPERIMENTAL INVESTIGATIONS

6.1 Tests Program

In order to investigate the fatigue behaviour of concrete by the wedge splitting test method, three different concrete compositions were tested: (1) a plain concrete; (2) a steel fiber reinforced concrete (steel FRC); and (3) a synthetic fiber reinforced concrete (synthetic FRC). More over, to characterize the materials four different kinds of testing condition were applied. Compressive strength was calculated from the compressive strength test method (cubic) and the tensile strength was estimated from both compressive test and splitting test method (cubic). The fracture properties of concrete, including F_{sp}-*CMOD* relationship, fracture energy, and σ-w relationship were investigated by a combination of the WST method under monotonic loading and by conducting inverse analyses. Finally, the fatigue behaviour of the three types of concrete was investigated using the WST-method under low cyclic fatigue loading and by conducting inverse analyses.

In the following sections, the concrete mixture of the tested concrete composites, tests set-up, and experimental results for monotonic loading and cyclic loading, interpreted by inverse analysis, are presented. The result of numerical investigations and comparison between numerical and experimental results are not included in this chapter.

6.2 Concrete Mix Composition

Although the material composition of a concrete, consisting of cement, additives, superplasticizer, aggregates, and fibers, has significant influence on the fatigue and fracture behaviour of concrete (see sections 3.4 and 3.5) it was not within the scope of this study to consider these effects. Hence, during the experimental investigation, all material variations have been excluded and the inclusion of two types of fiber has been taken into consideration. The mix composition of the three concrete types is presented in Table 6.1.

In this study, a total number of 48 specimens, for three types of concrete compositions, were manufactured at Thomas Concrete Central laboratory and then shipped to Chalmers laboratory for mechanical tests. After casting, the specimens were covered with plastic and stored in a climate room with a constant temperature of 20˚C and relative humidity of 65%. The specimens were shipped after two weeks to the mechanical testing laboratory at Chalmers where they were stored in water until the time of testing. Two weeks prior to testing the notches were prepared by using a wet diamond saw. For the plain concrete and steel fiber reinforced concrete, six specimens were prepared for monotonic loading and three specimens were used for cyclic loading by WST method. For synthetic fiber reinforce concrete, the behaviour under monotonic and cyclic loading was investigated using three specimens for each loading case by the same method. For the plain and steel fibre reinforced concrete, the compressive strength and splitting tensile strength were evaluated from 3 cube specimens ($150\times150\times150$ mm^3) in each case. The tensile strength of the synthetic

FRC was estimated from its compressive strength and a separate splitting test was not conducted.

Since flow properties of concrete are of importance (particularly for a self-compacting concrete), rheology tests were conducted using a rheometer (Viscometer 5 type BML) and the results are presented in the Table 6.1; for the test method see Section 6.3.

Table 6.1 Concrete mix composition

Constituents	**Type**	**Density**	**Plain Concrete**	**Steel FRC**	**Synthetic FRC**
Cement	CEM I 42,5N ANL (Degerham)	3150	400	400	400
Water	Drinkable	1000	160	160	160
Water/binder ratio	---	---	0.4	0.4	0.4
Sand 0-4	Sea sand	2670	478	478	474
Sand 0-8	Östad	2670	478	478	474
Gravel 8-16	Tagene	2700	644	639	627
Filler	Lime (L40)	2670	190	190	190
Fiber I	Dramix™ 65/35	7850	---	39.3	---
Fiber II	Barchip MACRO	910	---	---	4.55
Superplasticizer	Sikament 56	1100	4.8	4.8	4.8
Air-entraining	SikaAir-s	1001	0.8	0.8	0.8
Time of	---	---	20	15	10
Flow Speed [mm]	---	---	715	700	760
T50 [s]	---	---	6.0	10	6.0
Viscosity [Pa s]	---	---	136.7	---	83.2
Yield Stress [Pa]	---	---	56	---	3
Separation [%]	---	---	4	---	-3

*All values for mix compositions are in [kg/m^3]

6.3 Test Set-up

Set-ups for two tests, the rheology test and Wedge splitting test, are explained in this section.

Rheology Test

The Rheological properties of concrete were determined using a rheometer (Viscometer 5 type BML), which was developed by Wallewik at IBRI (Island). In this test method, concrete is placed between two concentric cylinders. The outer cylinder rotates in an oscillatory mode; frequency and amplitude are selected by the operator. The torque induced by the movement is measured in the inner cylinder. This configuration allows the operator to calculate the viscosity and the yield stress of the concrete as a function of frequency. The advantageous of this instrument is that it allows the operator to calculate the intrinsic values of the material. The result of this test is shown in Table 6.1 for three types of tested concrete.

Wedge-Splitting Specimens

According to Löfgren (2004), who has used WST method to investigate fracture properties of steel fiber reinforced concrete, for short fibers, maximum length of 30 mm, a 150 mm WST specimen should be sufficient. However, the specimen size seems to have some effect on the scatter. The scatter is smaller for a 200 mm specimen due to a larger fracture area.

Since the Steel fibers used in this investigation were of the type with hooked end, from Dramix™: RC-65/35-BN (length of 35 mm, diameter of 0.55 mm, and tensile strength of 1100 MPa), then a WST specimen with the following dimensions was used in this study, see Figure 6.1.

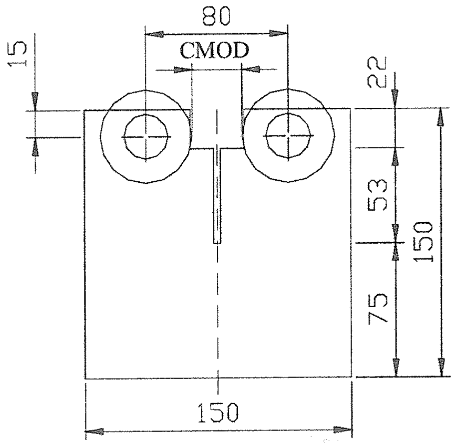

Figure 6.1 The geometry of the wedge splitting specimens used in this study, specimen thickness is 150 mm.

6.4 Experimental Results for Monotonic Loading

The result of compressive test, tensile test, wedge splitting test under a monotonic loading, and inverse analysis are presented as follows:

Compressive and tensile strength

Based on the test results from compressive and tensile tests, the properties of three types of concrete were calculated according to CEB-FIP Model Code 1990; see Table 6.2. Each property was determined as the average value of three specimens. In the case of compressive strength, the coefficient of variance for plain concrete, steel FRC, and Synthetic FRC are 3.3%, 1.9%, and 0.4%, respectively. While the coefficient of variance for tensile tests are 5.5% and 7.0%, for plain concrete and steel FRC, respectively. The tensile strength from splitting test was calculated based on BBK 94, Boverket (2003),using a coefficient of 0.8.

Table 6.2 Properties of tested concrete according to CEB-FIP Model Code 1990.

Concrete Type	Age at the time of testing	Compressive Strength	Tensile Strength (from compressive test)	Tensile Strength (from splitting test)	Modulus of Elasticity E_{ci} - E_c
	[Day]	[MPa]	[MPa]	[MPa]	[GPa]
Plain Concrete	50	80.6	4.4	4.5	43.1-36.6
Steel FRC	50	94.5	4.9	6.3	45.5-38.6
Synthetic FRC	50	86.0	4.6	---	44.0-37.4

Wedge splitting test under the monotonic loading

The load history and CMOD history of the monotonic tests are shown in Figure 6.2. For all three types of concrete, the experiments were loaded under a force control regime until the vertical force reached -500N. Then the test was continued under a CMOD control regime till a CMOD of 2.25 mm. The program of the monotonic and cyclic loading is presented in Appendix C.

The test results from the WST specimens under the monotonic loading are presented in Figure 6.3 (a) to (d). It was found that the scatter in the test results was quite large and the coefficient of variance could be as high as 34%, 27%, and 29% for plain concrete, steel FRC, and Synthetic FRC, respectively; see Figure 6.4. It is believed that a major factor contributing to the large scatter in the test results is related to variation in orientation and distribution and the inherent variation in plain concrete. For steel fiber reinforced concrete, a scatter of the test result as high as 40% has been reported by Löfgren (2005). When counting the number of fibers crossing the fracture plane it was found that it exceeded the theoretical value for random 3-D orientation in all steel FRC specimens. Based on the theory explained in the section 5.3, the average fiber efficiency factor was 0.54, which will be used in order to adjust the σ-w relationship after inverse analysis. The coefficient of variance for the number of fibers crossing the fracture surface was 22%; this value has been reported between 10 and 30% for steel FRC by Löfgren (2005).

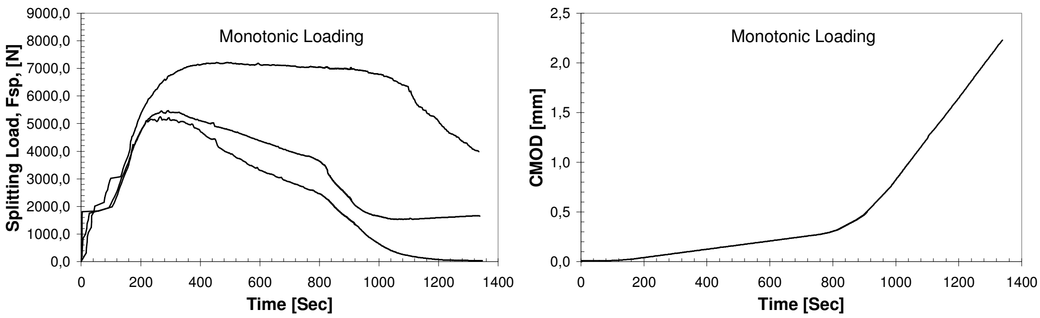

(a) *(b)*

Figure 6.2 *(a) Splitting load history and (b) CMOD history of the WST specimens under the monotonic loading for the three types of concrete.*

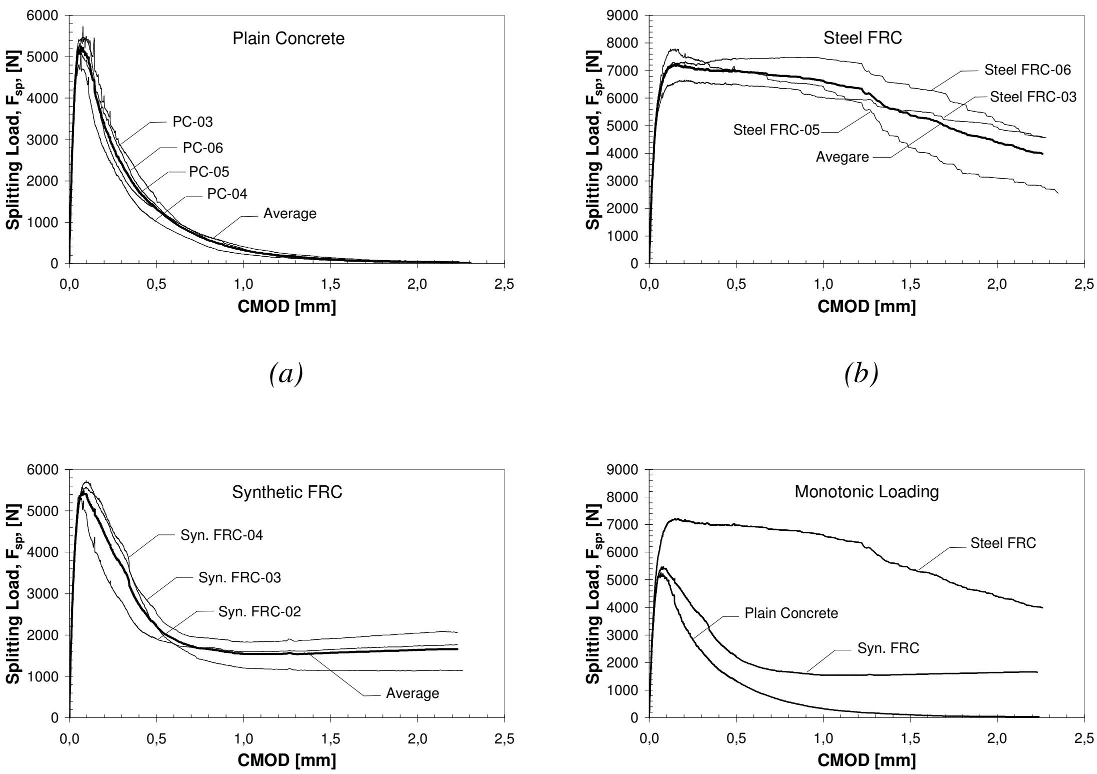

(a) *(b)*

(c) *(d)*

Figure 6.3 *Typical result from the WST experiments under monotonic loading, splitting force versus CMOD for: (a) Plain concrete, (b) Steel fiber reinforced concrete, (c) Synthetic fiber reinforced concrete, (d) Comparison of the results for all the three cases.*

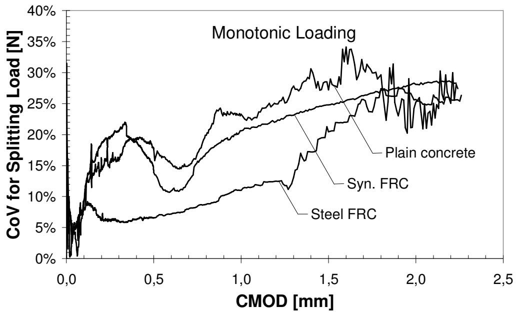

Figure 6.4 Comparison of the scatter in the test result for the monotonic loading, coefficient of variance (CoV).

Based on the experimental data, the dissipated energy was calculated versus CMOD; see Figure 6.5. Apparently, the energy dissipation for steel FRC is much greater than the plain concrete and synthetic FRC. In the case of plain concrete, the energy dissipation reaches approximately a constant value at CMOD of 1.3 mm (indicating an almost completely fractured specimen) while for the steel FRC and synthetic FRC, the energy dissipation keeps increasing until CMOD of 2.24 (where the test was stopped). At CMOD of 2.24 mm, the energy dissipation in steel FRC is 8.2 and 6.7 times greater than the energy dissipation at the same CMOD in the plain concrete and synthetic FRC, respectively. Of interest is that a 150 Nm/m^2 of energy dissipation corresponds to CMOD of 2.24, 0.64, and 0.26 mm in plain concrete, steel FRC, and synthetic FRC, respectively. This behaviour is explained based on the action of fiber bridging and fiber pullout in fiber reinforced concrete, which dissipates the energy in the wake of the crack tip; see sections 4.4, 4.5, and 4.6 for more explanation.

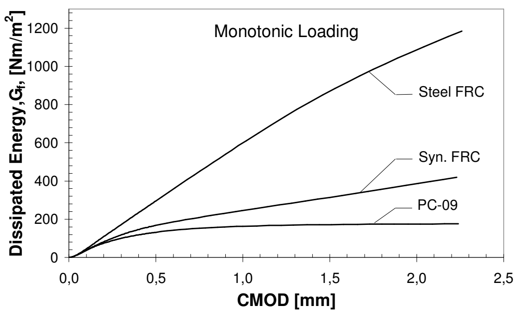

Figure 6.5 Effect of steel and synthetic fiber inclusion on the dissipated energy at different CMODs.

Inverse analysis

The inverse analysis were conducted by using a Matlab® program developed at DTU by Østergaard (2003). The program determines a bi-linear relationship based on the crack hinged model, developed by Olesen (2001); see Østergaard and Olesen (2004). The response was determined until CMOD of 2.24 mm (for which the experimental data was available). However as steel FRC and synthetic FRC meet larger CMOD (if the tests were continued), the slope of the second line in σ-w relationship may not be correct and it is not reasonable to calculate the critical crack opening, w_c, based on the estimated σ-w relationship. Basically, the test can be continued until a CMOD equal to half a fiber length where it reaches the critical crack opening. Otherwise it is recommended to rely on the estimated σ-w relationship until half the proceeded CMOD.

The result from the experiment and the inverse analysis for splitting force are presented in Figure 6.6 to Figure 6.8 for the plain concrete, steel FRC, and synthetic FRC, respectively. In these figures, the ratio between the experiment and the inverse analysis showing the relative error is also shown. Furthermore, these ratios, for three types of concrete, are compared in Figure 6.9. As can be seen in these figures, the agreement between experiments and the inverse analysis is not constant along the CMOD axis, and also the pattern varies for types of concrete. In the case of plain concrete, the ratio is limited between 0.89 and 1.07 for CMODs lower than 1.0 mm. After a CMOD of 1.0 mm, the ratio keeps increasing up to 1.85 at the CMOD of 2.0 mm; see Figure 6.6 (b). By using a multi-linear approximation of the σ-w relationship, it may be possible to reach better agreement. The ratio of the splitting loads, for the steel FRC and synthetic FRC dose not show significant difference along the CMOD axis compared with the plain concrete; although there are some peak points corresponding to the high ratio of analytical and experimental splitting force. These ratios are between 0.95 and 1.05 for the both steel and synthetic FRC, except for a region around CMOD of 0.03 to 0.04 mm, in the case of synthetic FRC.

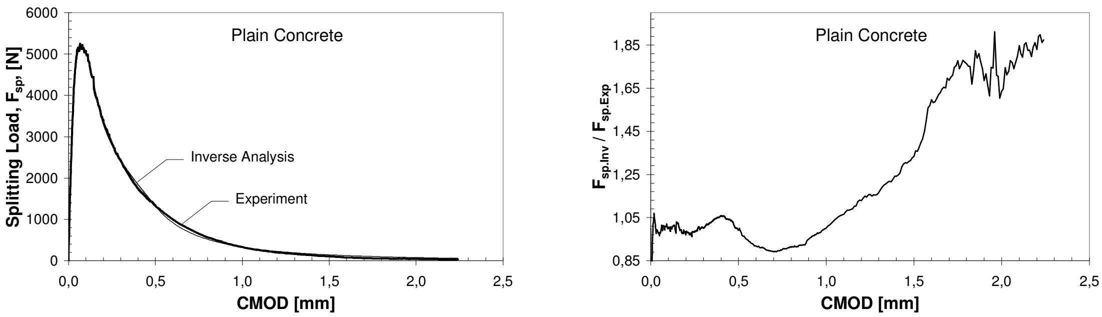

(a) *(b)*

Figure 6.6 *Comparison of the results from the experiment and inverse analysis for the plain concrete: (a) the splitting load (b) fraction of the splitting loads taken from the experiment and inverse analysis.*

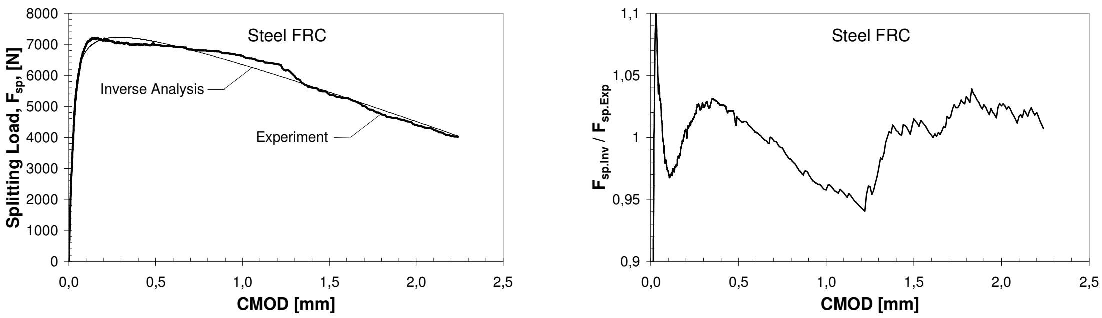

(a) *(b)*

Figure 6.7 Comparison of the results from the experiment and inverse analysis for the steel FRC: (a) the splitting load (b) fraction of the splitting loads taken from the experiment and inverse analysis.

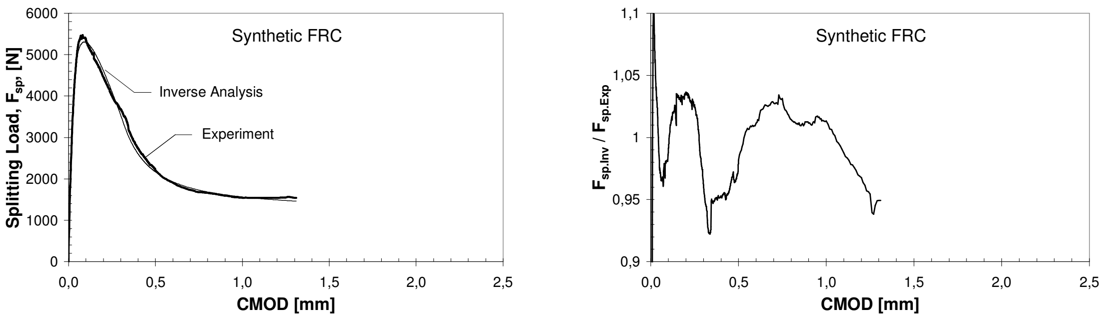

(a) *(b)*

Figure 6.8 Comparison of the results from the experiment and inverse analysis for the synthetic FRC: (a) the splitting load (b) fraction of the splitting loads taken from the experiment and inverse analysis.

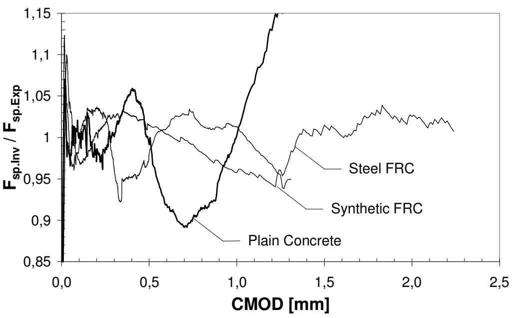

Figure 6.9 Comparison of the fraction of the splitting loads taken from the experiment and inverse analysis for the three types of concrete.

The result from the experiments and the inverse analysis for dissipated energy are presented in Figure 6.10 to Figure 6.12 for the three types of concrete. In these figures, the ratio between the experiment and the inverse analysis is also shown. Furthermore, these ratios, are compared in Figure 6.9. As can be seen in these figures, not similar to the ratio between splitting loads, the agreement between experiments and the inverse analysis for dissipated energy is good and constant along the CMOD axis for all three concrete types. In the case of plain concrete, the ratio is limited between 0.98 and 1.02, except for a region of very small CMOD before the peak load. The disagreement observed in the splitting loads of plain concrete with CMOD of higher than 1 mm, Figure 6.6 (b), cannot be seen in Figure 6.10 (b). The reason could be for the small values of splitting load after the CMOD of 1mm, which yield small fracture energy. Similar to the plain concrete, the ratio of the dissipated energy for the steel FRC and synthetic FRC dose not show significant difference along the CMOD axis; although there is a peak region corresponding to the high ratio of the analytical and experimental dissipated energy for a very small CMOD.

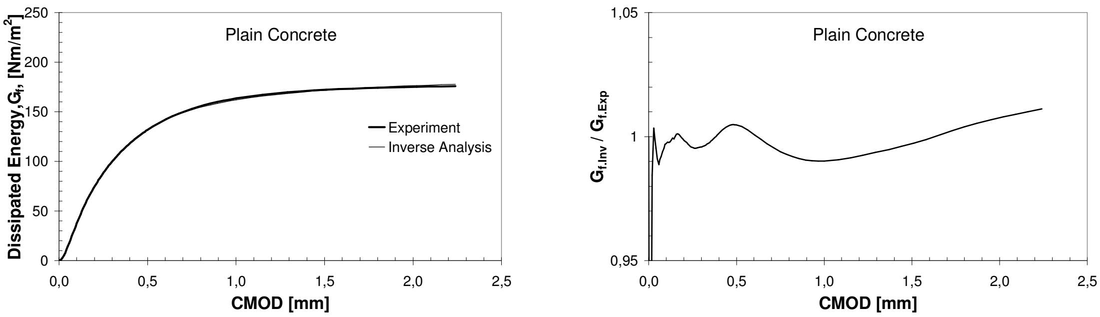

(a) *(b)*

Figure 6.10 Comparison of the results from the experiment and inverse analysis for the plain concrete: (a) the dissipated energy (b) fraction of dissipated energies taken from the experiment and inverse analysis.

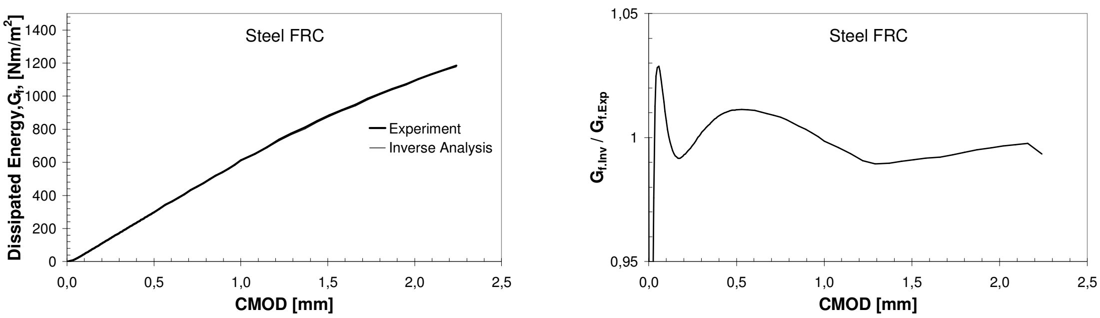

(a) *(b)*

Figure 6.11 Comparison of the results from the experiment and inverse analysis for the steel FRC: (a) the dissipated energy (b) fraction of dissipated energies taken from the experiment and inverse analysis.

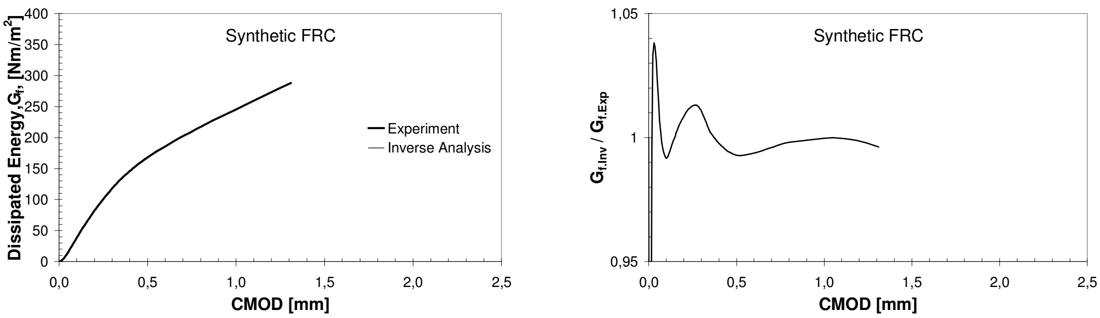

(a) *(b)*

Figure 6.12 Comparison of the results from the experiment and inverse analysis for the synthetic FRC: (a) the dissipated energy (b) fraction of dissipated energies taken from the experiment and inverse analysis.

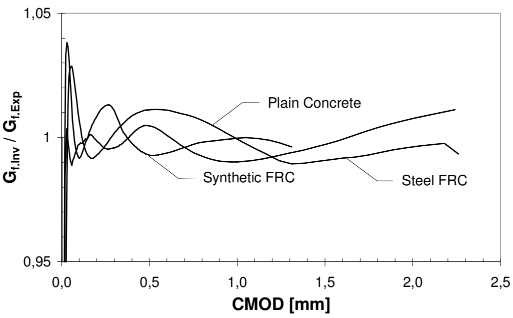

Figure 6.13 Comparison of the fraction of the dissipated energy taken from the experiment and inverse analysis for the three types of concrete.

The stress-crack opening relationship were determined by conducting inverse analysis on the results from the WST under monotonic load and adjusted using the fiber efficiency factor. The bi-linear stress-crack opening relationships are presented in Figure 6.14. It should be noted that, the inverse analysis does not respond well for the synthetic FRC. It is mainly for the hardening behaviour of the synthetic FRC after CMOD of 1.3 mm. The experimental results show that after the CMOD equal to 1.3 mm, the splitting load increases by 7.7 % till it reaches the end of the experiment, i.e. CMOD of 2.24 mm. In fact the inverse analysis stops at this point where the hardening behaviour appears. It suggests a negative slope for the second estimated line, a_2, however the Matlab® program limits this slope to a positive value, therefore the analyses was stopped automatically before the line with negative slope starts.

From Figure 6.14 it is observed that inclusion of both steel and synthetic fibers significantly changes the shape of the stress-crack opening relationship. As explained before, the exact critical crack opening, w_c, can not be calculated from the estimated σ-w relationship as the test were just proceeded until CMOD of 2.24 mm as it only provides information of the σ-w relationship for crack openings up to about 1 mm.

However, it can be concluded that fibers affect the σ-w relationship so that the zero stress is reached at significantly larger crack openings compared to the plain concrete.

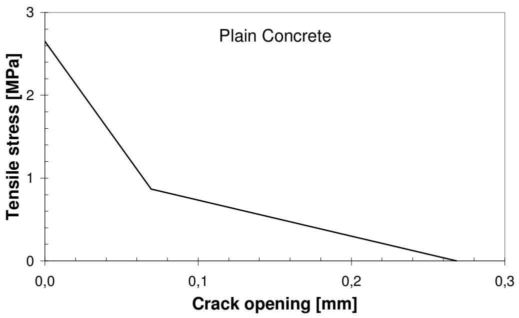

(a)

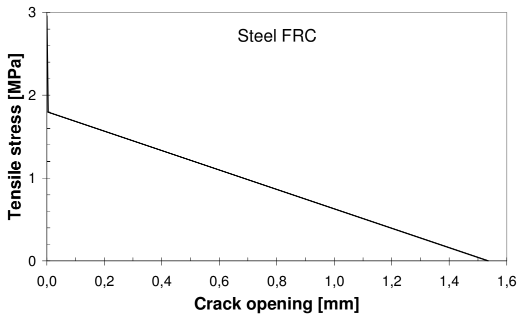

(b)

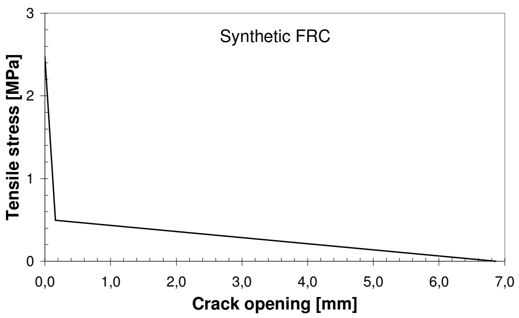

(c)

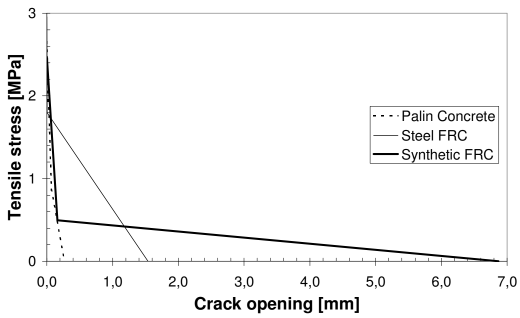

(d)

Figure 6.14 Bi-linear σ-w relationship for (a) plain concrete (b) steel FRC (c) synthetic FRC (d) comparison of all three types of concrete.

6.5 Experimental Results for Dynamic Loading

Since the aim of this research was to investigate the applicability of the WST method for fatigue loading, the main attention was paid to this part. It should be noted that the MTS machine, which was used for the WST specimens under both monotonic and cyclic loading, is very sensitive and precise tuning should be done. A brief description of how to work and tune the testing machine for the explained test method is attached to this report; see Appendix D.

The load history and CMOD history of the cyclic test are shown in Figure 6.15 and Figure 6.16. For all three types of concrete, the experiments were loaded under a displacement control regime. Similar to the monotonic tests, the cyclic tests were supposed to be loaded under a CMOD control regime, but as the results where unstable, a vertical displacement controlled loading was applied and more stable results were obtained.

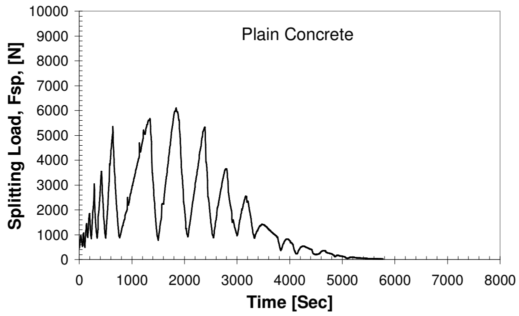

(a)

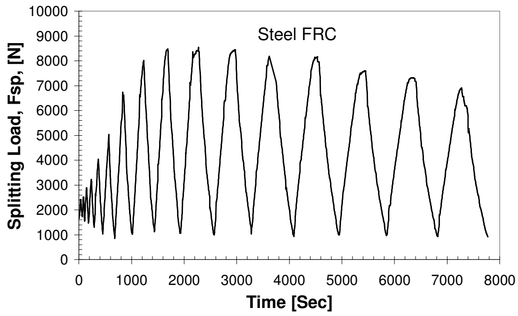

(b)

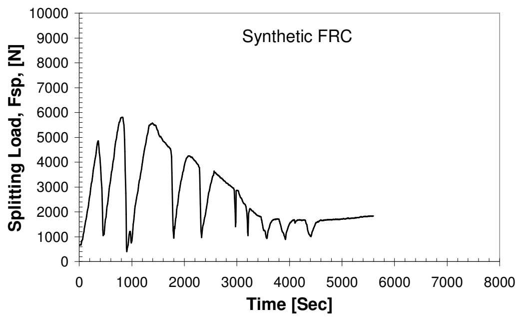

(c)

Figure 6.15 Splitting load history of the WST specimens under the cyclic loading for (a) plain concrete, (b) steel FRC, and (c) synthetic FRC.

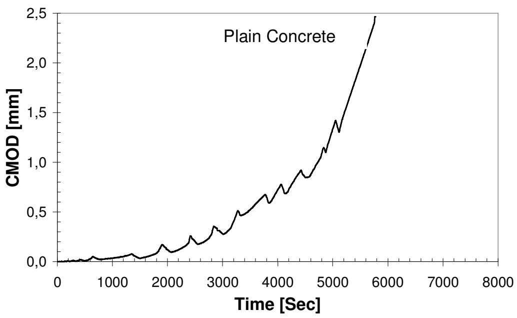

(a)

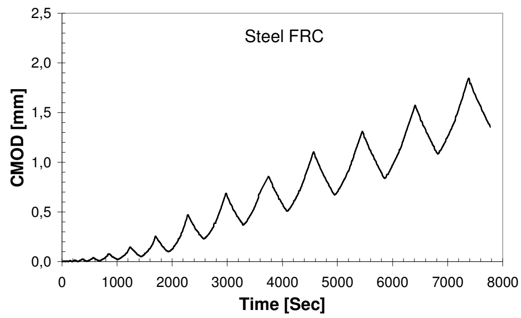

(b)

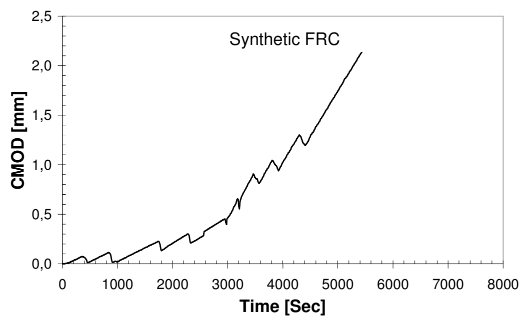

(c)

Figure 6.16 CMOD history of the WST specimens under the cyclic loading for (a) plain concrete, (b) steel FRC, and (c) synthetic FRC.

The test results from the WST specimens under the low-cycle fatigue loading are presented in Figure 6.17. Since some specimens have been used to tune the MTS machine for cyclic loading, just one complete experiment data for each type of concrete is presented here. As it can be seen from the diagrams, the energy dissipation under the cyclic loading slightly increases by inclusion of the synthetic fibers into the plain concrete and remarkably increases by the inclusion of the steel fibers. Based on the mechanisms explained in the former chapters, the addition of fibers is found to have a significant effect on the dissipated energy because of the fiber bridging and fiber pullout actions. The fracture surface of the broken specimens shows a combination action of these tow phenomena. For the steel FRC, approximately 40% of the fibers on the fracture surface were fractured and the rests were pulled out.

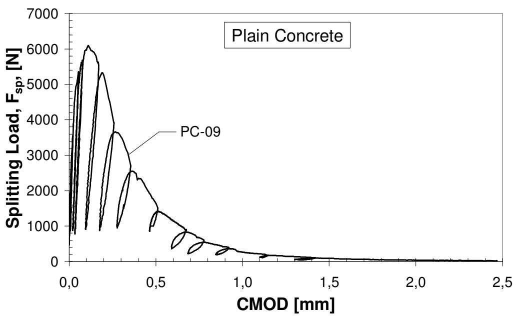

(a)

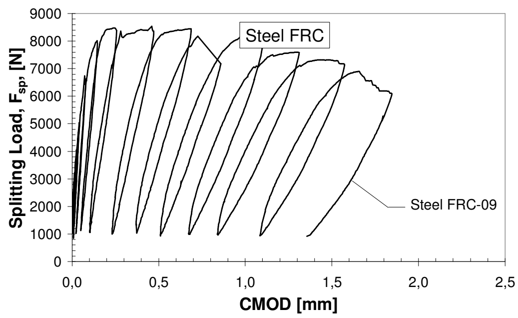

(b)

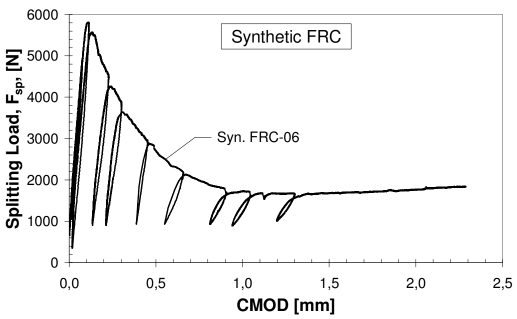

(c)

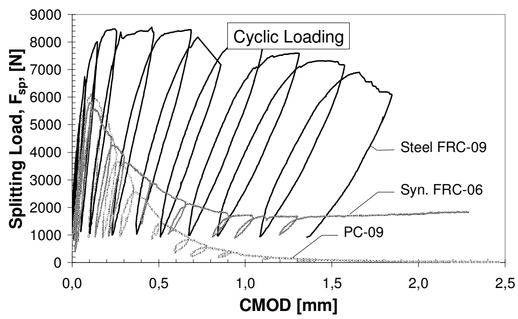

(d)

Figure 6.17 Typical result from the WST experiments under cyclic loading, splitting force versus CMOD for: (a) Plain concrete, (b) Steel fiber reinforced concrete, (c) Synthetic fiber reinforced concrete, (d) Comparison of the results for all the three cases.

The results of monotonic and cyclic loading are presented for each types of concrete in Figure 6.18. In all three cases, no damage can be observed in the cyclic result compared with monotonic result. This may be interpreted by the load history or the scatter of the fatigue result. Since the cycle results are based on one tested specimen, more experimental data for cyclic loading are required to be able to understand the behaviour.

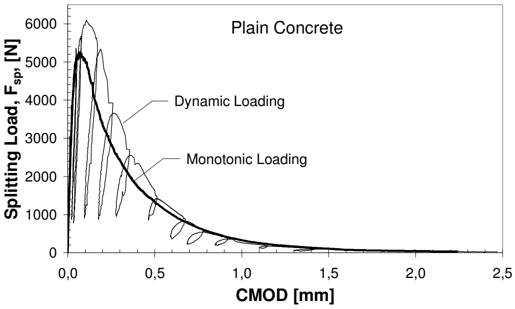

(a)

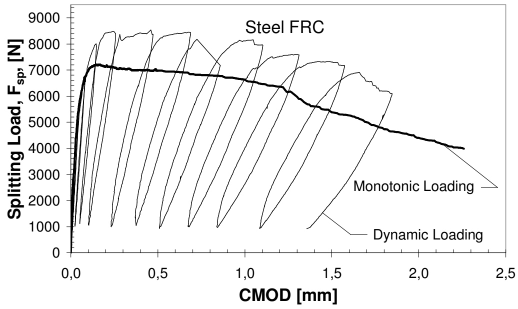

(b)

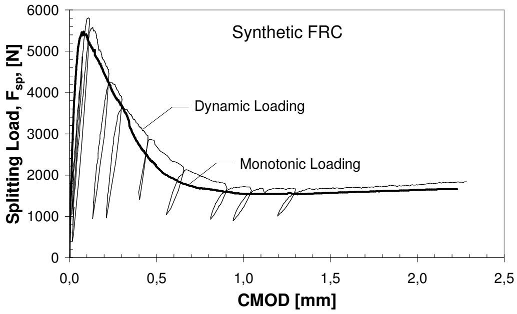

(c)

Figure 6.18 Comparison of the results from the monotonic and cyclic loading for (a) plain concrete, (b) steel FRC, and (c) synthetic FRC.

Inverse analysis

Based on the experimental data, the F_{sp}-*CMOD* curve was divided into 14 cycles of loading and unloading and inverse analysis using Matlab® program was conducted for loading part of each cycle in order to investigate the applicability of inverse analysis for each loading part of a cyclic test. Moreover, estimation of the σ-w relationship for a cyclic test, make it possible to calculate the modulus of elasticity and consequently the stiffness degradation after some specific cycles.

In order to apply the inverse analysis, it was assumed that each reloading path is similar to a monotonic loading. This assumption was fulfilled by determining the splitting force and CMOD of each reloading part and normalizing to a zero splitting force and CMOD; see Figure 6.19. After applying inverse analyses on each reloading, it was seen that the inverse analysis can not estimate the σ-w relationship for the reloadings belonged to those cycles with the splitting force less than 1000 N, i.e. cycles-9 to -14, while the σ-w relationship and stiffness for cycles-3 to -8 seems reasonable.

Elastic modulus was calculated for each cycle; the stiffness degradation is presented in Figure 6.20. It is seen that the stiffness is reducing from 41 for cycle-3 to 10 GPa for cycle-8 in a linear way; see Figure 6.20. The stiffness degradation should be reduced based on the number of cycles, CMOD of unloading, and loading history.

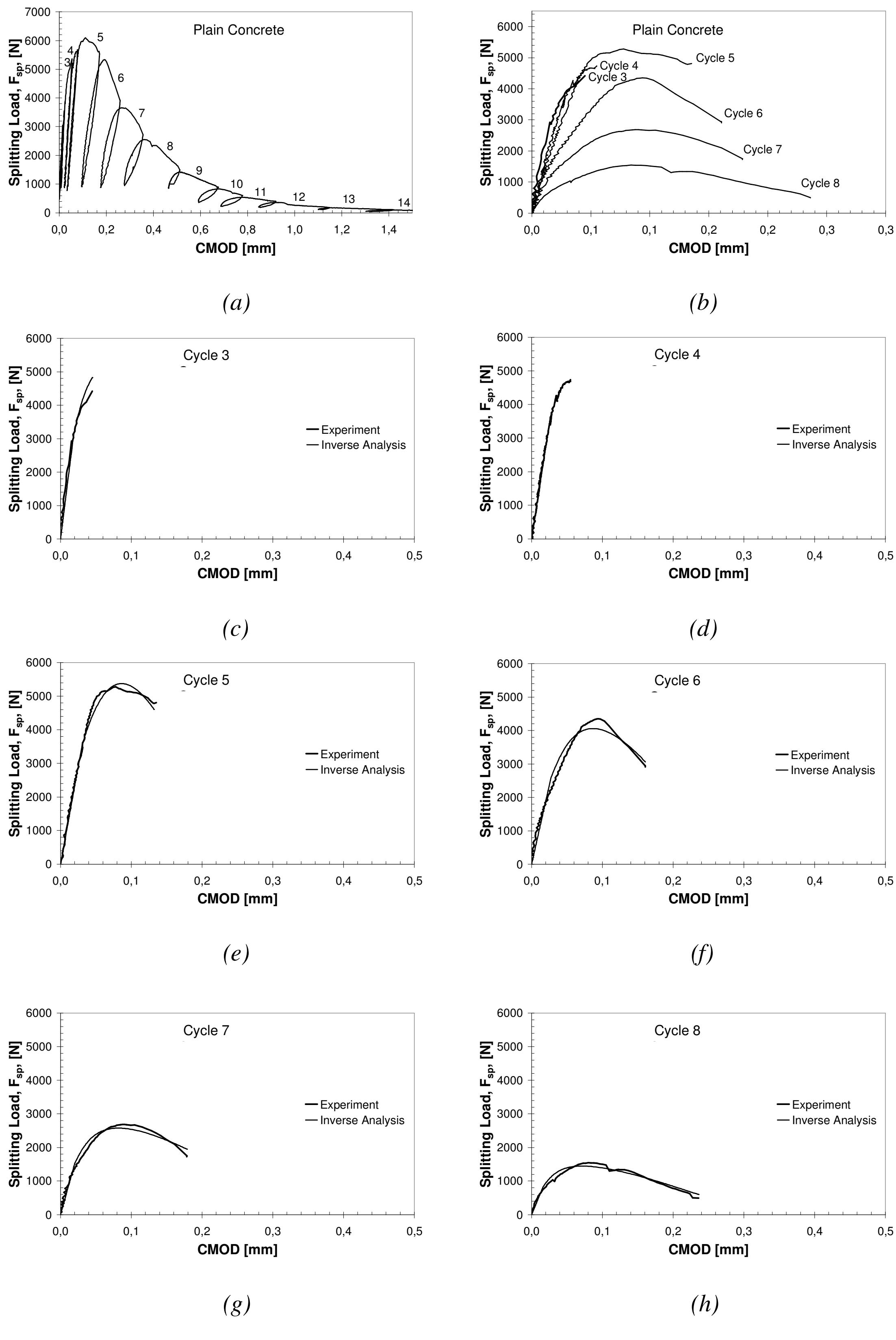

Figure 6.19 Comparison of the results from the experiment and inverse analysis for the plain concrete under cyclic loading for some cycles: (a) cycles numbering, (b) normalized curves and, (c) to (h) cycle-3 to cycles-8.

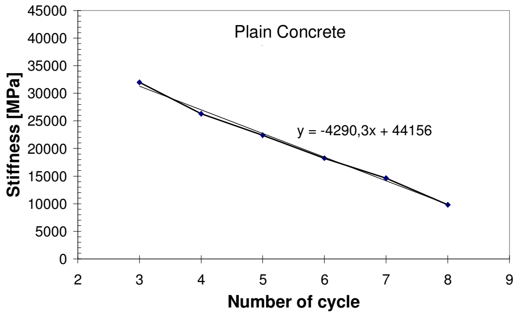

Figure 6.20 Stiffness of each cycle for the plain concrete under the cyclic loading.

7 NUMERICAL INVESTIGATIONS

7.1 Introduction

In Finite Element modelling, the constitution relationships of the materials, the equilibrium conditions and the deformation compatibility functions should be known. Generally, it is relatively easy to apply FE analysis in a continuum but for a cracked concrete element, additional equations to model the crack initiation and propagation have to be induced. The application of fracture mechanics can fulfil this objective. Usually, discrete crack approach and smeared crack approach are mainly adopted in such finite element simulations.

In this study, a WST specimen was modelled by using the finite element program Diana; see Diana User Manuals. From the analyses, F_{sp}-CMOD relationships were investigated for three types of concrete, i.e. plain concrete, steel FRC, and synthetic FRC. These analyses were conducted under monotonic and cyclic loading conditions similar to the experimental load history. In each case the finite element analyses (FEA) were compared with the corresponding experimental results.

In the following sections, the properties and procedures of the FE model will be presented and the FEA results will be compared with the experimental results based on the F_{sp}-$CMOD$, σ-w, and G_f-$CMOD$ relationships.

7.2 Modelling Features

As previously stated, discrete crack models and smeared crack models are two main approaches used in the FE analysis. Early in the application of finite element analysis to concrete structures (Rashid 1968), it became clear that it is often much more convenient to represent cracks by changing the constitutive properties of the finite elements than to change the topography of the finite element grid. The earliest procedure involved dropping the material stiffness to zero in the direction of the principal tensile stress once the stress was calculated as exceeding the tensile capacity of the concrete. Simultaneously, the stresses in the concrete were released and reapplied to the structure as residual loads. Models of this type exhibit a system of distributed or "smeared" cracks. A discrete crack model treats a crack as a geometrical entity. In the FE method, unless the crack path is known in advance, discrete cracks are usually modelled by altering the mesh to accommodate propagating cracks.

In this study, FE analyses were conducted on half a WST specimen, considering the symmetry, with dimensions similar to the experimental specimens; see Figure 7.1. All the elements outside the crack were assumed to have linear elastic and isotropic behaviour, while the crack was modelled as a discrete crack with nonlinear interface elements. The interface elements relate the forces acting on the interface to the relative displacement of the two sides of the interface; see Diana User Manuals – material library, chapter 21. The interface element can be considered as nonlinear springs describing the Mode I fracture properties, furthermore plane stress conditions were assumed. The constitutive law for discrete cracking in Diana is based on a total deformation theory, which expresses the tractions as a function of the total relative displacements, the crack width and the crack slip.

In order to provide symmetrical properties on the interface elements, these elements were fixed in the X direction while they were free to move in the other direction. The support was modelled by constraining the vertical movements. This is presented by a simple support in the figure, which is representative of the real conditions.

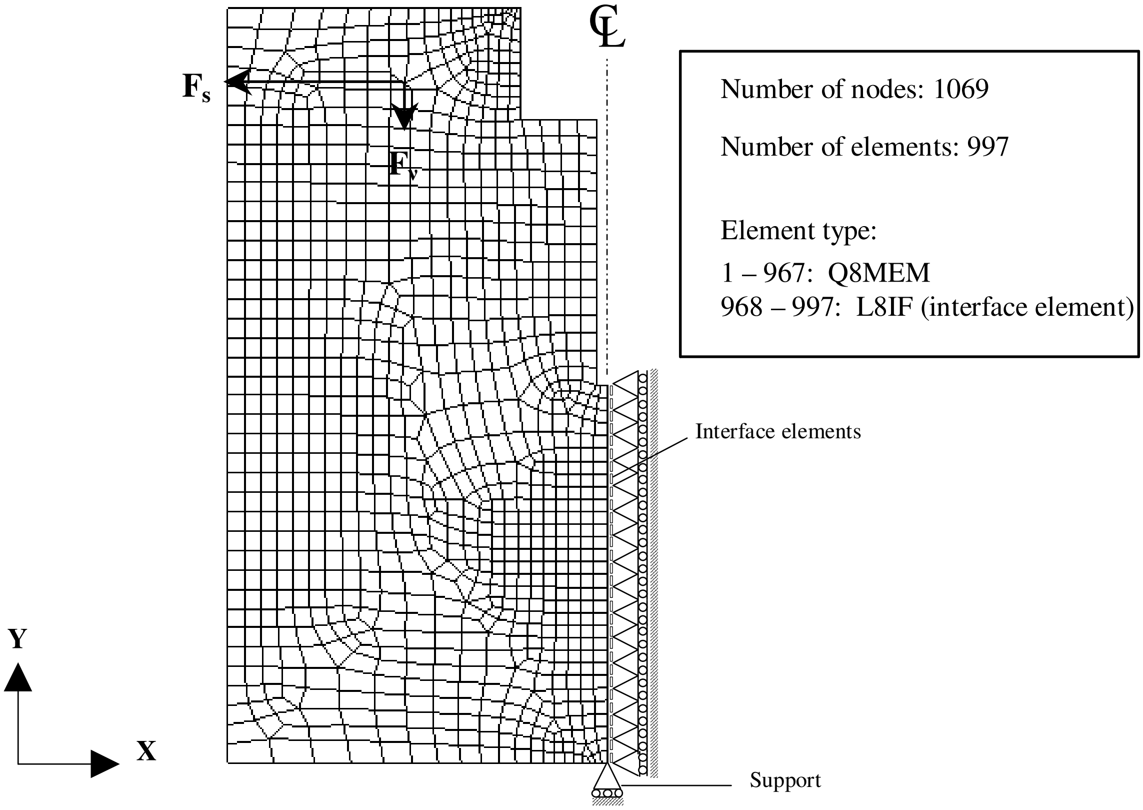

Figure 7.1 Properties of the FE model developed in Diana for half a WST specimen with the dimensions similar to the experimental specimen.

7.3 Modelling Procedure

As previously discussed in chapter 5, in an experiment a wedge splitting specimen is subjected to both vertical and horizontal loads. In this section results of two different loading regimes, with and without the vertical component, are compared to understand and evaluate the effect of the vertical component.

In the first case, an analysis was conducted on a WST specimen under force control regime including both vertical, F_v, and horizontal component, F_{sp}. Based on the Equation 5.4, the splitting force is calculated as $1.866F_v$, providing $\alpha=15°$. In the second case, an analysis was carried out under a deformation control regime consisting of the horizontal deformation. Results of these two analyses are presented in Figure 7.2.

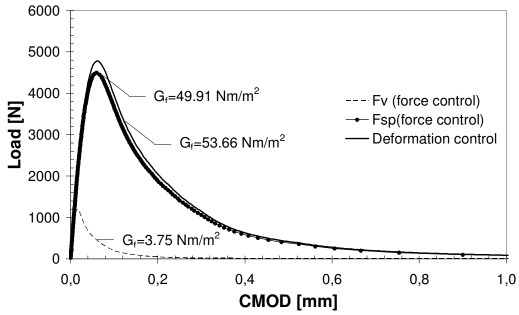

Figure 7.2 Comparison of the load-CMOD relationship for two different loading regime: force control loading regime consisting of both vertical and horizontal component, and deformation control loading regime consisting of just horizontal component.

In the figure above, the dissipated energies were calculated: for the case of the force control analysis this corresponds to the total area under the F_V-CMOD and F_{sp}-CMOD curves; and for the case of the deformation control analysis it corresponds to the area under the F-CMOD curve. It should be mentioned that, since the model includes half a WST specimen, considering the symmetry of the specimen, the CMODs values was multiplied by two, thus the load versus CMOD in the figure above represents the fracture energy of a complete WST specimen. Obviously, the total energy is dissipated by horizontal component in the deformation control analysis while it is dissipated by both horizontal and vertical components of load in the force control analysis. As it is calculated, the energy dissipated by the vertical force is almost 7.5% of the energy dissipated by the horizontal load in the case of load control regime. This corresponds well to the figures quoted by Shah (1991) who states that the contribution of the vertical component of the load can be estimated to be between 5 and 9%.

The rest of the analyses conducted in this study were performed under a deformation control loading regime, consisting of just the horizontal component, and the results were modified by the coefficient of 7.5% and compared with the experimental results. The main reasons for this was that it simplified the analyses of the tests conducted under cyclic CMOD control.

7.4 Numerical Results for Monotonic Loading

In the present section, results of inverse analysis, performed using the program package Diana, are presented. Based on the discussion made in section 7.3, all the analyses were conducted in a deformation control loading regime consisting of just the horizontal force component. The fracture energy introduced to the FE analysis was calculated from test data and modified by the coefficient of 7.5%. The FE analyses were conducted in an non-automatic way, that is the best fit of the F_{sp}-CMOD relationship was investigated manually by changing the input parameters such as tensile strength, f_t, and fracture energy, G_f, of concrete. A bi-linear σ-w relationship was applied for the steel FRC and synthetic FRC while an exponential softening, based on a model proposed by Hordijk (1986), was used for the plain concrete; see Appendix E for Hordijk model.

The results from the experiments and the inverse analyses are presented in Figure 7.3 to Figure 7.5 for the plain concrete, steel FRC, and synthetic FRC, respectively. In these figures, the ratio between experimental and analyses results are also shown. Furthermore, these ratios, for the three types of concrete, are compared in Figure 7.6. Almost the same agreement which where observed in the inverse analysis using the Matlab® program can be seen in figures. There is a good agreement between experiments and the inverse analyses up to a CMOD of 1.0 mm for the plain concrete. In Figure 7.3(b), the ratio is limited between 0.85 and 1.05 for CMODs lower than 1.0 mm. After a CMOD of 1.0 mm, the ratio of the splitting loads keeps increasing up to 2.05 at the CMOD of 2.24 mm. Basically, this disagreement for CMODs of greater than 1.0 mm can be interpreted by low values of splitting force for the plain concrete but the influence on the dissipated energy (or fracture energy) is relatively limited. It may also be due to the properties of the concrete, which had a high strength and good aggregate bond that resulted in aggregate rupture; hence, indicating a reduced tail. By using a different *σ-w* relationship, e.g. a multi-linear approximation, it may be possible to reach a better agreement. The ratio of the splitting loads, for the steel FRC and synthetic FRC dose not show any significant difference along the CMOD axis, as the plain concrete, except for CMODs greater than 1.3 mm for synthetic FRC, where the Fsp-CMOD curves bend over with a negative slope. These ratios are between 0.95 and 1.05 for the steel and between 0.9 and 1.05 for the synthetic FRC, except for CMOD of greater than 1.3mm. Similar to the result of inverse analysis from Matlab® program, there are some peak points corresponding to the high ratio of analytical and experimental splitting force for very small CMODs in all three types of concrete.

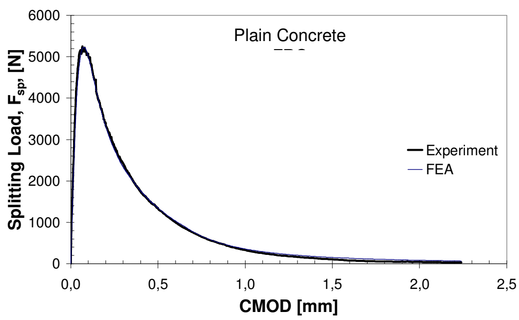

(a)

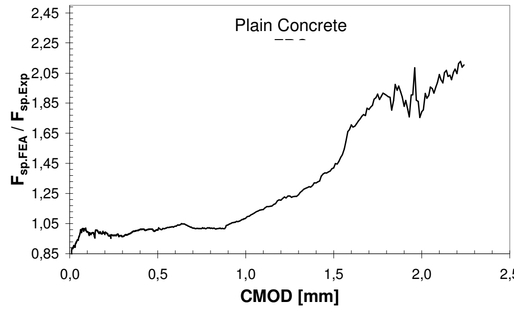

(b)

Figure 7.3 Comparison of the results from the experiment and FE analysis for the plain concrete: (a) the splitting load (b) fraction of the splitting loads taken from the experiment and FE analysis.

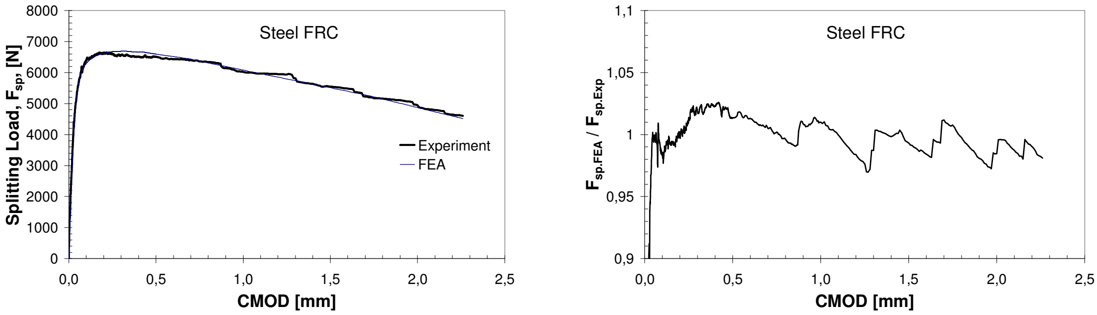

(a) (b)

Figure 7.4 Comparison of the results from the experiment and FE analysis for the steel FRC: (a) the splitting load (b) fraction of the splitting loads taken from the experiment and FE analysis.

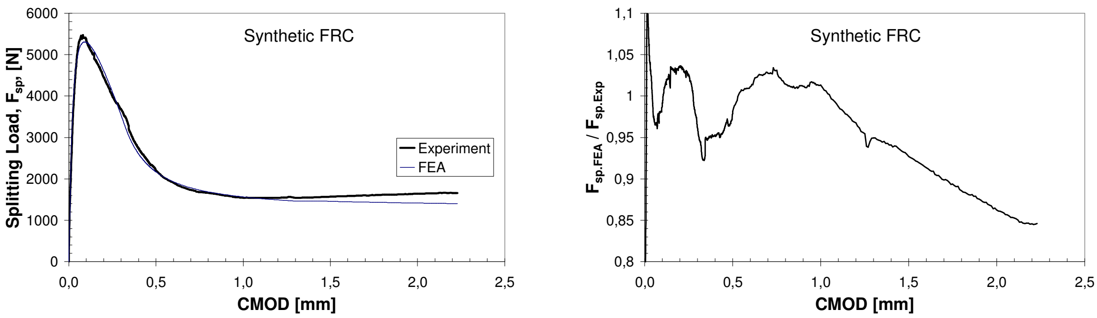

(a) (b)

Figure 7.5 Comparison of the results from the experiment and FE analysis for the synthetic FRC: (a) the splitting load (b) fraction of the splitting loads taken from the experiment and FE analysis.

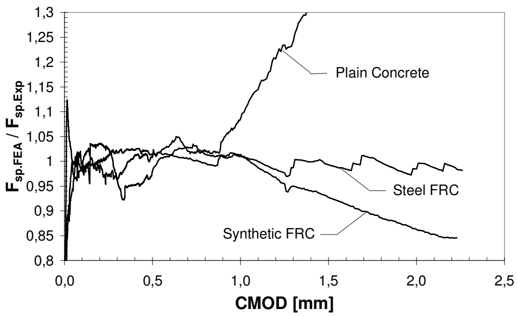

Figure 7.6 Comparison of the fraction of the splitting loads taken from the experiment and FE analysis for the three types of concrete.

The result from the experiments and inverse analysis carried out by Diana for dissipated energy are presented in Figure 7.7 to Figure 7.9 for the three types of concrete. In these figures, the ratio between the experiment and the inverse analysis is also shown. As can be seen in the figures, the agreement between experiments and the inverse analysis for dissipated energy is good for all three concrete types. In the case of plain concrete and synthetic FRC, the ratio is limited between 0.95 and 1.05, while for the case of steel FRC it is limited between 0.9 and 1.0, except for a region with very small CMODs before the peak load. These ratios for three types of tested concrete are shown in Figure 6.8.

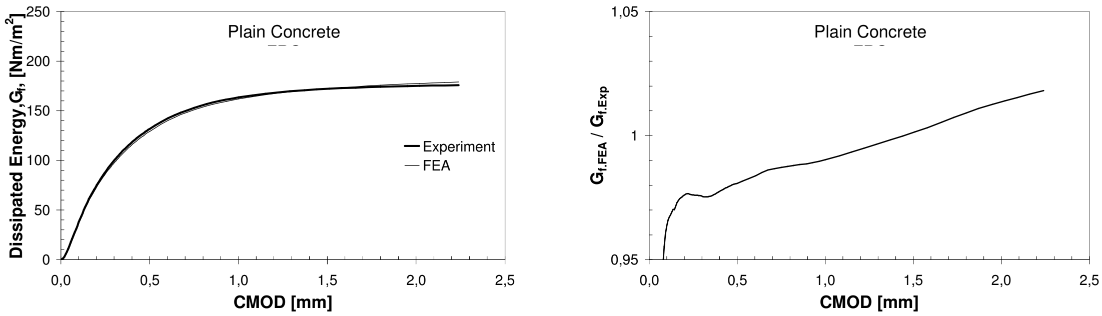

(a) *(b)*

Figure 7.7 Comparison of the results from the experiment and FE analysis for the plain concrete: (a) the dissipated energy (b) fraction of dissipated energies taken from the experiment and FE analysis.

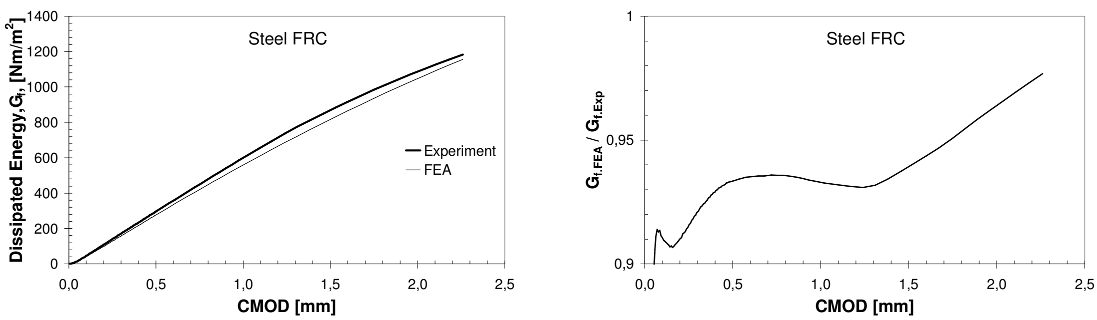

(a) *(b)*

Figure 7.8 Comparison of the results from the experiment and FE analysis for the steel FRC: (a) the dissipated energy (b) fraction of dissipated energies taken from the experiment and FE analysis.

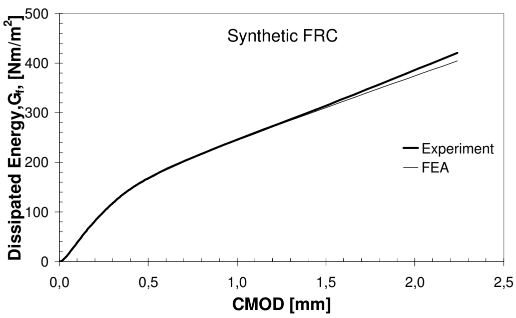

(a)

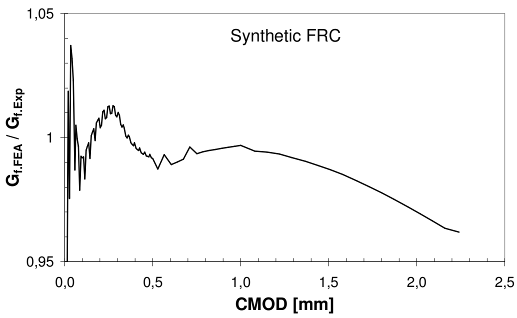

(b)

Figure 7.9 Comparison of the results from the experiment and FE analysis for the synthetic FRC: (a) the dissipated energy (b) fraction of dissipated energies taken from the experiment and FE analysis.

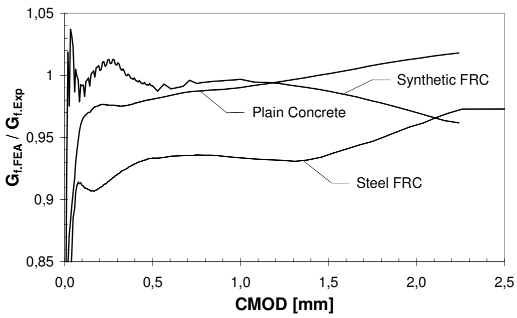

Figure 7.10 Comparison of the fraction of the dissipated energy taken from the experiment and FE analysis for the three types of concrete.

The σ-w relationships, from EF analyses, are presented in Figure 7.11 where a nonlinear relationship based on Hordijk model; see Hordijk (1986) and Appendix E, for the plain concrete and a bi-linear relationship for the steel and synthetic FRC were used. As it can be seen, the inclusion of fibers remarkably influences the shape of the relationship. As previously cleared, the experiments and inverse analysis were carried out until a CMOD of 2.2 mm, thus good estimations of the σ-w relationships are expected until CMOD of 1.0 mm. Consequently, it is not wise to calculated critical crack openings, w_c, where the stress is zero from these diagrams. Also a good agreement is seen for estimated σ-w relationships using Matlab® program and FE analysis; compare Figure 7.11 and Figure 6.14.

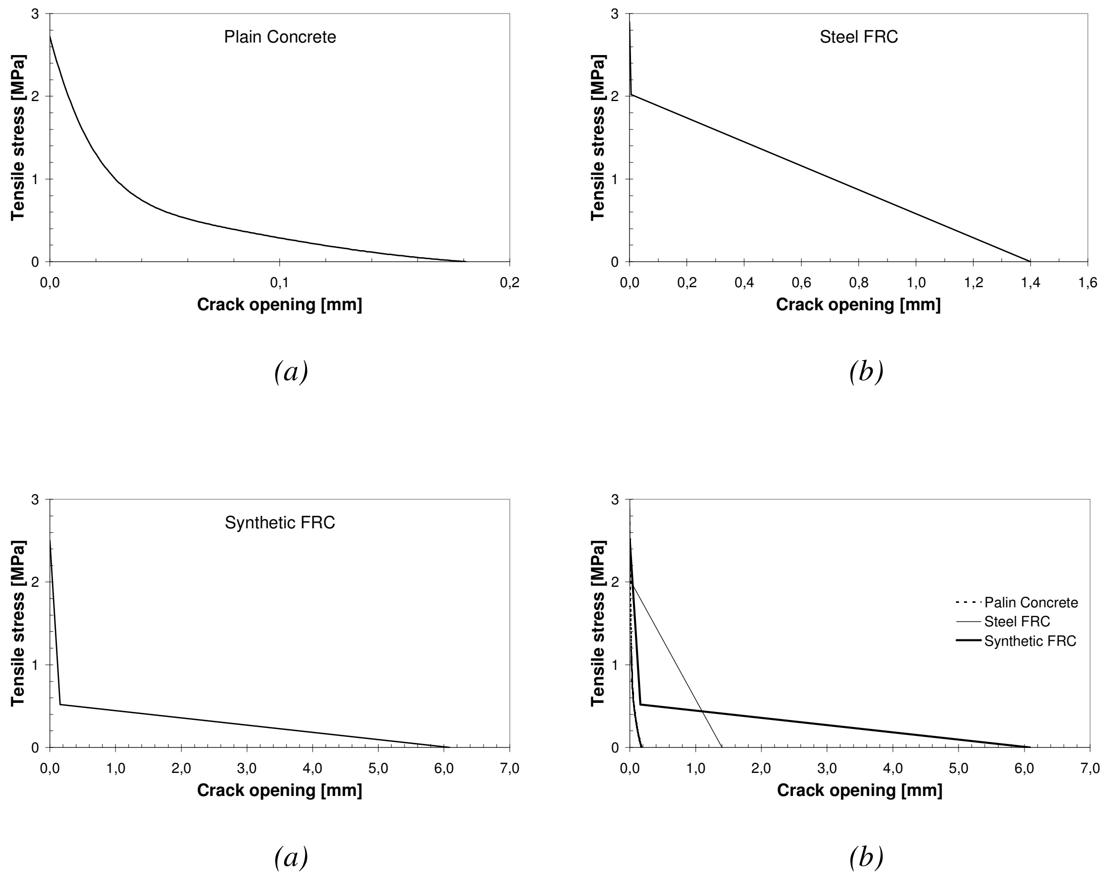

Figure 7.11 Bi-linear σ-w relationship for: (a) plain concrete (b) steel FRC (c) synthetic FRC (d) comparison of all three types of concrete.

7.5 Modelling Procedure for Cyclic Loading

In the present section, the result of FE analyses performed using Diana is presented. It should be noted that it was not the aim of this project to find the best numerical fit, i.e. the material properties which best fits the experimental data. On the other hand, as stated before, for FE analysis this optimisation should be done manually. Although, for monotonic loading, attempts were made to find a reasonably good agreement between numerical analysis and experimental data, but in the case of cyclic loading more time is required to complete the analysis; moreover this is quite time consuming as the analyses were not that stable.

In Diana, three different unloading patterns are provided and these are named: secant unloading (straight line back to the origin), elastic unloading (immediate return using the linear elastic stiffness) and cyclic unloading via hysteresis loops according to the continuous function model by Hordijk; see Hordijk (1986) and Appendix E. The latter model is only applicable in combination with the nonlinear tension-softening criterion of Hordijk et al. Extensive attempts were made to apply cyclic unloading via hysteresis loops according to continuous function model by Hordijk, but the analyses were extremely unstable and frequently the step sizes had to be adjusted.

7.6 Numerical Results for Cyclic Loading

In this section the result of elastic unloading are presented. One result for plain concrete analysed under cyclic loading of Hordijk model is presented in Appendix E just to give an idea of how the Hordijk unloading and reloading pattern looks like.

Elastic unloading, which was the case for inverse FE analysis under cyclic loading, dose not consider stiffness degradation but it may be utilised to estimate the energy loss in each unloading and reloading cycle due to crack propagation. The experimental and numerical results from the WST specimens under the cyclic loading are presented in Figure 7.12 to Figure 7.15. The same loading history that was applied in the experiments was applied in the numerical analyses. As it can be seen, the energy loss for each unloading and reloading cycles is not estimated properly by elastic unloading while it is approximated better with the Hordijk model; see Appendix E. the general trend of energy dissipation for three types of concrete can be observed in inverse analysis, that is, for a specific CMOD the highest energy dissipates with the steel FRC; see Figure 7.15.

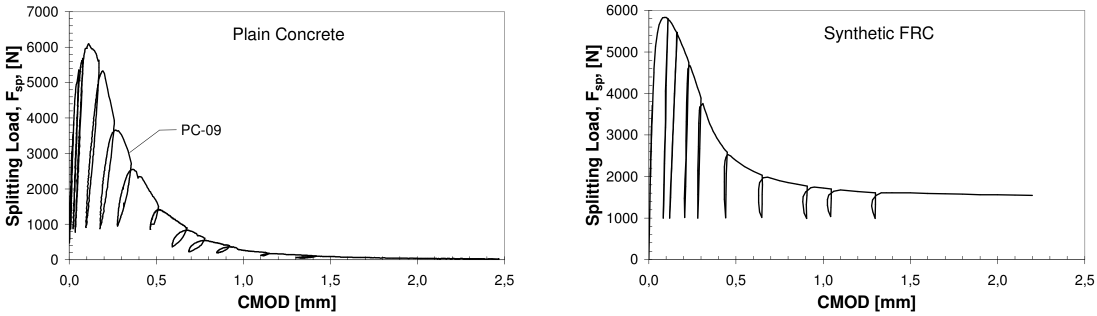

(a) *(b)*

Figure 7.12 Splitting load versus CMOD for the plain concrete under cyclic loading from: (a) experimental data and (b) FE analysis with elastic unloading.

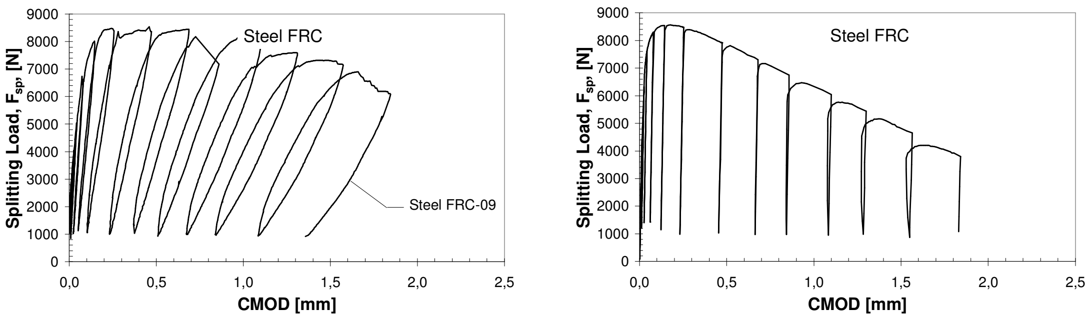

(a) *(b)*

Figure 7.13 Splitting load versus CMOD for the steel FRC under cyclic loading from: (a) experimental data and (b) FE analysis with elastic unloading.

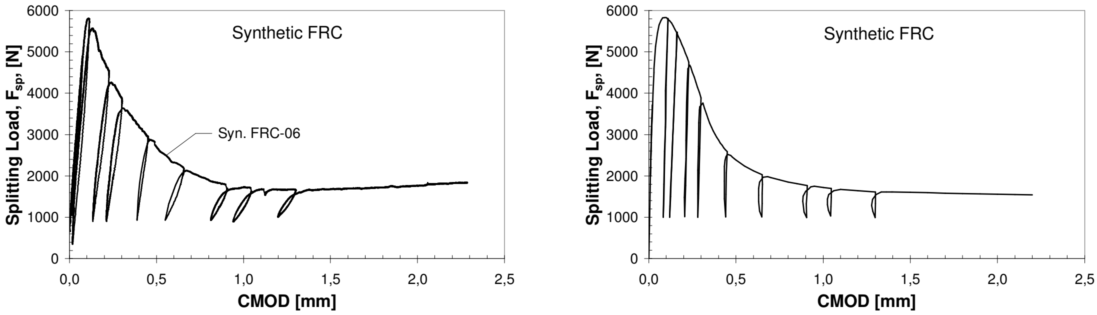

(a) *(b)*

Figure 7.14 Splitting load versus CMOD for the synthetic FRC under cyclic loading from: (a) experimental data and (b) FE analysis with elastic unloading.

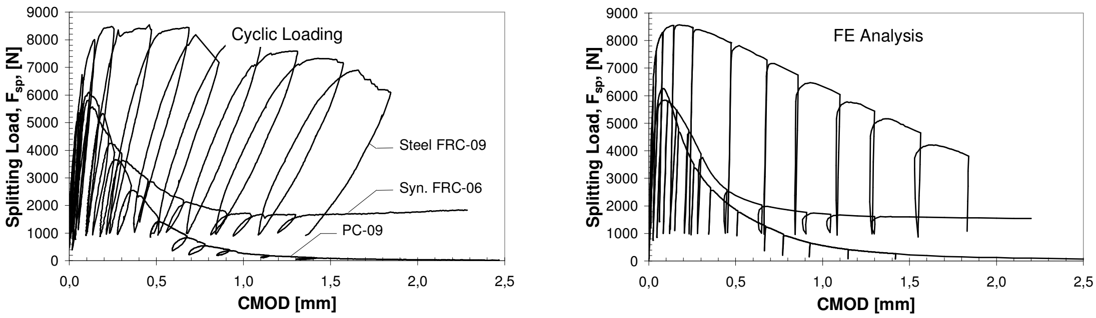

(a) *(b)*

Figure 7.15 Splitting load versus CMOD for all the three types of concrete under cyclic loading from: (a) experimental data and (b) FE analysis with elastic unloading.

8 CONCLUSIONS

8.1 Summary

Since brittle materials are considered to have no significant post-crack ductility, fibrous composites have been developed to provide brittle materials by ductile mechanical properties. One of the greatest benefits to be gained by using fiber reinforcement is improved long-term serviceability of structures. One aspect of serviceability that can be enhanced by the use of fibers is control of cracking. In addition to crack control and serviceability benefits, use of fibers at high volume percentages can substantially increase the composite's tensile strength.

The main benefit of the inclusion of fibers in the concrete matrix is the increased ability to absorb energy, which was observed in the conducted experiments. The action of fiber bridging and fiber pullout in FRC dissipates energy in the wake of crack tip. Consequently, it is feasible to slow down and inhibit the growth of the flaws in the second stage of fatigue failure development by introducing dispersed fibers as reinforcements.

Different methods are used to explore the fatigue properties of concrete, as there is no standardized method of fatigue testing. The aim of this study was to investigate the possibility of using the wedge splitting test (WST) method in order to determine the fatigue behaviour of concrete. Compared other fracture test methods, e.g. Three-point Bending Test (TPBT) and Uni-axial Tension Test (UTT), the Wedge splitting test is a simple test method to determine the fracture properties of concrete, which rarely has been used to investigate the fatigue properties of concrete.

In this thesis, the fatigue behaviour of plain concrete, steel fiber reinforced concrete, and synthetic fiber reinforced concrete were studied experimentally and numerically, by the WST method. In the experimental part, experiments were performed using WST specimens under monotonic as well as under cyclic loading. In the numerical part, inverse analyses were conducted under similar loading conditions as the experimental part using a Matlab® program, developed at DTU by Østergaard (2003), and FE analysis using the commercial available program package Diana. Through numerical analysis, bi-linear *σ-w* relationship and energy dissipation were determined. For this a systematic approach for material testing based on fracture mechanics presented by Löfgren (2005), which covers material testing, inverse analysis, and adjustment of the *σ-w* relationship for fiber efficiency, were applied.

8.2 General Conclusions

As the first general conclusion, it can be concluded that the inclusion of steel and synthetic fibers improves the fracture behaviour of concrete. For instance, at a CMOD of 2.0 mm, the energy dissipation is 8 times greater for the steel FRC and 2 times greater for the synthetic FRC compared to the energy dissipation at the same CMOD in the plain concrete. This behaviour is explained based on the action of fiber bridging and fiber pullout in fiber reinforced concrete, which dissipates the energy in the wake of the crack tip; see sections 4.4, 4.5, and 4.6 for more explanation.

According to the σ-w relationships estimated by inverse analysis, it is found that inclusion of fibers affects the shape of the σ-w relationship remarkably, so that for steel and synthetic fiber reinforced concrete, the zero stress is reached at significantly larger crack openings compared to the plain concrete.

It is found that the scatter in the test results of monotonic loading was quite large and the coefficient of variance could be as high as 34%, 27%, and 29% for the plain concrete, steel FRC, and Synthetic FRC, respectively. It is believed that a major factor contributing to the large scatter in the test results is related to the variation in fiber orientation and distribution and the intrinsic variation of fracture properties of plain concrete.

Based on the result of the inverse analysis conducted by using a Matlab® program, there is a reasonably good agreement between experiments and inverse analyses for all there types of concrete except for CMODs greater than 1.0 mm in the case of plain concrete, where the ratio of the splitting loads taken from inverse analysis and experiments exceeds 1.1. This ration is limited between 0.9 and 1.1 for the three types of concrete with CMODs lower than 1.0 mm.

Based on the result from the experiments and the inverse analysis for dissipated energy, a good agreement between experiments and inverse analysis was observed. The ratio between energy dissipation calculated from the inverse analysis conducted by Matlab® program and the experiments is limited between 0.95 and 1.1 for all three types of concrete except for a region of very small CMODs before the peak load.

From the test results of the WST specimens under the low-cycle fatigue loading, it is found that the energy dissipation under the cyclic loading slightly increases with the inclusion of the synthetic fibers and remarkably increases with the inclusion of the steel fibers. Based on the explained fatigue mechanisms of the steel FRC, the addition of fibers is found to have a significant effect on the dissipated energy because of the fiber bridging and fiber pullout actions.

Based on the stable results achieved from the WST method under the cyclic loading, it is concluded that the WST method can be applicable to investigate the fatigue behaviour of all three types of tested concrete, considering the WST geometry and test set-up used in these experiments.

The inverse analyses for the plain concrete, using the Matlab® program, suggests that a σ-w relationship can be determined for each reloading part of a fatigue test. Thus the stiffness degradation through a fatigue test can be calculated for each cycle

Finally, the inverse analysis using the FE method by Diana estimates the contribution of the vertical load to be 7.5 % of the horizontal load role in the process of dissipating energy through a force control regime of loading. As a consequence, if a FE analysis is performed under a deformation control loading, consisting of just horizontal component, then the results should be modified by the coefficient of 7.5% (for the WST geometry and test set-up used in these experiments). Likewise, if a WST experiment is conducted, it should be noted that if the fracture energy is to be determined from the test result it needs to be modified by the coefficient of 7.5% (for the WST geometry and test set-up used in these experiments).

8.3 Suggestions for Further Research

A large scatter of fatigue test result has been reported in literature; on the other hand, there is no standardized fatigue test method for concrete. While there is extensive research on the wedge splitting test as a test method for determining fracture properties of concrete, few studies have been carried out to investigate the fatigue behavior of concrete using the wedge splitting test method. Since a WST is easy to conduct and stable results have been reported in the literature, it may be of interest to evaluate and develop the WST method as a standardized method of fatigue test for concrete.

The result from inverse analysis, using a Matlab® program developed at DTU by Østergaard (2003) based on the crack hinged model developed by Olesen (2001), shows a good agreement with the test data for the three types of tested concrete. It is always important to determine the σ-w relationship of concrete, e.g. by a bi-linear or multi-linear estimation. It may be possible to apply the same model, i.e. crack hinge model, for a fatigue test data and obtain σ-w relationship for each cycle. Knowing about this relationship makes it possible to determine the stiffness degradation after each unloading and reloading cycle based on the test data for the WST method.

The low cycle fatigue, which was the case in this study, corresponds to a real environmental condition when a concrete element is exposed to an earthquake load. It would be valuable to carry out an experimental and numerical investigation of a WST method under a high cycle fatigue load, which simulates other types of fatigue loads, e.g. water or wind wave load. This would be a further step toward introducing a fatigue design for hydraulics structures or tall building, which are faced with high cycle fatigue loadings.

9 References

ACI 446.1R-91 (2003): *Fracture Mechanics of Concrete:(Reapproved 1999) Concepts, Models and Determination of Material Properties*, 2003, 146 pp.

ACI 544.2R-89 (2003): *Measurement of Properties of Fiber Reinforced Concrete*, 2003, Vol. 6, 11 pp.

Antrim, J.C (1976): *A Study of the Mechanism of Fatigue in Cement Paste and Plain Concrete.* PhD Thesis, Purdue University,

ASTM Designation: E 1823 - 96^{E1} (2001): *Standard Terminology Relating to Fatigue and Fracture Testing*, 2001, Vol. 03.02, pp. 1058-1077

Brandt, Andrzej M. (1995): *Cement-based Composites: Materials, Mechanical Properties and Performance.* Spon, London, 1995, 470 pp.

Brühwiler, E., Wittmann, F. H. (1990): The Wedge Splitting Test, a New Method of Performing Stable Fracture Mechanics Tests. *Engineering Fracture Mechanics,* Vol. 35, No. 1-3, 1990, pp. 117-126

Svensk Byggtjänst (2000), *High Performance Concrete Structures: Design Handbook*, Svensk Byggtjänst, PP. 127 pp.

Hideyuki Horii, Hak Chul Shin, Tirath Manojya Pallewatta. (1992): Mechanism of Fatigue Crack Growth in Concrete. *cement and Concrete Composite,* Vol. 14, 1992, pp. 83-89

Hilsdorf, Hurbert, K., Kesler, Clyde E. (1966): Fatigue Strength of Concrete Under Varying Flexural stresses. *ACI Journal,* V.63, No. 10, 1966, pp. 1059-1076

Holmen, J.O. (1979): *Fatigue of Concrete by Constant and Variable Loading.* Trondheim, 1979, xii, 218 pp.

Jin-Keun Kim Yun-Yong Kim. (1999): Fatigue crack growth of high-strength concrete in wedge-splitting test. *Cement Concrete Research,* Vol. 29, 1999, PP. 705-712

Löfgren, I. (2005): *Fiber-reinforced Concrete for Industrial Construction - a Fracture Mechanics Approach to Material Testing and Structural Analysis.* Structural Engineering and Mechanics, Chalmers University of Technology, Göteborg, 146 pp.

Löfgren, I. (2004): The Wedge Splitting Test – a Test Method for Assessment of Fracture Parameters of FRC. *Fracture Mechanics of Concrete Structures,* 2004,

M. Grzybowski , and Meyer (1993): Damage Accumulation in Concrete With and Without Fiber Reinforcement. *ACI Material Journal,* Vol. 90, No.6, 1993, PP. 594-604

M.K. Lee, B.I.G. Barr. (2004): An overview of the fatigue behaviour of plain and fibre reinforced concrete. *cement and Concrete Composite,* Vol. 26, 2004, pp. 299-305

Murdock, J., Kesler, C. E. (1960): The Mechanism of Fatigue in Cement Paste and Plain Concrete, No. 587, University of Illinois

Neville, A. (2003): *Properties of Concrete.* Longman Group, Harlow, 2003, xix, 844 pp.

Shah, S. P., Carpinteri, A. (1991): *Fracture Mechanics Test Methods for Concrete: Report of Technical Committee 89-FMT Fracture Mechanics of Concrete: Test Methods.* Chapman and Hall, London, 1991, xii, 287 pp.

Svensk byggtjänst (2000), *High performance concrete structures : design handbook*, Svensk byggtjänst, PP. 127

T. Paskova, and Meyer. (1994): Damage Mechanics Based Model for Cyclic Response of Concrete. *Fracture and Damage in Quasibrittle Structures,* Vol.85, No. 4, 1994, PP. 254-261

Zhang, J. (1998): *Fatigue Fracture of Fiber Reinforced Concrete - An Experimental and Theorethical Study.* Denmarks Tekniske Universitet, Lyngby, 1998, 169 pp. pp.

RILEM TC 162-TDF (2002): Test and Design Methods for Steel Fiber Reinforced Concrete, Bending Test, Final Recommendation. *Materials and Structures*, Vol. 35, Nov 2002, pp. 579-582

RILEM TC 162-TDF (2001): Test and Design Methods for Steel Fiber Reinforced Concrete, Recommendations for Uni-axial tension test. *Materials and Structures*, Vol. 34, Jan-Feb 2001, pp. 3-6

APPENDIX A Short Terminology Relating to Fatigue and Fracture Testing

Alternating load – see**; loading amplitude**

Clipping – in fatigue spectrum loading, the process of decreasing or increasing the magnitude of all loads (strains) that are, respectively, above or below a specified level, referred to as clipping level; the loads (strains) are decreased or increased to the clipping level (see figure)

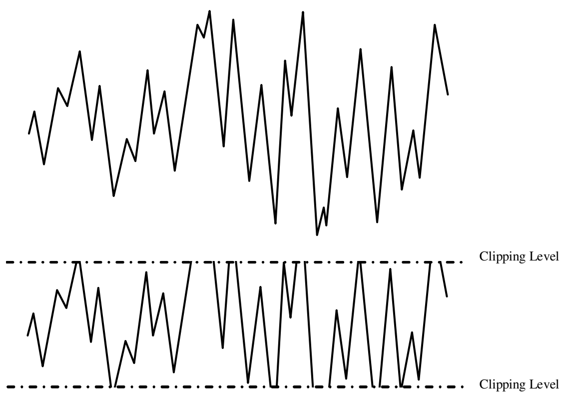

Clipping of fatigue spectrum loading

Compliance [L L^{-1}], n – the ratio of displacement increment to load increment.

Confidence interval – an interval estimate of a population parameter computed so that the statement '' the population parameter included in this interval'' will be true, in the average, in a stated proportion of the times such computations are made based on different samples from the population.

Confidence level (or coefficient) – the stated proportion of the times the confidence interval is expected to include in the population parameter.

Confidence limits – the two statistics that define a confidence interval.

Constant amplitude loading – in fatigue loading, a loading (strains) in which all of the peak loads (strains) are equal and all of the valley loads (strains) are equal.

Constant life diagram – in fatigue, a plot (usually in rectangular coordinates) or a family of curves each of which is for a single fatigue life, N, relating stress amplitude , S_a, to mean stress, S_m, or maximum stress, S_{man}, or both, to minimum stress, S_{min}. The constant life fatigue diagram is usually derived from a family of S-N curves each of which represents a different stress ratio (S or R) for a 50% probability of survival.

Corrosion fatigue – the process be which fracture occurs prematurely under conditions of simultaneous corrosion and repeated cyclic loading at lower stress levels or fewer cycles than would be required in the absence of the corrosive environment.

Counting method – in fatigue spectrum loading, a method of counting the occurrences and defining the magnitude of various loading parameters from a load-time history; (some of the counting methods are: level crossing count, peak count, mean crossing peak count, range count, range-pair count, rain-flow count, racetrack count).

Crack displacement [L] – the load-induced separation vector between two points (on the facing surface of a crack) that were initially coincident.

DISCUSSION – in practice E 561, displacement is the distance that a chosen measurement point on the specimen displaces normal to the crack plane. Measurement points on the C(W) and C(T) specimen configurations are identified as locations V0, V1, and V2.

Crack extension, Δa [L] – an increase in crack size.

DISCUSSION – foe example, in practice E561, Δa_p or Δa_e is the different between the crack size, either a_p (physical crack size) or a_e (effective crack size), and a_o (original crack size).

Crack-extension force, G [FL^{-1} or FLL^{-2}] – the elastic energy or unit of new separation area that is made available at the front of an ideal crack in an elastic solid during a virtual increment of forward crack extension.

DISCUSSION – this force concept implies an analytical model for which the stress-strain relations are regarded as elastic. The preceding definition of G applies to either static cracks or running cracks. From past usage, G is commonly associates with linear-elastic methods of analysis, although the J (see J-internal) also may be used for such analyses.

Crack-extension resistance, K_R [$FL^{-3/2}$], G_R [FL^{-1}]or J_R [FL^{-1}] – a measure of the resistance of a material to crack extension expressed in terms of the stress-intensity factor, K; crack-extension force, G; or values of J derived using the J-integral concept.

DISCUSSION – see definitions of R-curve.

Crack length, a [L] – see crack size and surface crack length. Also see crack length in the description of terms. For example, in the C(T) specimen, a is measured from the line connecting the bearing points of load applications; in the M(T) specimen, a is measured from the perpendicular bisector of the central crack.

Crack-mouth opening displacement (CMOD), $2\upsilon_m$ [L] – the Mode 1 (also called opening-mode) component of crack displacement resulting from the total deformation (elastic plus plastic), measured under load at the location on a crack surface that has the greatest elastic displacement per unit load.

DISCUSSION – in part-through surface-crack (PS) specimens, CMOD is measured on the specimen surface at the midpoint of the crack length.

Crack-plane orientation – an identification of the plane and direction of a fracture in relation to product configuration. This identification is designates by a hyphenated code with the first letter(s) representing the direction normal to the crack plane and the second letter(s) designated the expected direction of crack propagation.

Crack size, a [L] – a linear measure of a principal planar dimension of a crack. This measure is commonly used in the calculation of quantities descriptive of the stress and displacement fields and is often also termed crack length or depth.

DISCUSSION – in practice, the value of a is obtained from procedures for measurement of physical crack size, a_p , original crack size, a_o, and effective crack size, a_e, as appropriate to the situation being considered.

Crack strength, σ_a [FL^{-2}] – the maximum value of the nominal stress that a cracked structures id capable of sustaining.

DISCUSSION -1 crack strength id calculated on the basis of the maximum load and the original minimum cross-section area (net cross section of ligament). Thus, it takes into account the original size of the crack but ignores any crack extension that may occur during the test.

DISCUSSION -2 crack strength is analogous to the ultimate tensile strength, as it is based on the ratio of the maximum load to the minimum cross-sectional area at the start of the test.

Crack-tip opening displacement (CTOD), δ; [L] – the crack displacement resulting from the total deformation (elastic plus plastic) at variously defines locations near the original (prior to load application) crack tip.

DISCUSSION – in common practice, δ is estimated for Mode 1 by inference from observations of crack displacement nearby or aqua, or both, from the crack tip.

Crack-tip plane strain – a stress-strain field (near the crack tip) that approaches plane strain to the degree required by an empirical criterion.

DISCUSSION – for example, in Mode 1, the criterion for crack-tip plane strain given by Test Method ASTM E 399 requires that plate thickness, B, must be equal to or greater than 2.5 $(K/\sigma_{YS})^2$.

Crack-tip plane stress – a stress-strain field (near the crack tip) that is not in plane strain.

DISCUSSION – In such situations, a significant degree of plane strain may be present.

Criterion of failure – complete separation, or the presence of a crack of specified length visible at a specified magnification. Other criteria ma be used but should be clearly defined.

Cycle – in fatigue, one complete sequence of values of load (strain) that is repeated under constant amplitude loading (straining). (see figure ---) the symbol N *see definition of fatigue life) is used to indicate the number of cycles.

DISCUSSION – In spectrum loading, definitions of cycles varies with the counting method.

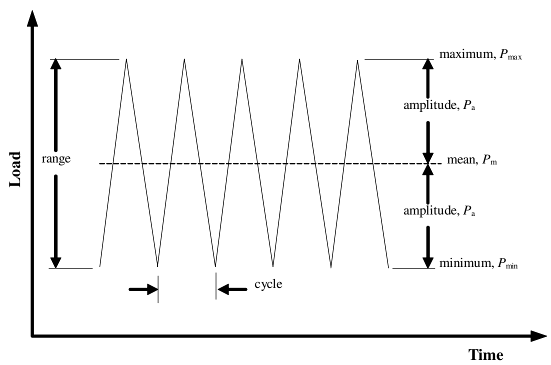

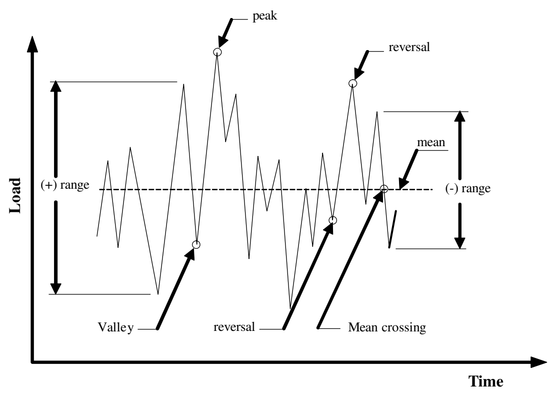

Fatigue loading basic terms

Cycles endure, n – in fatigue, the number of cycles of specified character (that produce fluctuating load) which a specimen has endures at any time in its load history.

Cycle ratio, D – the ratio of cycles endures, n, to the estimated fatigue life, N_f, obtained fro the stress versus fatigue life (S-N) of the strain versus fatigue life (Є-N) diagram for cycles of the same character, that is, $D=n/N_f$.

Cyclic loading – see fatigue loafing.

Dynamometer – an elastic calibration device used to verify the indicated loads applied by a fatigue testing system. It shall consist of an instrumented member having mass, stiffness, and end displacements such that the inertial effects of the specimen and its attachments to the testing machine for which the verification of loads is desired are duplicated within 5 %. The instrumentation shall permit an accurate determination of the magnitude of the average strain in a region of the uniform transverse cross section when the dynamometer is subjected to a tensile or compressive force along its longitudinal axis, within 1% of the true strains. A strain gaged specimen is often used as a dynamometer.

Dynamometer dynamic loads [F] – the maximum and minimum loads (or the mean load and the load amplitude) that correspond to the readings obtained from the dynamometer output according to an existing static calibration. Such loads are considered true specimen dynamic loads for the purpose of this terminology.

Dynamometer range [F] – the range of load for which the dynamometer may be used for verification purpose. A dynamometer for use in tension and in compression will have two dynamometer ranges, one in tension and one in compression.

Effective crack size, a_e [L] – the physical crack size augmented to account for crack-tip plastic deformation.

DISCUSSION – sometimes the effective crack size, a_e, is calculated from a measured value of a physical crack size, a_p, plus a calculated value of a plastic-zone adjustment, r_Y. Another methods for calculation of a_e involves comparing the compliance from the secant of a load-deflection trace with the elastic compliance from a calibration for the given specimen design.

Effective thickness B_e [L] – for compliance-based extension measurements:

$$B_e = B - (B - B_N)^2 / B$$

Effective yield strength, σ_N [FL_{-2}] – an assumed value of uniaxial yield strength, that represents the influences of plastic yielding upon fracture test parameters.

DISCUSSION – 1 It is calculated as the average of the 0.2 % offset yield strength, σ_{YS}, and the ultimate tensile strength, σ_{TS} , for example :

$$\sigma_{Y} = (\sigma_{YS} + \sigma_{YS})^{2}$$

DISCUSSION – 2 In estimating σ_Y, influence of testing conditions, such as loading rate and temperature, should be considered.

Environment – in fatigue testing, the aggregate of chemical species and energy that surrounds a test specimen.

Environment chamber – in fatigue testing, the container of the bulk volume surrounds a test specimen.

Environment composition [ML^{-3}] – in corrosion fatigue testing, the concentration of the chemical components in the fluid environment surrounding s test specimen.

Environment hydrogen content [ML^{-3}] – in corrosion fatigue testing, the hydrogen gas concentration of the fluid environment surrounding a test specimen.

Fatigue- the process of progressive localized permanent structural change occurring in the material subjected to the conditions that produce fluctuating stresses and strains at some points and that may culminate in cracks or complete fracture after a sufficient number of fluctuations.

Discussion- fluctuation may occur both in load and with time (frequency) as in the case of ''random vibration''

Discussion- the Value of S_N that is commonly found in the literature is the value of S_{max} or S_a at which 50 % of the specimens of a given sample could survive N stress cycles in which S_m=0. This is also known as the median failure strength for N cycles.

Fracture toughness- a generic term for measures of resistance to extension of a crack.

Discussion- the term is sometimes restricted to results of fracture mechanics tests, which are directly applicable in fracture control. However the term commonly includes results from tests of notched or pre-cracked specimens, which do not involve fracture mechanics analysis. Results from tests of the latter type are often useful for fracture control, based upon either service experience or empirical correlations with tests analysed using fracture mechanics.

Discussion- R-curves normally depend upon specimen thickness and, for some material, upon temperature and strain rate.

Fatigue limit for *p* % survival – the limiting value of fatigue strength for *p* % survival as *N* becomes very large; *p* may be any number, such as 95, 90 and so forth.

Fatigue loading- periodic, or not periodic, fluctuating loading applied to a test specimen or experienced by a structure in service.

Fatigue strength at N cycles, S_N [FL^{-2}] - is a value of stress for failure at exactly N cycles as determined from an S-N diagram. The value of S_N thus determined is subjected to the same conditions as those, which apply to the S-N diagram.

Fracture toughness- a generic term for measurement of resistance to extension of a crack

Hysteresis Diagram – in fatigue, the stress-strain path during a cycle

Load cell – a device which indicates the applied force by means of an electrical voltage increases linearly with applied load.

Load range – in fatigue loading, the algebraic difference between successive valley and peak loads or between successive peak and valley loads.

Load ratio – in fatigue, the algebraic ratio of the two loading parameters of a cycle.

Maximum load – in fatigue, the highest algebraic value of applied load in a cycle.

Notched tensile strength – the maximum nominal stress that a nothched tensile specimen is capable of sustaining.

Physical crack extension – an increase in physical crack size.

Fatigue strength at N cycles, S_N [FL^{-2}] - is a value of stress for failure at exactly N cycles as determined from an S-N diagram. The value of S_N thus determined is subjected to the same conditions as those, which apply to the S-N diagram.

Plane-strain fracture toughness – the crack extension resistance under conditions of crack-tip plane strain.

R-curve- a plot of crack-extension resistance as a function of stable crack extension, Δa_p or Δa_e.

S-N curve for 50 % survival – a curve fitted to the median values of fatigue life at each of several stress levels. It is an estimate of relationship between applied stress and the number of cycles to failure that 50 % of the population would survive.

APPENDIX B Some Fatigue Tests on Plain Concrete Performed by Different Investigators

Investigator(s)	Concrete type	Loading condition	Test geometry	Aim of the work
Horii, Shin, and Pallewatta (1992)	Plain concrete f_c = 26.1 MPa f_t = 3.39 MPa	Low cycle fatigue P_{max}=80% of the maximum static load P_{min}=0 (almost) With the frequency of 0.2 Hz	Wedge Splitting Test 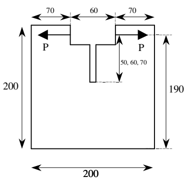	To propose an analytical model of fatigue crack growth in concrete in order to identify the governing mechanism happening in the fracture process zone
Subramaniam and Shah (2003)	Plain concrete E= 33.67 GPa υ = 0.187	Low cycle fatigue loading on two different specimens: 1) Notched 3PBT, and 2) hollow concrete cylinders subjected to torsion P_{max} = 75%, 85%, and 95% of the average quasi-static peak load P_{min}=5% of the average quasi-static peak load (kept constant)	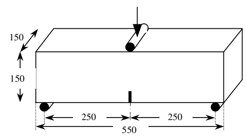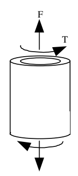	To characterize the quasi-static and low-cycle fatigue response of concrete subjected to biaxial stresses in the biaxial tension region, where the principal tensile stress is larger than or equal to the principal compressive stress in magnitude.
Taylor and Tait (1999)	Cement mortar with and without f_c = 40 MPa (in both cases)	Cyclic load frequency=0.1, 1, 5, 10, 20 (Hz) P_{max} - P_{min} = 50% to 95% of the ultimate load P_{max} = 50% to 95% of the ultimate load (in steps of 5%)	Double Torsion Test 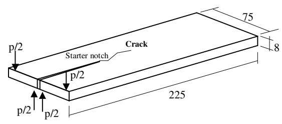	To investigate the effect of fly ash on the fatigue resistance of cement mortar.
Kim and Kim (1996)	High strength concrete, f_c = 26, 52, 84, and 103 MPa	P_{max}/P_{min} = 75%, 80%, 85%, 95% With the frequency of 1 Hz.	Compressive cylinder 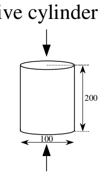	To investigate the fatigue behaviour of high strength concrete.
Suresh, Tschegg, and Brockenbrough (1989)	Plain concrete f_c = 52.9 MPa	Subjected to cyclic compressive loading, S_{max} = -15.25 MPa S_{min} = -0.25 MPa With the frequency of 5 Hz.	Notched specimen 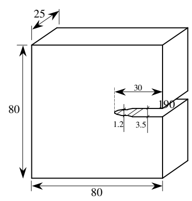	To investigate the mechanisms of fatigue crack growth under uniaxial cyclic compressive loading.

Saito (1988)	Plain concrete f_c = 63.7 MPa f_t = 5.31 MPa Static bond strength is equal to 2.10 MPa.	Sinusoidal loading S_{max} = 76.5, 81.2, 85.9, and 90.6% of the average static bond strength S_{min} = 7.6% of the average static bond strength. With the frequency of 5 Hz.	Uniaxial tension test 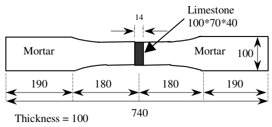	To obtain the *S-N* curve for the case subjected to direct tensile loading.
Alliche and Francois (1986)	Cement paste	Compressive cyclic loading, S_{max} / S_{min} =10	Compressive cylinder 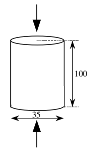	To investigate the fatigue behaviour of cement paste
Slowik, Plizzari, and Saouma (1996)	Plain concrete f_c = 30 MPa	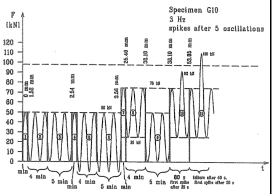 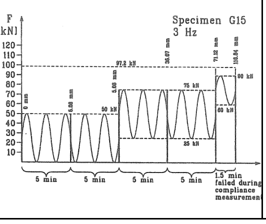	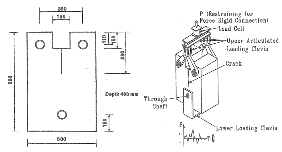 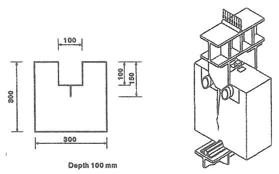	To investigate the fracture response of concrete under low-cycle variable amplitude loading at frequency up to 10HZ.

APPENDIX C Load History of Monotonic and Cyclic Loading for Experiments

Table 1 Static load history for the plain concrete, steel FRC, and synthetic FRC

Function Name	Control Mode (Axial)	Unit	Rate of Loading	End level		
				Relative	Absolute	Force [N] Strain [mm] Displacement. [mm]
Data	---	---	---			---
Cod plot	---	---	---			---
Start ramp	Force	[N/Sec]	5.000		●	-250,00
Ramp 2	Force	[N/Sec]	10.000		●	-500.00
Ramp 3	Strain	[mm/Min]	0.010000	●		-0,010000
Ramp 4	Strain	[mm/Min]	0.015000	●		-0.010000
Ramp 5	Strain	[mm/Min]	0.025000	●		-0,25000
Ramp 6	Strain	[mm/Min]	0.010000	●		-0.020000
Ramp 7	Strain	[mm/Min]	0.060000	●		-0.025000
Ramp 8	Strain	[mm/Min]	0.10000	●		-0.10000
Ramp 9	Strain	[mm/Min]	0.12500	●		-0.050000
Ramp 10	Strain	[mm/Min]	0.20000		●	-0.75000
Ramp 11	Strain	[mm/Min]	0.25000		●	-1.2500
Ramp 12	Displacement	[mm/Min]	0.50000	●		-2.0000

Table 2 Cyclic load history for the plain concrete

Function Name	Control Mode (Axial)	Unit	Rate of Loading	End level		
				Relative	Absolute	Force [N] Strain [mm] Displacement. [mm]
Data	---	---	---			---

Cod plot	---	---	---			---
Start ramp	Displacement	[mm/Min]	0.10000		●	-0.025000
Ramp 2	Displacement	[mm/Min]	0.20000	●		-0.05000
Ramp 3	Displacement	[mm/Min]	0.10000		●	-0.025000
Ramp 4	Displacement	[mm/Min]	0.20000		●	-0.1000
Ramp 5	Displacement	[mm/Min]	0.20000		●	-0.15000
Ramp 6	Displacement	[mm/Min]	0.20000		●	-0.15000
Ramp 7	Displacement	[mm/Min]	0.20000		●	-0.09000
Ramp 8	Displacement	[mm/Min]	0.20000		●	-0.20000
Ramp 9	Displacement	[mm/Min]	0.20000		●	-0.10000
Ramp 10	Displacement	[mm/Min]	0.20000		●	-0.30000
Ramp 11	Displacement	[mm/Min]	0.20000		●	-0.13000
Ramp 12	Displacement	[mm/Min]	0.20000		●	-0.40000
Ramp 13	Displacement	[mm/Min]	0.20000		●	-0.14100
Ramp 14	Displacement	[mm/Min]	0.20000		●	-0.60000
Ramp 15	Displacement	[mm/Min]	0.20000		●	-0.19000
Ramp 16	Displacement	[mm/Min]	0.050000		●	-0.67000
Ramp 17	Displacement	[mm/Min]	0.20000		●	-0.18000
Ramp 18	Displacement	[mm/Min]	0.10000		●	-0.85000
Ramp 19	Displacement	[mm/Min]	0.20000		●	-0.32000
Ramp 20	Displacement	[mm/Min]	0.10000		●	-0.90000
Ramp 21	Displacement	[mm/Min]	0.20000		●	-0.47000
Ramp 22	Displacement	[mm/Min]	0.10000		●	-1.0900
Ramp 23	Displacement	[mm/Min]	0.20000		●	-0.94000
Ramp 24	Displacement	[mm/Min]	0.05000		●	-1.3100
Ramp 25	Displacement	[mm/Min]	0.20000		●	-1.0900
Ramp 26	Displacement	[mm/Min]	0.10000		●	-1.4500
Ramp 27	Displacement	[mm/Min]	0.20000		●	-1.2250
Ramp 28	Displacement	[mm/Min]	0.10000		●	-1.7000
Ramp 29	Displacement	[mm/Min]	0.20000		●	-1.4500
Ramp 30	Displacement	[mm/Min]	0.20000		●	-2.6000
Ramp 31	Displacement	[mm/Min]	0.20000		●	-0.025000
Ramp 32	Displacement	[mm/Min]	0.20000		●	-3.0000

Ramp 33	Displacement	[mm/Min]	0.20000		●	-3.5000
Ramp 34	Displacement	[mm/Min]	0.20000		●	-4.0000
Ramp 35	Displacement	[mm/Min]	0.20000		●	-4.5000
Ramp 36	Displacement	[mm/Min]	0.20000		●	-5.0000
Ramp 37	Displacement	[mm/Min]	0.20000		●	-5.5000
Ramp 38	Displacement	[mm/Min]	0.20000		●	-6.0000

Table 3 *Cyclic load history for the steel FRC*

Function Name	**Control Mode (Axial)**	**Unit**	**Rate of Loading**	**End level**		
				Relative	**Absolute**	**Force [N] Strain [mm] Displacement. [mm]**
Data	---	---	---			---
Cod plot	---	---	---			---
Start ramp	Displacement	[mm/Min]	0.10000		●	-0.025000
Ramp 2	Displacement	[mm/Min]	0.20000	●		-0.05000
Ramp 3	Displacement	[mm/Min]	0.10000		●	-0.025000
Ramp 4	Displacement	[mm/Min]	0.20000		●	-0.1000
Ramp 5	Displacement	[mm/Min]	0.20000		●	-0.025000
Ramp 6	Displacement	[mm/Min]	0.20000		●	-0.15000
Ramp 7	Displacement	[mm/Min]	0.20000		●	-0.025000
Ramp 8	Displacement	[mm/Min]	0.20000		●	-0.20000
Ramp 9	Displacement	[mm/Min]	0.20000		●	-0.025000
Ramp 10	Displacement	[mm/Min]	0.20000		●	-0.30000
Ramp 11	Displacement	[mm/Min]	0.20000		●	-0.025000
Ramp 12	Displacement	[mm/Min]	0.20000		●	-0.40000
Ramp 13	Displacement	[mm/Min]	0.20000		●	-0.025000
Ramp 14	Displacement	[mm/Min]	0.20000		●	-0.60000
Ramp 15	Displacement	[mm/Min]	0.20000		●	-0.067000
Ramp 16	Displacement	[mm/Min]	0.20000		●	-0.14000
Ramp 17	Displacement	[mm/Min]	0.20000		●	-1.0000
Ramp 18	Displacement	[mm/Min]	0.20000		●	-0.22000

Ramp 19	Displacement	[mm/Min]	0.20000		●	-1.4000
Ramp 20	Displacement	[mm/Min]	0.20000		●	-0.46000
Ramp 21	Displacement	[mm/Min]	0.20000		●	-1.8000
Ramp 22	Displacement	[mm/Min]	0.20000		●	-0.67000
Ramp 23	Displacement	[mm/Min]	0.20000		●	-2.2000
Ramp 24	Displacement	[mm/Min]	0.20000		●	-1.0000
Ramp 25	Displacement	[mm/Min]	0.20000		●	-2.6000
Ramp 26	Displacement	[mm/Min]	0.20000		●	-1.33000
Ramp 27	Displacement	[mm/Min]	0.20000		●	-3.0000
Ramp 28	Displacement	[mm/Min]	0.20000		●	-1.6600
Ramp 29	Displacement	[mm/Min]	0.20000		●	-3.5000
Ramp 30	Displacement	[mm/Min]	0.20000		●	-2.1400
Ramp 31	Displacement	[mm/Min]	0.20000		●	-4.0000
Ramp 32	Displacement	[mm/Min]	0.20000		●	-2.6850
Ramp 33	Displacement	[mm/Min]	0.20000		●	-4.4000
Ramp 34	Displacement	[mm/Min]	0.20000		●	-0.02500
Ramp 35	Displacement	[mm/Min]	0.20000		●	-5.0000
Ramp 36	Displacement	[mm/Min]	0.20000		●	-0.025000
Ramp 37	Displacement	[mm/Min]	0.20000		●	-10.000

Table 4 Cyclic load history for the synthetic FRC

Function Name	**Control Mode (Axial)**	**Unit**	**Rate of Loading**	**End level**		
				Relative	**Absolute**	**Force [N] Strain [mm] Displacement. [mm]**
Data	---	---	---			---
Cod plot	---	---	---			---
Start ramp	Force	[N]	10.000		●	-500
Ramp 2	Displacement	[mm/Min]	0.02000		●	-0.050000
Ramp 3	Displacement	[mm/Min]	0.02000		●	-0.025000
Ramp 4	Displacement	[mm/Min]	0.02000		●	-0.10000
Ramp 5	Displacement	[mm/Min]	0.20000		●	-0.025000

Ramp 6	Displacement	[mm/Min]	0.20000		●	-0.15000
Ramp 7	Displacement	[mm/Min]	0.20000		●	-0.025000
Ramp 8	Displacement	[mm/Min]	0.20000		●	-0.20000
Ramp 9	Displacement	[mm/Min]	0.20000	●		0.15000
Ramp 10	Displacement	[mm/Min]	0.20000		●	-0.30000
Ramp 11	Displacement	[mm/Min]	0.20000	●		0.20000
Ramp 12	Displacement	[mm/Min]	0.20000		●	-0.40000
Ramp 13	Displacement	[mm/Min]	0.20000	●		0.20000
Ramp 14	Displacement	[mm/Min]	0.20000		●	-0.60000
Ramp 15	Displacement	[mm/Min]	0.20000	●		0.20000
Ramp 16	Displacement	[mm/Min]	0.20000		●	-0.80000
Ramp 17	Displacement	[mm/Min]	0.20000	●		0.20000
Ramp 18	Displacement	[mm/Min]	0.20000		●	-1.0000
Ramp 19	Displacement	[mm/Min]	0.20000	●		0.20000
Ramp 20	Displacement	[mm/Min]	0.20000		●	-1.2000
Ramp 21	Displacement	[mm/Min]	0.20000	●		0.20000
Ramp 22	Displacement	[mm/Min]	0.20000		●	-1.6000
Ramp 23	Displacement	[mm/Min]	0.20000	●		0.20000
Ramp 24	Displacement	[mm/Min]	0.20000		●	-2.0000
Ramp 25	Displacement	[mm/Min]	0.20000	●		0.20000
Ramp 26	Displacement	[mm/Min]	0.20000		●	-2.5000
Ramp 27	Displacement	[mm/Min]	0.20000	●		0.20000
Ramp 28	Displacement	[mm/Min]	0.20000		●	-3.5000
Ramp 29	Displacement	[mm/Min]	0.20000	●		0.20000
Ramp 30	Displacement	[mm/Min]	0.20000		●	-4.5000

APPENDIX D How to Tune MTS Machine and Perform Wedge Splitting Tests

Sine the MTS Model 793.10 MultiPurpose TestWare is used newly at Chalmers laboratory, it took some days and a lot of testing specimens until the behaviour and the response of the machine have been understood. In order to avoid all those tries and errors, done during this master thesis, for the next operator, the way that I dealt with the MTS machine is explained briefly. There are also four electronic documentations, provided by the MTS TestStar, which is recommended as the main reference.

1. Introduction

The Model 793.10 MultiPurpose TestWare is an advanced test designer available to MTS Series 793 Controllers. With MultiPurpose TestWare, it is possible to

- Create complex test procedures that include command, data acquisition, event detection, and external control instructions.
- Generate programs based on profiles created with a text editor application, a spreadsheet application, or the Model 793.11 Profile Editor application.
- Acquire and monitor real-time trend or fatigue data.

1. Range of application

The MPT application is not a stand-alone application. It must be used in conjunction with other applications in the Model 793.00 System Software bundle. Before the MPT application is started, following steps should be done:

1. Create a station configuration file with the Station Builder application.

2. Start the Station Manager application and open the station configuration file.

3. Select MPT from the Application menu of Station Manager.

After following these procedures for the first time, the station manager should be opened and defined station should be selected.

(Station Manager is accessible through: Start/All Programs/MTS TestStar/Station Manager)

Performing a test:

Following steps are needed:

1. Turn on the MTS TestStardata processor (from the switch on the back) and run the TestStar Software from: C:\Documents and Settings\All Users\Start Menu\Programs\MTS TestStar. Then click on Station Manager.

2. "Open Station" Window opens and Byggpress_Ext from the window and your Parameters Sets should be selected.

3. Turn on the hydraulic System of the machine by clicking on the 4 controlling buttons (Power low, Power high, Power low, Power high).

Note: If you see that Station Limits in the Station Option is in its upper limit, use one of methods stated in the manual: System Software Vol 1 pages 98 and 99 (Method 1 or method 2)

This sort of out range error usually happens when you start the machine after a long rest (like a day).

4. In order to let the machine to warm up and meet a stable condition, it is recommended to run the procedure "Warm-up' and let the machine to follow it for 10 minutes, as follows:

- Click on: Open Procedure
- Chose: Warm up
- Click on program stop (after 10 min)

Note: make sure that you do not have any specimen (or anything else) in the cross-head path

5. A new Test Procedure should be made or a prescribed Test Procedure should be applied.

6. Making a New Test Procedure: with a Test Procedure, the loading procedure is defined. Different modes such as force, strain, or displacement can be select.

- From the Process Palette, your desired command can be chosen for your procedure.

- the procedure should be saved after each edition.

Note: it is also possible to edit the Test Procedure during loading provided that the test should be stopped by "Program Stop" bottom and the Testing status should be unlocked by " Toggle Execute/Edit mode" bottom and the editor window can be opened by "Procedure Editor". After editing the procedure, the Procedure Window should be saved and closed in order to complete the edition. By clicking on " Toggle Execute/Edit mode" + "Program Run" the tests will be followed by the new Test procedure.

Note: the modification of Test Procedure during testing is not recommended, but it any case this edition should be done quickly in order to avoid creep and relaxation effect on the test.

7. In order to do a good monitoring of the test, six windows are needed to be opened as follows:

- Station Manager: this is the main window and includes all main function of testing.
- Signal Audio Offset: this window gives you the opportunity to set three parameters to zero: Axial, Displacement, Axial Force, and Axial Strain.
- Manual Controls: the cross-head of the machine can be manually controlled by this windows if the Active Mode set to Displacement and 'Enable Manual Command' become on.
- Scope 1: through this window the two parameters versus time are plotting simultaneously. It is wise to have Axial command-Time and Axial Strain-Time if the test is doing under strain control (or Axial command-Time and Axial force-Time if the test is doing under force control). Through this window the coincidence of Axial Command and measured value of one parameter can be monitor.
- Meters 1: Axial Displacement, Force, Strain, Command, error, and etc can be monitored by this window.
- cod plot: as long as you click on the " Toggle Execute/Edit mode " bottom, it starts to plot the defined plot file in the Test Procedure.

8. Preparing the Specimen: after putting the specimen on the cross-head, the upper cross-head can be controlled by the Remote Control Station if it is already enabled. It is recommended to set the axial force to zero before the upper cross-head touches the specimen, by ‘’Single Auto Offset’’ window on the monitor. In order to be sure that the specimen is in full contact with the upper cross-head properly, the specimen can be loaded up to a low value (e.g. 300 N), by either Remote station Control or Manual Control. It can be also done by Manual command in the monitoring phase, if it has been already enabled. After setting Axial Displacement and Axial Strain to zero, the test is ready to start.

9. Starting the testing: the test starts by "Program Run" bottom in the "Station Manager" Window and it will be switched off automatically after following all the predefined Test Procedure. After finishing the test, it should be unlocked by clicking on "Toggle Execute/Edit mode". The saved data of the test is accessible via: C:\tsiis\mpt\Specimens

10. Turning off the Machine: all the windows excluded Station Manager should be closed. The Hydraulic System should be off by clicking on ‘’off’’ bottom in "Station Controls" panel of the "Station Manager" window; and finally the "station manager" can be closed by Path: File/Exit. The operator will be asked by saving the new setting

on the station manager. The TestStar Processor also should be off by its switch on the back.

Note: In the case of Cyclic loading, the test is mush more stable under displacement control rather than Strain or Force control. It also gives the opportunity to manually edit the test procedure during testing with a very slight effect of relaxation and creep which dose not influence the global behaviour and can not be seen in the Force-Strain diagram.

APPENDIX E A Brief Introduction to Nonlinear Tension Softening (Hordijk et al.)

Hordijk, Cornelissen & Reinhardt proposed an expression for the softening behaviour of concrete which also results in a crack stress equal to zero at a crack width $\Delta u_{n.ult}$; see Fig 1(a), also see Diana User Manuals – section 21.1.3 for the function.

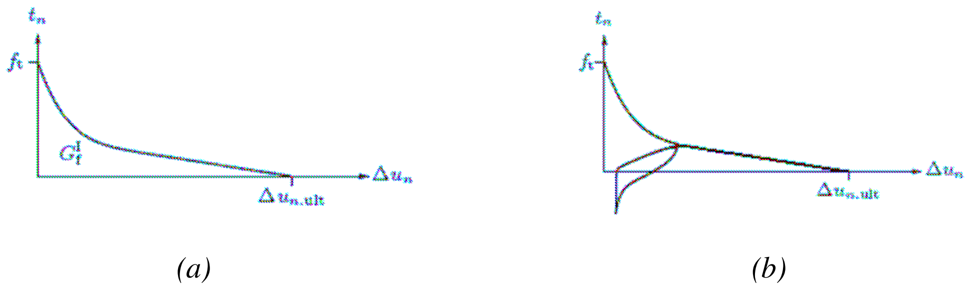

Fig 1 (a) Nonlinear tension softening (Hordijk et al.), and (b) Hysteresis model (Hordijk)

Unloading and reloading can be modeled according to a secant approach, an elastic approach or by application of hysteresis. In the secant approach, the relation between the traction and the relative normal displacement is linear up to the origin, after which the initial stiffness is recovered. In the elastic approach, the initial stiffness is recovered immediately after the relative normal displacement has become less than the current maximum relative normal displacement; see Fig 1(a). The third possibility is to apply the hysteresis model of Hordijk in which unloading and reloading follow different paths; see Fig 1(b).

One result from FE analysis performed by Diana with hysteresis model of Hordijk on plain concrete is presented in Fig 2.

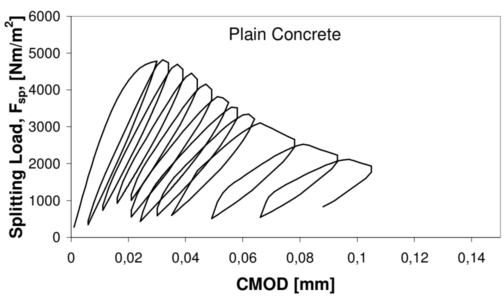

Fig 2 Typical result from the FE analysis conducted by Diana for the plain concrete using the hysteresis model of Hordijk.